In vivo Measurement of Ectopeptidase Activity Using Electroosmotic Perfusion-Microdialysis

by

Rachael-Anh Elizabeth Wilson

B.S. in Chemistry, George Mason University, 2014

Submitted to the Graduate Faculty of the

Dietrich School of Arts & Sciences in partial fulfillment

of the requirements for the degree of

Doctor of Philosophy

University of Pittsburgh

2019

UNIVERSITY OF PITTSBURGH

DIETRICH SCHOOL OF ARTS AND SCIENCES

This dissertation was presented

by

Rachael-Anh Elizabeth Wilson

It was defended on

May 29, 2019

and approved by

Dr. Adrian C. Michael, Professor, Department of Chemistry

Dr. Seth Horne, Associate Professor, Department of Chemistry

Dr. Jun Chen, Assistant Professor, Department of Electrical and Computer Engineering

Dissertation Director: Dr. Stephen G. Weber, Professor, Department of Chemistry

In vivo Measurement of Ectopeptidase Activity Using Electroosmotic Perfusion-Microdialysis

Rachael-Anh Elizabeth Wilson, Ph. D.

University of Pittsburgh, 2019

Insulin regulated aminopeptidase (IRAP, EC 3.4.11.3) is a promising drug target for treatment of cognitive impairment. This membrane-bound ectopeptidase is densely concentrated in areas of the brain associated with cognition and is known to hydrolyze neuropeptides involved in memory and learning *in vitro*. A hypothesis is that inhibition of IRAP may extend the lifetime of beneficial neuropeptides in the extracellular space, mitigating the effects of diseases such as Alzheimer's. A challenge in testing this hypothesis is the lack of available methods for quantitatively measuring ectopeptidase activity *in vivo*.

This work describes the development of analytical techniques to aid in the understanding of ectopeptidases and the fate of neuropeptides in the extracellular space. We have done this by enhancing the sensitivity and quantitative capabilities of detection methods including capillary liquid chromatography-tandem mass spectrometry for online collection of neuropeptides and by the development of a novel sampling technique called electroosmotic perfusion-microdialysis (EOP-MD). With EOP-MD, substrate peptides are perfused using electroosmotic flow and hydrolysis products along with unhydrolyzed substrate are collected at the microdialysis probe. The advantage of using this approach compared to conventional microdialysis is that the volume of substrate and the residence time in the tissue can be controlled using current. Additionally, spatial resolution is dependent on the distance between the EOP and MD probes, which is approximately 100 μm. We have demonstrated this approach by observing leucine enkephalin hydrolysis in the anesthetized rat brain in the presence and absence of the IRAP inhibitor HFI-419.

Table of Contents

List of Tables

List of Figures

List of Equations

Preface

This work is dedicated to Marcus and Iris. Marcus, this work could not have been done without your endless support, strength, and optimism. Thank you for always being by my side and encouraging me to pursue my goals. Iris, you are the light of my world and the inspiration for everything I do. You will do great things!

The past five years have shown me how truly blessed I am. Over and over again God has shown me that I am not alone in my journey and it is only through the support of many remarkable people that this work has been accomplished. Foremost, my family, especially my mom and sisters for providing constant support and encouragement over the past five years as well as being there for Iris when I could not. I truly could not have done this without you. I must also thank my advisor, Dr. Stephen Weber, who welcomed me into his lab and taught me so much about science and life in general. Your support and mentorship have been invaluable to me. I would also like to thank my undergraduate advisor, Dr. Abul Hussam, for introducing me to analytical chemistry and encouraging me to go to graduate school. Thank you to Dr. Andrea Jacquins-Gerstl for being an amazing co-worker and friend. There aren't words to describe how much I appreciate your support. Finally, I want to thank my co-workers in the Weber Lab for being alongside me throughout this work. I will always value your friendship.

1.0 Introduction

Ectopeptidases are important drug targets in the search for therapies to address central nervous system afflictions, including cognitive impairment and pain.[1] These membrane-bound enzymes have active sites open to the extracellular space (ECS) and act as the primary regulation mechanism for neuropeptides, a diverse class of signaling molecules.[2] Neuropeptides are released in small concentrations by volume transmission into the ECS, where they elicit effects through interactions with receptors.[3-4] Unlike classical neurotransmitters, such as dopamine and serotonin, their effects are modulated by degradation by ectopeptidases rather than cellular reuptake.[5] Resulting hydrolysis products can also act in signaling with activities different from the parent peptide. Thus, release of a particular peptide can initiate a cascade of effects throughout the central nervous system.

Central infusions of neuropeptides such as the enkephalins, galanin, oxytocin, and vasopressin have beneficial effects on cognition and learning, seizure activity, emotional disorders, and brain plasticity.[6-10] Thus, it is possible that specific inhibitors to target certain ectopeptidases may extend the extracellular lifetime of these beneficial neuropeptides. The potential benefits of using the endogenous neuropeptide system to treat cognitive diseases include high drug specificity and fewer side effects.[11]

Despite the benefits of exploiting this system to treat central nervous system diseases, difficulty in studying ectopeptidases and their substrates *in vivo* limits our understanding of the effects of inhibition, both desired and undesired. This is especially a problem for ectopeptidases such as insulin regulated aminopeptidase (IRAP, EC 3.4.11.3), an important drug target for cognitive enhancers but whose role in the brain and natural endogenous substrates are largely

unknown.[12] There is an unmet need for quantitative *in vivo* methods for probing ectopeptidase activity and understanding the fate neuropeptide hydrolysis products in the ECS.[13] Insight into these processes will help determine the biological roles of these important signaling molecules as well as potential effects of pharmacological manipulation.

1.1 Insulin Regulated Aminopeptidase (IRAP)

A number of ectopeptidases play a role in modulating the activity of neuropeptides in the ECS including dipeptidyl peptidase IV (EC 3.4.14.5), aminopeptidase N (EC 3.4.11.2), and neutral endopeptidase (EC 3.4.24.11). These ectopeptidases are relatively well-characterized in terms of binding site specificity and artificial substrates and inhibitors are readily available for probing enzymatic activity.[2] The focus of this dissertation will be on developing methods for the study of IRAP, a recently discovered ectopeptidase that has shown promise as a drug target for the development of cognitive enhancers.[12]

IRAP was first discovered in the mid-1990s when it was found to be co-localized with the GLUT4 transporter in adipocytes.[14-15] It was hypothesized that the protein had a role in glucose shuttling and was also found to have aminopeptidase activity, suggesting a function in regulating peptide hormones.[14-15] Shortly after, a third group identified IRAP in the placenta as placental leucine aminopeptidase/ oxytocinase, where it was thought to have a role in regulating oxytocin levels throughout pregnancy.[16] The authors noted that IRAP was likely synthesized as a transmembrane protein but was detectable in a soluble form in placental plasma.[16] IRAP was found to be widely distributed in tissues throughout the body including skeletal muscle, cardiac tissue, digestive organs, and the brain, further contributing to the mystery of the function of this

peptidase.[16] *In vitro* studies showed that IRAP hydrolyzed several neuropeptides involved in cognitive and emotional processing, including the enkephalins[17-18], dynorphin A 1-8,[19] arginine-vasopressin[17, 20], oxytocin[17, 21], somatostatin[20]. A role for IRAP in regulating these particular neuropeptides seems to be mirrored in histological studies showing that IRAP is highly concentrated in areas involved in cognition, including the hippocampus, prefrontal cortex, and the amygdala, though it is also widely distributed in other areas of the brain.[22]

In 2001, IRAP was identified as the angiotensin IV (AT4, VYIHPF) receptor.[23] AT4 was thought to be an inactive byproduct of the renin-angiotensin system but in the 1970-80s it was found that intracerebroventricular (icv) infusions of the AT4 precursor angiotensin II (AT2) stimulated the release of vasopressin[24], and dopamine[25-26]. This led to the discovery that AT2 also enhances rodent performance in memory and learning[27-38] tests, reverses some forms of cognitive impairment[39-43], and protects against the effects of ischemia[44-45]. It was later concluded that the beneficial effects of AT2 are dependent upon its metabolism to AT4.[33, 46-55] Discovery of a distinct AT4 receptor further suggested a bioactive role for AT4.[56-57] When this receptor was later identified as IRAP, it was hypothesized that the cognitive effects of AT4 were due to binding and inhibition of IRAP, extending the lifetime of cognitive-enhancing peptides in the extracellular space. [23, 58-60] While there is still debate over the identity of IRAP as the AT4 receptor[61], perfusion of specific inhibitors shows similar cognitive effects as those seen with AT4 and its ligands.[62-67] Thus, IRAP has become a target for the development of drugs to treat cognitive impairment, though the role of IRAP in the brain and relevant *in vivo* substrates are still unknown.[66, 68-69]

1.2 *In vivo* Sampling Methods

Understanding the roles of ectopeptidases has been limited, in part, by challenges in studying endogenous neuropeptides. Low concentrations (pM) in the extracellular space require the use of careful sample handling and highly sensitive and specific detection methods.[70] This makes it difficult to accurately measure not only basal levels but also changes in concentration due to binding or degradation processes.[13]

One *in vivo* sampling technique that has been used to study neuropeptides in the ECS is push-pull perfusion (PPP).[71-74] This method involves a probe consisting of two capillaries, one for perfusion and the other for collection. Artificial cerebrospinal fluid (aCSF) is infused through the perfusion probe while vacuum is applied at the collection end. This process must be carefully balanced so that fluid is replaced at the same rate that it is withdrawn.[75] Extracellular contents are contained within the collection capillary, where they can be analyzed offline. The main advantage of PPP is that analytes can be collected at nearly 100% efficiency, meaning nearly all the fluid perfused into the ECS, along with analytes that have diffused into the fluid, is recovered in the collection capillary.[76] This is especially important for low-abundance analytes, such as neuropeptides. An accompanying disadvantage is that there is no barrier preventing large analytes such as soluble enzymes and proteins from entering the collection probe, leading to possible degradation of collected analytes as well as technical issues, such as capillary clogging. Another downside is that low flow rates (nL/ min) must be used to minimize tissue damage.[76-77] This results in impractical sample volumes.

The most common sampling method for studying neuropeptides is microdialysis, in which a microbore probe consisting of inlet and outlet tubing connected by a molecular weight cutoff membrane is inserted into the ECS of a particular brain region.[78-79] The probe is continuously

perfused with a physiological solution, such as aCSF, creating a concentration gradient that drives analytes across the membrane. Dialysate is collected at the probe outlet. This method allows continuous, online collection at practical (μL/ min.) flow rates. Online collection of neuropeptides is ideal, both to prevent degradation upon collection[80] and to minimize adsorptive losses[81] from these mass-limited samples due to sample handling and storage. Additionally, microdialysis can be coupled with a variety of separation and detection methods to suit the needs of the analyte of interest.

1.3 Neuropeptide Separation and Detection

Although a main advantage of using microdialysis is the ability to collect microliter sample volumes, an accompanying problem is analyte dilution. Capillary liquid chromatography (cLC) is particularly suited to this challenge due to small column diameters (≤150 μm), which decrease radial dilution and improve concentration sensitivity.[82-83] A drawback is that small columns are also susceptible to volume overload, in which large injection volumes result in altered peak shapes and decreased sensitivity.[83-87] Fortunately, capillary columns have limited thermal mass, which allows the use of fast and efficient temperature changes to focus large volume injections and mitigate the effects of volume overload.[88-91]

Coupling cLC with tandem mass spectrometry (MS^2) has emerged as the gold standard for *in vivo* neuropeptide detection.[92] By using mass detection, substrates and hydrolysis products can be detected simultaneously and with high sensitivity.[93] In addition, it is amenable to online neuropeptide analysis, though this approach has only been used sparingly.[94-97] Though cLC-MS is

becoming an increasingly popular method for studying neuropeptides in microdialysate, quantitative detection at basal levels is still a challenge.

1.4 Measuring Enzyme Activity *In vivo*

Portions of this section are based on a review that was published in *Annual Review of Analytical Chemistry*[98]

Direct *in vivo* measurements of endogenous neuropeptides using the aforementioned approaches could be invaluable in determining where a particular neuropeptide acts and the relative quantities at which it is present, but more information is required to understand the relative affinity of a peptide substrate for an ectopeptidase of interest as well as the kinetics of substrate hydrolysis. This information is critical in elucidating the relevant *in vivo* substrates of a particular ectopeptidase, such as IRAP.

Methods for measuring enzyme activity *ex vivo* or *in vivo* tend to fall into the categories of either imaging-based techniques or sampling-based techniques. Imaging-based techniques such as fluorescence[99-101], and magnetic resonance imaging[102-103] often rely on detectable probes or labels to generate or dampen a signal when enzymatic activity occurs. This work has been particularly useful for qualitative clinical applications, such as identifying the location of a tumor. These techniques also have the advantage of being minimally invasive. Conversely, sampling-based techniques involve implantation of a physical probe into the tissue. Such approaches are frequently applied to biochemical or pharmacokinetic studies and offer the ability to locally affect the sampling environment by perfusion of drugs or other analytes.

1.4.1 Imaging-based Techniques

Among the imaging-based techniques, fluorescence is common. Several fluorescent probes have been developed for imaging tumors in rodents based on the upregulated activity of certain enzymes, including cysteine and serine proteases[104] and more specifically, cathepsin D[105], asparaginyl endopeptidase[106], and β-galactosidase.[107] Design of these probes involves creative chemistry and strategies for enhancing signal-to-noise ratio, but *in vivo* applications are largely focused on the spatiotemporal aspects of cancer detection and monitoring rather than quantitative elucidation of the role of a particular peptidase.

A historically important *ex vivo* approach for measuring enzymatic activity in the brain is *in situ* zymography (ISZ), which uses a "dye quenched," or DQ-collagen to measure matrix metalloproteinase (MMP) activity in brain tissue slices. A fluorescent signal is generated upon hydrolysis of the derivatized collagen substrate, providing information about both the activity of the enzyme as well as location. This approach has been used in both frozen[108] and fixed[109-111] tissues to study MMP roles in ischemia[108], seizures[110], and long-term potentiation[112] in the brain. This concept has also been applied *in vivo* using Förster (or fluorescence) resonance energy transfer (FRET)[113]-based substrates, which consist of a fluorophore and a quencher separated by an amino acid linker sequence. The linker confers enzymatic specificity and fluorescence is detected upon hydrolysis. A method known as differential *in vivo* zymography utilizes this concept, with different fluorophores corresponding to different enzymes.[114] This has allowed monitoring of MMP activity changes throughout zebrafish development. The limitation of zymography is that it is almost exclusively used to study MMPs.

Magnetic resonance spectroscopy (MRS) has been used to study enzymatic activity of natural substrates by observing the magnetization transfer among functional groups on different

molecules containing the same active nucleus, such as ^{31}P. This has allowed the *in vivo* measurement of creatinine kinase and ATP synthase activity in the liver and muscle as well as other phosphorylation events.[115] ^{1}H MRS has been used to monitor the levels of 2-hydroxyglutarate in brain tumors, a metabolite and possible biomarker for isocitrate dehydrogenase-mutated gliomas.[116] Another MRS approach that has been used in the brain is the perfusion of ^{15}N-labeled glutamate along with $^{15}NH_4Cl$ for a period of time allowing for [5-^{15}N]-glutamine synthesis followed by perfusion of $^{14}NH_4Cl$.[117] By monitoring the decline in [5-^{15}N]-glutamine its hydrolysis rate can be determined. This approach has been combined with microdialysis collection of extracellular glutamine to study glutamine export to the extracellular space.[118] MRS-based techniques offer the ability to make quantitative rate measurements along with imaging capabilities. A weakness is that their detection limits (mM) are relatively high for neuropeptide studies.

Mass spectrometry imaging (MSI) is a versatile and sensitive approach that allows identification of chemical species while maintaining spatial resolution. This is particularly important in elucidating the function of a peptide substrate or ectopeptidase in the brain. The major advantage of matrix-assisted laser desorption/ionization (MALDI)-based approaches is that natural substrates and hydrolysis products, both known and unknown, can be analyzed directly without further chemical modification.[119] MALDI coupled with time of flight (TOF) analyzers has been combined with *in situ* histochemistry to map angiotensin degradation in mouse kidney slices[120] and to study the effect of different aminopeptidase inhibitors on dynorphin B metabolism in the rat brain using frozen tissue slices.[119] The Li group used MALDI-LTQ-Orbitrap XL to perform multiple data dependent acquisition steps in a spiral sequence at each raster step.[121] This allowed the identification of one novel and 38 known endogenous neuropeptides in blue crab

(*Callinectes sapidus*) brain slices.[121] The power of MSI lies in the ability to detect natural substrates and products with high sensitivity and specificity. The downside is that it is limited to *ex vivo* analyses.

1.4.2 Sampling-based Techniques

As previously stated, microdialysis is the most commonly used *in vivo* sampling technique and has been applied to the study of enzymatic activity in the ECS. Enzymatic studies using microdialysis usually involve introducing a substrate by retrodialysis. The substrate diffuses out of the probe, where it is hydrolyzed by ectopeptidases, and resulting products as well as unhydrolyzed substrate diffuse back to the probe. Alternatively, substrates can be centrally infused into the brain and products collected in a particular brain region using microdialysis. These approaches have been used to investigate Peptide E[122], beta-endorphin[123], dynorphin A[124], angiotension II[50], and substance P[94] degradation in the rat striatum. Klintenberg and Andren extended this approach to find differences in dynorphin A metabolism in unilaterally 6-hydroxydopamine lesioned rat striata.[125] By lesioning one side of the brain and implanting probes bilaterally, the authors found lower levels of dynorphin A hydrolysis products in the lesioned side of the brain compared to the intact side, suggesting that dynorphin A metabolism is altered in Parkinson's disease.[125]

Though the majority of neuropeptide degradation studies are qualitative in nature, the Stenken group has attempted to develop models for quantifying enzyme activity using microdialysis.[126-127] These studies have been performed *in situ*[128-129] and *in vivo*[130], though not in the brain. Substrates, in some cases isotope-labeled, are introduced to the tissue by retrodialysis. The concentration collected at the outlet of the probe is compared to that which was introduced at

the inlet. This relates to the extraction fraction (EF) of the probe and is a function of membrane properties, analyte mass transport through the probe and the medium, perfusion flow rate, and substrate uptake and degradative processes in the tissue.[131] Changes in EF throughout an experiment were attributed to enzymatic activity.[132] Though this metric was sensitive to changes in enzymatic activity *in vitro* and *in situ*, changes in microdialysis EF were not sensitive enough to detect changes in enzymatic activity in *in vivo* studies looking at glucose metabolism[133] and MMP-1/9 activity[134]. The latter work suggested that this is because EF is more affected by analyte mass transport than enzymatic processes *in vivo*.[131, 135-136]

The complex processes dictating analyte delivery to the tissue limit quantitation of enzymatic activity by microdialysis. Clearance mechanisms in the ECS change the concentration gradient external to the probe which changes the amount of substrate that is delivered to the tissue.[131, 136-137] This requires long equilibration times to achieve steady-state.[130] Treatments that block uptake or metabolic processes alter the concentration gradient, which could change the recovery of the probe.[137] Thus, measurements made in the absence of inhibitor may not be directly related to those made with inhibitor treatment. Since enzymatic rates are concentration-dependent, many experiments are necessary to assess the effects of experimental factors such as probe geometry and flow rate and conclude that a change in EF is due to a biological process rather than some other form of mass transport.[138] Even so, there is a narrow range of clearance rates that can be detected in this way. [131, 136]

Our group has developed a method for probing the extracellular space using electroosmotic perfusion, in which current is used to perfuse substrate peptides into the tissue, where they are hydrolyzed in the ECS by ectopeptidases.[139-140] Hydrolysis products and unhydrolyzed substrate

are collected and analyzed to determine enzyme activity. Because the analyte residence time can be controlled by current, quantitative parameters of enzyme activity can be determined.

1.4.2.1 Electroosmotic Perfusion-based Sampling

Substrate peptide-containing solutions are perfused into the tissue via a fused silica capillary. Electroosmotic flow results from a current passing through the solution (Figure 1).[141] An uneven distribution of positive ions in the double layer move in the direction of the negative electrode, resulting in bulk fluid flow.[141-142]

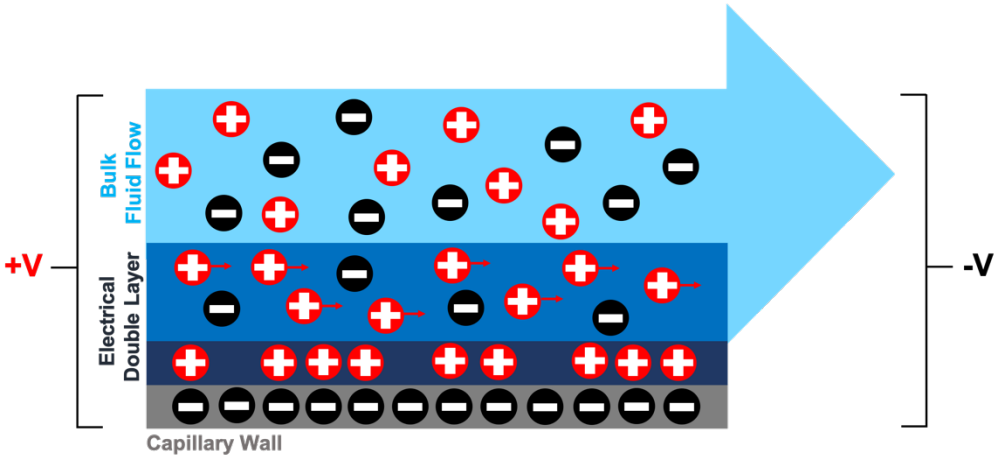

Figure 1 Schematic of the double layer that forms due to interactions between surface charges at the capillary wall and mobile ions in the electrolyte solution, resulting in bulk fluid flow when an electric field is applied.

The electroosmotic flow rate (m^3/s), U_{eo}, is dependent upon the applied current (A), i, as seen in Equation 1:

Equation 1

$$U_{eo} = -\frac{\varepsilon_w \zeta}{\eta}\frac{i}{\sigma_{el}}$$

where ε_w is the permittivity of water (F/m), η is the dynamic viscosity (Pa s), ζ is the potential at an imaginary plane between the fixed charges on the surface of the capillary and the solution (V),

and σ_{el} is the conductivity of the electrolyte solution (S/m).[143] An analogous expression based on a modified Darcy's law can be used to describe the superficial electroosmotic velocity (u_{eo}) in a porous medium in the absence of a pressure gradient (Equation 2):

Equation 2

$$u_{eo} = \frac{\varepsilon_w \zeta}{\eta} \frac{\Delta V}{L}$$

where ΔV is the voltage-drop over a distance, L.[144-146] Equation 2 demonstrates mathematically that the electroosmotic velocity can in fact be controlled using current.

To compare EOP to pressure-driven methods such as push-pull perfusion, we can compare Equation 2 to Equation 3, the superficial velocity of a pressure-driven fluid, u_p, through a porous medium:

Equation 3

$$u_p = -\frac{\Delta P}{L} \frac{\kappa}{\eta}$$

where ΔP is the pressure-drop over and κ is the hydraulic permeability of the medium, which is approximately 10^{-15} m^2 in the gray matter[147] of the brain. At constant current, electroosmotic flow is not dependent upon the permeability of the tissue[148], which varies throughout the brain[147]. This means that electroosmotic flow is more uniform in a heterogenous medium whereas pressure-driven flow will favor flow through tissue that has lower permeabilities, such as white matter.[149] This quality gives electroosmotic flow an advantage over pressure-driven flow for measuring ectopeptidase activity.

Xu, et al. first reported the use of electroosmotic sampling in a study of leucine-enkephalin (LE, YGGFL) degradation in OHSCs.[139] A tissue culture was placed on an insert membrane in

contact with a bath consisting of a solution of LE and an internal standard yaGfl, where lowercase letters denote a D-amino acid. The internal standard is resistant to hydrolysis and serves as a measure of the substrate concentration in the absence of hydrolysis. A 150 μm ID x 30 cm long capillary was placed on the surface of the tissue in the CA3 region of the hippocampus, with its distal end in contact with an electrolyte solution in which a platinum electrode was immersed. A second platinum electrode was placed in the tissue bath to complete the circuit. When an electric field was applied, electroosmotic flow drove peptides from the bath, through the tissue, and into the collection capillary. The contents of the collection capillary were then ejected into a vial and analyzed using HPLC-EC. By measuring hydrolysis in the presence of multiple inhibitors, it was determined that a bestatin-sensitive aminopeptidase is primarily responsible for LE degradation to GGFL in the ECS of the hippocampal CA3 region. It was also reported that the Michaelis Menten constant, K_m, for LE conversion to GGFL was 1.2 ± 0.5 mM, which was consistent with other literature reports. This work was the first to determine Michaelis Menten parameters based on live tissue measurements. Wu, et al. later used a similar approach to quantify coenzyme A degradation in the ECS of OHSCs using with online capillary electrophoresis – laser induced fluorescence.[150]

In single-probe electroosmotic perfusion studies the spatial resolution is largely dictated by the inner diameter of the collection capillary. The perfusion volume of the peptide is also not easily controlled. For these reasons, Rupert, et al. developed a two-probe electroosmotic push-pull perfusion (EOPPP) technique.[140] With EOPPP, peptide substrates were perfused using a pulled-tip source capillary ("push") and hydrolysis products and unhydrolyzed substrate were collected using the collection capillary ("pull"). The advantage of this technique is that the spatial resolution is dependent upon the distance between the two probes (40-100 μm). This allowed comparison of galanin hydrolysis between two regions within the hippocampus, the CA1 and the CA3.[140] This

method also provided quantitative evidence that LE degradation is higher in the CA1 region compared to the CA3, which may contribute to higher instances of cell death in the CA1 during oxygen-glucose deprivation (OGD), an ex vivo model for ischemia.[148, 151] It was also shown that administration of bestatin following OGD statistically reduced cell death in the CA1. This work demonstrates the importance of performing quantitative measurements of ectopeptidase activity in a spatially-resolved manner in order to understand the mechanisms of peptide modulation.

The *ex vivo* work described here represents a major technological stride in studying ectopeptidases in brain tissue. The next logical step for improving the versatility of this technique is to adapt it for *in vivo* use. This dissertation describes the steps we have taken to develop a method for *in vivo* ectopeptidase activity measurements in the anesthetized rat. Our approach was to first develop novel focusing techniques for enhancing sensitivity of peptide detection with cLC[152], then to apply proteomics-based strategies for peptide quantitation to the online detection of endogenous neuropeptides[97], and finally to design and fabricate a device capable of performing electroosmotic perfusion *in vivo*. Though this method can be used to study virtually any ectopeptidase in the ECS, our emphasis is on its application to the study of IRAP activity and potential substrates.

2.0 Improving the Sensitivity, Resolution, and Peak Capacity of Gradient Elution in Capillary Liquid Chromatography with Large-Volume Injections by Using Temperature-Assisted On-column Solute Focusing

Capillary HPLC (cLC) with gradient elution is the separation method of choice for the fields of proteomics and metabolomics. This is due to the complementary nature of cLC flow rates and electrospray or nanospray ionization mass spectrometry (ESI-MS). The small column diameters result in good mass sensitivity. Good concentration sensitivity is also possible by injection of relatively large volumes of solution and relying on solvent-based solute focusing. However, if the injection volume is too large or solutes are poorly retained during injection, volume overload occurs which leads to altered peak shapes, decreased sensitivity and lower peak capacity. Solutes that elute early even with the use of a solvent gradient are especially vulnerable to this problem. In this paper we describe a simple, automated instrumental method, Temperature-Assisted On-column Solute Focusing (TASF), that is capable of focusing large volume injections of small molecules and peptides under gradient conditions. By injecting a large sample volume while cooling a short segment of the column inlet at sub-ambient temperatures, solutes are concentrated into narrow bands at the head of the column. Rapidly raising the temperature of this segment of the column leads to separations with less peak broadening in comparison to solvent focusing alone. For large volume injections of both mixtures of small molecules and a bovine serum albumin tryptic digest, TASF improved the peak shape and resolution in chromatograms.

TASF showed the most dramatic improvements with shallow gradients, which is particularly useful for biological applications. Results demonstrate the ability of TASF with gradient elution to improve the sensitivity, resolution, and peak capacity of volume overloaded samples beyond gradient compression alone. Additionally, we have developed and validated a double extrapolation method for predicting retention factors at extremes of temperature and mobile phase composition. Using this method, the effects of TASF can be predicted, allowing determination of the usefulness of this technique for a particular application.

2.1 Introduction

With the advent of electrospray ionization mass spectrometry (ESI-MS), capillary HPLC (cLC) has become a widely used separation method. Due to reduced volumetric flow rates and increased ionization efficiency, cLC couples particularly well with ESI-MS.[82, 153-155] This has led to cLC's dominance in the fields of proteomics[156-161], metabolomics,[155, 158, 162-167] and *in vivo* determination of neuropeptides.[168-172] Combined with gradient elution, peak capacities exceeding 800[173-174] have been achieved. In their work with ultra-high-pressure cLC, Shen et al. were able to identify over 2000 peptides and 5000 metabolites using tandem MS for detection.[174] High sensitivity with small volume samples is particularly important as interest in developing cLC for clinical use is growing,[163, 175-179] with some recent methods achieving full or partial FDA validation.[82] Of course, the increased concentration sensitivity of cLC systems[82, 154, 165, 180-186] can be advantageously applied to any analysis based on small volume samples.

A disadvantage accompanying the use of small diameter columns is the potential for volume overload, the situation in which the injection volume is large enough to alter a solute's peak shape.[154, 187-190] While a solvent gradient/reversed phase cLC system may not be highly susceptible to volume overload for the more hydrophobic solutes, the more polar solutes still can suffer from broadening due to volume overload.[187, 189] Of course, which solutes in a sample fall into the "more polar" class and suffer volume overload and which fall into the "more hydrophobic" class and do not depends on the injection volume and the particular chromatographic conditions.[89, 187, 189, 191] Volume overload decreases the overall peak capacity and sensitivity of the method.[187, 189-190, 192] Manipulating the gradient to avoid having solutes in the early eluting, "more polar" class flies in the face of gradient optimization[188, 193-195] which attempts to use all of the peak capacity available in the specified separation time. What is needed is a general approach for focusing large-volume injections (>100% of the column volume) that allows an analytical method to take advantage of the full peak capacity of the gradient system and sensitivity of a capillary scale column.

Due to low thermal mass and thin silica walls, rapid heating and cooling of cLC columns is possible without increasing bandspreading from radial thermal gradients.[196-197] Additionally, elevated temperature is effective in improving the efficiency of capillary columns.[198] However, elevated temperatures also add to the challenge of managing large volume injections because increasing temperature typically decreases retention making volume overload more of a problem. Since retention in LC is temperature dependent, transient temperature changes can be used to alter retention factors in chromatographically useful ways.[199-203] Solute trapping using sub-ambient temperatures has been explored. Holm, et al., developed a capillary column oven in which the column was placed on a "cold zone" held at 0 °C during injection then manually moved in space

to a “hot zone” for the separation phase. Using this approach, the authors were able to minimize peak widths of large-volume injections of the antioxidant Irganox 1076 (clog P 13.9)[204] in a neat acetonitrile mobile phase.[205] Eghbali, et al., used dry ice and boiling water to cool/heat circulating nitrogen gas, allowing focusing of the protein lysozyme at -20 °C near the end of the column.[206] While each work demonstrated the effectiveness of temperature focusing, the former involved very hydrophobic solutes and the authors of the latter work doubted the usefulness of their approach for small molecules.[206] Additionally, neither approach was automated which limits throughput and threatens irreproducibility.

We have previously shown that temperature-assisted solute focusing (TASF) is effective in improving volume-overloaded isocratic separations of hydroxybenzoate esters beyond that achieved with solvent focusing alone.[207-208] With TASF the head of the column is cooled to sub-ambient temperatures during injection. This results in focusing of solutes into narrow bands at the head of the column. Subsequently raising the temperature increases solute velocity to achieve a separation in a reasonable time. However, previous TASF studies were done using small molecules and under isocratic conditions and with a simple approach to controlling temperature. In this paper we demonstrate that our fully automated TASF apparatus used with reversed-phase LC (RPLC) is a practical method for focusing large volume injections of both small molecules (values of log P (or clog P) range from 1.16 to 4.75)[209-210] and peptides and can also focus solute bands beyond gradient compression alone. In order to be able to simulate or predict the outcome of a TASF-enhanced separation, values of both very high and very low retention factors, k’, are needed. We developed and validated a double extrapolation procedure based on an equation by Neue and Kuss[211] and the van ‘t Hoff relationship for obtaining such k’ values.

2.2 Experimental

2.2.1 Reagents and Solutions

Uracil, acetanilide, methyl and ethyl esters of *p*-hydroxybenzoic acid (parabens), acetophenone, propiophenone, butyrophenone, benzophenone, valerophenone, hexanophenone, heptanophenone, and octanophenone were from Sigma-Aldrich (St. Louis, MO). Stock solutions, 25 mM, were made in acetonitrile (Chromsolv, LC-MS grad, Fisher Scientific, Fair Lawn NJ. Samples were diluted to concentrations from 5 to 20 μM with deionized water. Sample concentrations were selected to maximize concentration while factoring in column loadability and solubility. Water was from a Millipore Milli-Q Synthesis A10 purification system (Billerica, MA). Peptide samples were from an LC-MS grade BSA tryptic digest from Fisher. The lyophilized sample was diluted, as per reagent instructions, to 1 pmol/μL in 95:5 0.1% formic acid: acetonitrile. Formic acid was from Sigma. The BSA sample was stored at -5 °C when not in use and used within 48 hours of thawing/dilution.

2.2.2 Instrumentation

A Thermo/Dionex UltiMate 3000 Nano LC (NCS-3500RS, Germering, Germany) system consisting of a nanoflow pump, a low-pressure loading pump, integrated column oven, and WPS-3000RS autosampler was used for this work. Autosampler temperature was set to 35 °C for small molecule work (to increase sample solubility) and 5 °C for BSA samples. Detection was achieved by a Waters Acquity TUV detector (Millford, MA) fitted with a 10 nL flow cell. Signal from the

detector was interfaced with an external Thermo analog-to-digital converter. Acquisition rate was 100 Hz. The system was controlled by Chromeleon software (version 6.8).

2.2.3 TASF Hardware

Hardware for this system is similar to that used previously.[208] Briefly, timed injections were made using an external 6-port Cheminert injection valve (C72x-669D, VICI Valco, Houston, TX) fitted with a 75 μm x 75 cm nanoViper capillary (Thermo) loop. Samples were loaded into the sample loop using the loading pump and autosampler of the NSC-3500 system. Focusing segment temperature was controlled by a 1.0 x 1.0 cm Peltier thermoelectric device (TEC, Custom Thermoelectric, 04801-rG30-34RB, Bishopville, MD). To improve heat transfer between the TEC and heat sink compared to our previous system, the TEC was silver soldered to a custom liquid cooled copper heat sink. Heat sink temperature was regulated using a HAAKE A80 temperature controlled cooler (Thermo, Paramus, NJ) pumping an ethylene glycol/water mixture at about 1 L/min. The TEC was powered by a MAXIM Integrated 1968 electronic TEC driver (Sunnyvale, CA). Temperature was monitored by a 36-gage type-T thermocouple from Omega Engineering (Stamford, CT) interfaced with a National Instruments 9211 4-channel thermocouple module (Austin, TX). TEC temperature was logged at 7 Hz and controlled using a simple feedback loop written in LabVIEW 2015 (NI). TEC control, remote start, and valve injection signals were made by a USB-6008 multifunction DAQ (NI). The downstream, isothermal segment of the column was heated resistively using a Kapton resistive heater (KH-106-10-P, Omega) and a Love Model 1500 proportional-integral-derivative (PID) controller (Dwyer Instruments, Michigan City, IN) as described previously.[212]

2.2.4 TASF Control

Temperature transients must be fast to ensure efficient release of focused bands as well as precisely controlled to ensure reproducibility and minimize temperature over- and undershoot. To achieve this, a commercially available electronic TEC driver was used to run a high power, low thermal mass TEC with control software written in-house. A simple feedback loop-based routine was developed in LabVIEW to control the driver. At the beginning of a day, the software "learns" the relationship between temperature and control voltage. This is achieved by setting an arbitrary temperature in the software for which the driver establishes a voltage to maintain that temperature at the TEC (±0.05 °C). Temperature measurements and voltage adjustments are made at 7 Hz. The program stores the maximum and minimum voltages required to reach the separation and focusing temperatures, respectively. In operation, a LabVIEW program initiates a temperature change at a programmed time. When the target temperature is raised, it applies a control voltage corresponding to a temperature that is a few degrees below the target. Then a feedback loop takes over. Based upon ΔT, the difference between the measured and target temperatures, the program increases the control voltage, in steps that can be defined by the user, to approach the target temperature. The steps become smaller as ΔT becomes smaller. When ΔT changes sign, so does the control voltage steps. For cooling, the process is analogous. By adjusting the voltage step size for a particular range of values of ΔT, the approach to the final voltage can be made more aggressive with a slight overshoot or gentler with no overshoot. While not a proportional-integral-derivative (PID) control algorithm, this program mimics a PID result and works equally well in the heating and cooling modes without the need for separate PID parameters in each operational mode.

2.2.5 Chromatographic Conditions

5 µL of each sample were delivered from the autosampler to the valve by the loading pump, which served to fill the 1 µL sample loop. A one-minute delay between autosampler injection and valve injection was employed to ensure the injection plug was centered in the sample loop.

2.2.6 Column Preparation

Columns were packed in-house following a previously developed method.[207-208] Briefly, 100 µm fused silica capillaries from Polymicro Technologies (Phoenix, AZ) were packed with Acquity CSH C18 1.7 µm particles (Waters). Column length, 14.2 cm, was controlled by defining the volume of slurry in the column packing bomb. Following packing with stationary phase the remainder of the capillary blank was packed with 8 µm solid silica spheres (Thermo). Column length was trimmed to a final length of 16.7 cm. We refer to these dual-phase columns as 'packed-void' columns. The column fluid volume, not including the packed-void segment, was estimated at 683 nL. A 5.0 cm x 100 µm, single-phase column was used for solute retention studies.

2.2.7 van`t Hoff Retention Studies

Temperature was controlled by the column oven of the Ultimate 3000 system. Extra-column time was determined to be 0.35 minutes by making 50 nL timed injections into the 25 µm ID detection capillary. Isocratic runs were performed for each solute under at least 4 different mobile phase compositions and 5 temperatures between 30 and 65 °C. See Table 1 (SI) for exact conditions used for each solute. The minimum temperature of 30 °C was dictated by the column

oven's lack of cooling capabilities. The order of temperatures was randomized and at least one hour of equilibration time was given between temperature changes to ensure temperature stability. Detection conditions were identical to those described above.

2.2.8 TASF Conditions

For TASF experiments the focusing temperature was -7.5 °C and the separation temperature was 65 °C. The temperature range was dictated by the maximum achievable by the TEC under experimental conditions. The lower temperature was the minimum practical based on our pump's maximum pressure and issues related to condensation at the TEC surface. The focusing temperature was held during the time of injection plus an additional 5 seconds. The column was equilibrated at the initial conditions for 5 minutes prior to the start of each run. The TEC was held at the focusing temperature for 1 minute prior to injection. Thus, the gradient time was coordinated to begin at the start of injection. After focusing, the temperature was raised quickly to the separation temperature and remained there for the remainder of the run. All runs were performed a minimum of three times.

2.2.9 Chromatography

Timed injections of solutions of small organic molecules (20 μM acetanilide, 15 μM acetophenone, 5 μM hexano- to octanophenone, and 7 μM benzophenone) from the 1 μL loop served to introduce samples. The volume of injection is deduced from the injection time and the flow rate, 1.00 μL/min. The initial gradient used consisted of 5-75% ACN over 12 minutes (5.8% ACN/min). UV absorbance was measured at 254 nm. Additional runs performed to create a variety

of gradient steepness were: 14.2% ACN/min and 2.7% ACN/min. To determine the usefulness of TASF with different injection volumes, the small molecule mixture described previously was injected at volumes of 50, 150, 250, 500, and 1000 nL. To maintain detectable signals, solute concentrations were increased accordingly. For this study, the gradient conditions were 5 to 75% ACN over 12 minutes.

For peptide experiments, 2 µL of the BSA sample were injected using an overfilled-loop. Gradient conditions were 5-40% ACN over 15 minutes with a flow rate of 1.00 µL/min. The separation temperature was 65 °C and the focusing temperature was -7.5 °C. The focusing temperature was held for 125 seconds. UV absorbance was measured at 214 nm.

All chromatograms were analyzed using a simple peak finding, integration and characterization program written in-house in MATLAB R2015a (MathWorks, Matick, MA).

2.3 Results and Discussion

2.3.1 Theory

A brief review of the dominant contributions to peak broadening when considering volume overload will explain conceptually how TASF works. Observed peak variance in time units, $\sigma_{t,obs}$, is dominated by independent broadening processes occurring before, during, and after separation on the column.[213]

Equation 4

$$\sigma^2_{t,\,obs} = \sigma^2_{t,\,pre} + \sigma^2_{t,\,col} + \sigma^2_{t,\,post}$$

Since post-column dispersion, $\sigma_{t,post}$, can be considered small with appropriate detection under both TASF and isothermal conditions it is not considered further.

Equation 5

$$\sigma^2_{t,\,obs} \approx \sigma^2_{t,\,pre} + \sigma^2_{t,\,col}$$

In volume overload, the variance due to the injection volume dominates the precolumn contribution. Thus, the injection variance is dependent on both injection volume, V_{inj}, and column characteristics, including radius, r_c, as seen in Equation 6.

Equation 6

$$\sigma^2_{t,\,pre} \approx \sigma^2_{t,\,inj} = \left[\frac{V_{inj}}{\sqrt{12\pi}\, r_c^2\, \varepsilon_{Tot}\, (1 + k_1)}\right]^2 \left(\frac{1 + k_{eff}}{u_{av}}\right)^2$$

ε_{Tot} represents the total porosity of the column. The retention factor during injection, k_1, and k_{eff}, the effective retention factor at elution as defined by Snyder and Dolan,[214] are temperature-dependent terms; u_{av} is the average linear velocity, which converts length units to time units. According to Equation 6, injection variance is largely dependent on the k_1 term and because this term is in the denominator, small values of k_1 result in larger values of σ_{inj}. TASF acts by lowering the temperature at the head of the column thus increasing k_1 and decreasing broadening due to injection.[192] This effect is most obvious for compounds that have relatively small retention factors at the column temperature.

Peak width in gradient elution is determined by way of Equation 7, which is based on linear solvent strength theory (LSST).[214]

Equation 7

$$\sigma^2_{t,\,col} = \frac{t_0}{\sqrt{N}}\, G(p)\,(1 + k_{eff})$$

where t_0 is the dead time of the column and $G(p)$ is the gradient compression factor. This factor, which is dependent on gradient steepness, represents the compression of the solute band on the column. It arises because the velocity of the solute front is lower than that of the rear.[214] TASF takes advantage of the temperature dependence of retention factors to minimize injection variance whereas gradients partially reverse the effects of column band spreading, reducing the column variance. Thus, the actions of TASF and gradients are independent of one another and can be used in conjunction to minimize observed peak broadening.[200]

2.3.2 Determination of Retention Factors at Extremes of Temperature and Mobile Phase Composition

In order to predict the effect of TASF, k_1, must be known accurately. As described above, TASF will employ temperatures of -7.5 ºC and 65 ºC. Determining k_1 for the more hydrophobic solutes at the former temperature and the more hydrophilic solutes at the latter temperature is challenging. While others have predicted retention factors at sub-ambient temperatures by extrapolation of linear van't Hoff plots[206], to our knowledge no prior studies have examined models for extrapolation of retention as a function of temperature *and* mobile phase composition. Thus, we sought a reliable method to extrapolate k_1 data obtained under more reasonable conditions to our extreme conditions.

Extrapolation requires a mathematical model for retention. Three models were considered, namely, LSST[214] (Eq. 8) and two equations from Neue and Kuss (Eq. 9, 10).[211]

Equation 8

$$\ln k = \ln k_0(T) - S(T)\phi$$

Equation 9

$$\ln k = \ln k_0(T) + 2\ln(1 + a(T)\,\phi) - \frac{S(T)\,\phi}{1 + a(T)\,\phi}$$

Equation 10

$$\ln k = \ln k_0 + \frac{D}{T} + 2\ln(1 + a\,\phi) - (1 + \frac{D}{T})\frac{S}{1 + a\,\phi}$$

Eqs. 8 and 9 are used at a given temperature, T (K), while Eq. 10 includes a temperature dependence. For each equation, k_0 or $k_0(T)$ is the retention factor in pure water and S and $S(T)$ describe the relationship between solute retention and ϕ. $S(T)$ and $k_0(T)$ are constants in Eqs. 8 and 9 for a given temperature, T, but vary with temperature. S *and* k_0 in Eq. 7 are constants.[211] In Equations 9 and 10, a and $a(T)$ account for curvature in the relationship between ln k and ϕ, D reflects temperature effects.

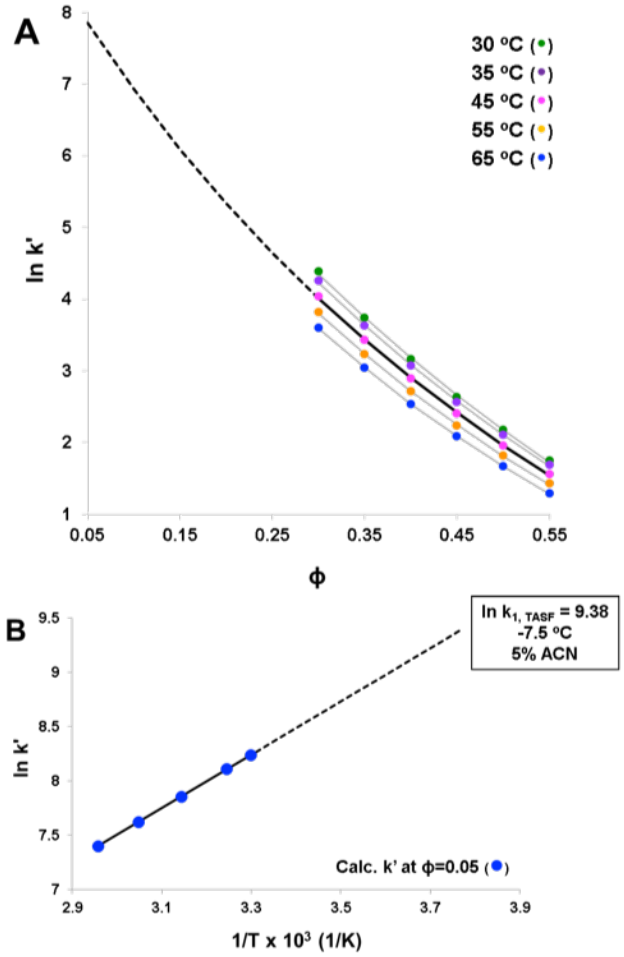

Figure 2 Illustration of k_1 determination process for hexanophenone. Figure 2A consists of experimental data obtained using the conditions described in the Experimental section. A single extrapolation based on Eq. 9 is shown. Figure 2B plots data found as shown in Figure 2A vs. 1/T and extrapolated to – 7.5 °C.

As Eqs. 8 and 9 have temperature-dependent constants, a two-step extrapolation was carried out. Figure 1 shows the basic idea. We first determined *k'* values for each solute at a minimum of five temperatures and four solvent compositions that led to a wide range of measureable values (~1 < k' < 35). These data form the basis for extrapolation [Table 1 (SI)]. As shown in Figure 2A, values of k' for a single temperature and a range of values of ϕ were used in a curve fitting procedure to determine the temperature-dependent constants in Eqs. 8 and 9. These values were used to

extrapolate to the lowest solvent strength, ϕ = 0.05. Figure 2A shows the fits of Eq. 9 for hexanophenone and the extrapolation for one temperature, the dashed line. This procedure was repeated for each temperature. The result is a set of (extrapolated) values for k' as a function of temperature at ϕ = 0.05. The second step is to plot these extrapolated values vs 1/T to determine the retention enthalpy at the lowest solvent strength, ϕ = 0.05, and further to extrapolate this van 't Hoff plot to the focusing temperature, -7.5 ºC (Figure 2B). For Equation 8, *ln* k_0 and *S* were determined at each temperature using linear regression. For Equation 9, the Solver function of Excel was used to determine the constants at each temperature by minimizing the sum of squared residuals between experimental and calculated values at each ϕ. Equation 10 was used differently. Solver was used to determine the constants for a single solute (e.g., all of the the points in Figure 1A) and *k'* was calculated by extrapolation to T = -7.5 °C. and ϕ = 0.05. The analogous procedures were used for some solutes to get k' for T = 65 °C. and ϕ = 0.05.

The accuracy of each model was determined using two methods. First, for those solutes for which experimental data *could* be obtained at ϕ = 0.05, the processes described above were carried out *without* using the data at ϕ = 0.05. van 't Hoff plots based on experimental k' values and the three sets of extrapolated values were compared [Figure 14 (SI)]. The model with the closest slope to the experimental data was considered to be most accurate. This turns out to be Eq. 9.

The second method was to compare the methylene group selectivity, α_{CH_2}, from extrapolated k' values to a known value. While literature on methylene selectivity at these particular conditions is not readily available, *ln* (α_{CH_2}) in pure water has been reported on four C18 phases at slightly different temperatures near room temperature.[215] Based on these data, at an average temperature of 26.8 ± 2.0 °C *ln* (α_{CH_2}) is 1.39 ± 0.01.[215] Fortuitously, under our experimental conditions (ϕ = 0.05 and -7.5 °C), the solvent strength is similar to water at room

temperature. This is because a decrease of 5 °C increases retention to about the same extent as a 1% increase in acetonitrile composition decreases retention.[216] Thus, the solvent strength in a water mobile phase near room temperature would remain about the same if we decreased the temperature from 26.8 °C to -7.5 °C and made the mobile phase composition 6.9% ACN (ΔT/ 5). This is similar to our sample composition at the lower temperature (5.0% ACN). Thus, we determined slopes of a plot of calculated ln k versus the number of methylene groups at ϕ = 0.05 and -7.5 °C for the straight-chain phenones [Figure 15 (SI)]. These slopes are α_{CH_2}. Its value was 1.33 when using Eq. 9 to calculate k' values. Values from the other two equations were very different [Figure 15 A, C (SI)]. Both of our validation methods point to the accuracy of Eq. 9 so retention data extrapolated using Eq. 9 were used for subsequent calculations.

2.3.3 Small Molecule Studies

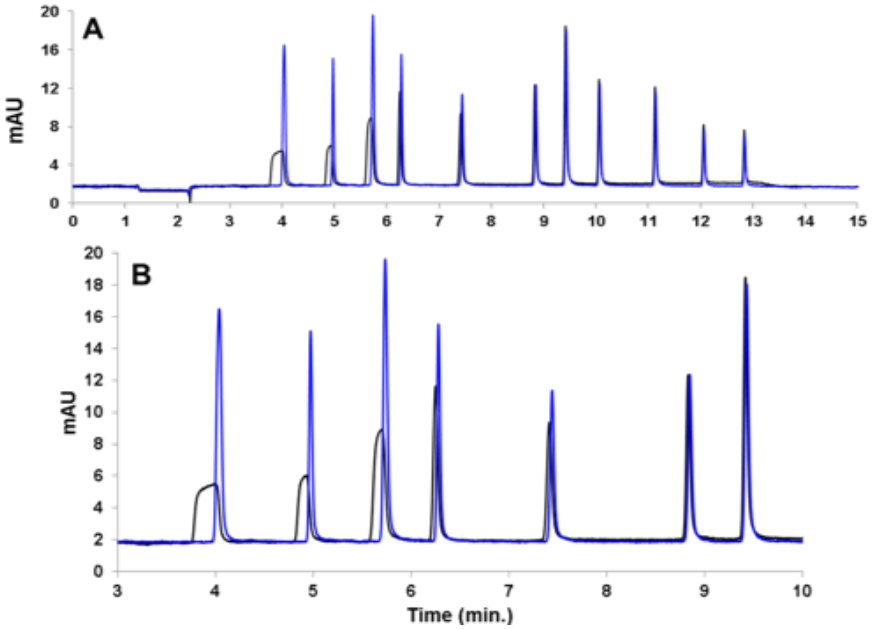

Figure 3 Chromatograms of 1000 nL injections of a small molecule mixture under isothermal (black line) and TASF (blue line) conditions with a gradient of 5-75% ACN over 12 minutes. Panel A illustrates all the solutes of the mixture whereas Panel B shows the early eluting peaks in more detail. The solutes in order of elution are: acetanilide, methylparaben, acetophenone, ethylparaben, propiophenone, butyrophenone, benzophenone, valerophenone, hexanophenone, heptanophenone, and octanophenone. Figures are representative of n = 3 replicates.

The utility of TASF for small molecules is illustrated in Figure 3, in which a chromatogram from a large-volume injection of a mixture of small molecules is dramatically improved compared to the isothermal separation (Figure 3A). This improvement is especially evident in Figure 3B, which shows the first seven peaks in greater detail. Volume overload is visually evident from the greater peak width of the first six peaks without TASF. This is consistent with what is expected based on Equation 6. The remainder of the separation is virtually identical to the isothermal results

as evident in Figure 3A. Figure 4 quantitatively illustrates the effectiveness of TASF for each peak in the chromatogram shown in Figure 2. For example, TASF decreases the full width at half-maximum, *FWHM*, of the acetanilide peak by a factor of 4.5 despite a low k' ($k_{1,isothermal}$ = 5.46, $k_{1,TASF}$ = 21.3) at the start of the gradient. Thus, TASF reduces volume overload but there is no degradation of peak shape for well-retained solutes. Decreased peak width for early eluting solutes provides more useable chromatographic space and thus higher peak capacities. By integrating the area under 1/*w* between the first and the last solute retention times[194] [Figure 16C (SI)], the peak capacity under TASF conditions was found to be 85 as compared to 70 for isothermal conditions. By improving peak width and resolution in the first 7.5 minutes of the separation, considerably more room is made for the detection of other polar compounds that may not be otherwise resolved.

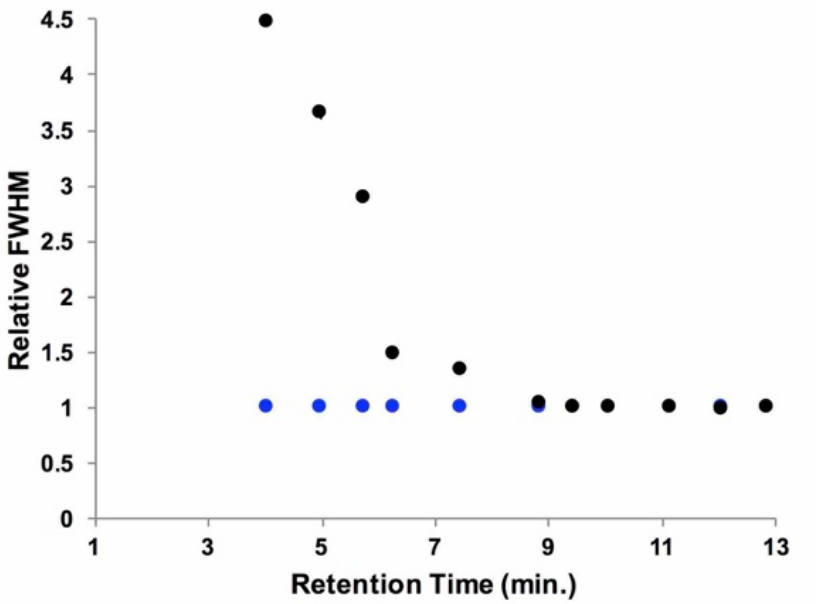

Figure 4 Relative FWHM (FWHM/ $FWHM_{TASF}$) for isothermal (black dots) and TASF (blue dots) separations based on the chromatograms depicted in Figure 3.

2.3.4 Injection Volume Studies

It is clear that TASF improves chromatography with large-volume injections but to determine the point at which TASF is *no longer essential* in gradient elution for a given injection volume, k_1, and $k_{eff,}$ a range of injection volumes and resulting half-widths were compared. Experimental results for first and third peaks of the mixture can be found in Figures 5A and 5B, respectively. Both acetanilide and acetophenone showed considerable improvement in peak width for a range of large volume injections. For acetophenone overloading effects were no longer apparent at injection volumes below 250 nL. At this point, the observed variance is dominated by column variance alone and minimal broadening due to injection is seen. However, with TASF, injection variance is almost completely eliminated, allowing observed widths of even 1000 nL injections to be at or less than peak widths of 50 nL injections (within 10%). A 10% loss of efficiency, as indicated by the red dashed line, is tolerable given the benefits of injecting large volumes. Using Equations 5 and 6, these results are modeled reasonably well (Figures 5C, D), illustrating the ability to predict the usefulness of TASF under particular conditions.

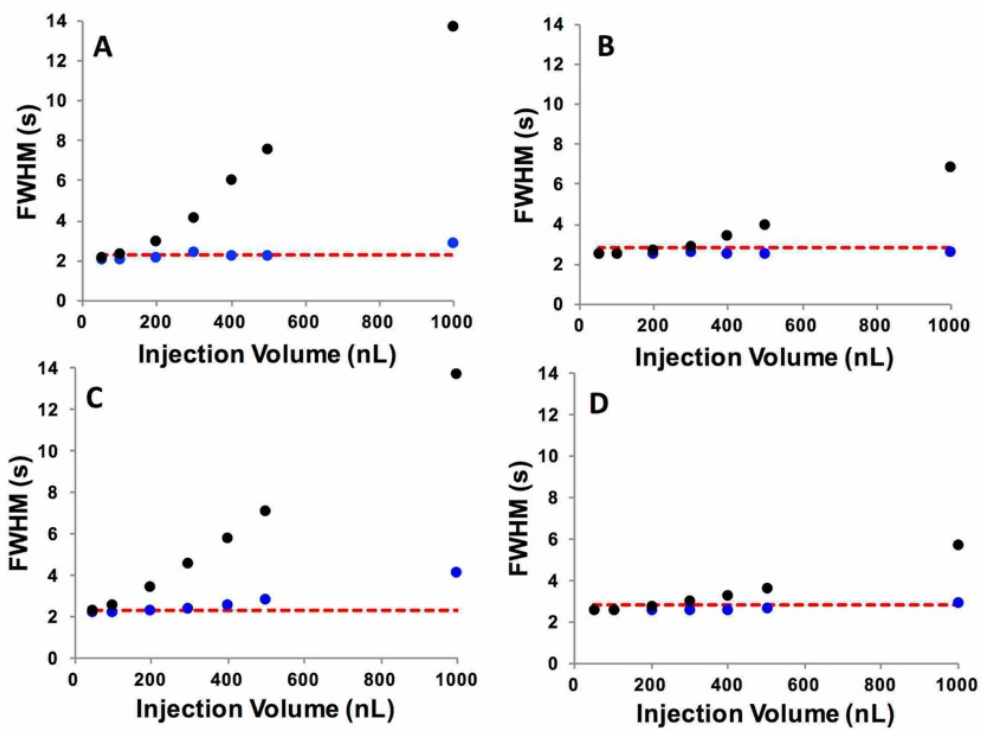

Figure 5 Experimental and predicted peak widths under isothermal (black dots) and TASF (blue dots) conditions for injection volumes ranging from 50-1000 nL. Panels A and B are the experimental values for acetanilide and acetophenone, respectively and Panels C and D are the calculated values for acetanilide and acetophenone, respectively found using Equations 6 and 7 and based on experimental conditions. The red dashed line indicates 10% greater peak width than that measured at the 50 nL injection volume. Calculations are based on n = 3 replicates at each condition.

2.3.5 Gradient Slope Studies

Gradient compression, *G(p)*, narrows solute zones due to increasing solvent strength, resulting in decreased peak widths.[187, 214] The gradient compression effect is dependent on the slope of the gradient, *b*, which can be calculated using the LSST parameter, *S*, the difference between the initial and final mobile phase composition, $\Delta\phi$, and the duration of the gradient, t_g.[214]

Equation 11

$$G(p) = \frac{\left\lfloor 1 + p + \frac{p^2}{3} \right\rfloor^{0.5}}{1 + p}$$

Equation 12

$$p = \frac{k_1 b}{(1 + k_1)}$$

Equation 13

$$b = \frac{S \Delta\phi t_0}{t_g}$$

It is of interest to determine the effects of TASF with changing gradient slope. This was examined by varying the t_g and final ϕ, resulting in gradient slopes of 0.2 (t_g = 24 min., ϕ_f = 0.7), 0.5 (t_g = 12 min., ϕ_f = 0.75), and 1.1 (t_g = 6 min., ϕ_f = 0.9). It is clear in Figure 6 that TASF focuses more polar solutes beyond gradient compression in each scenario. Furthermore, this effect is greatest for the shallowest gradient slope, as seen in Figure 7. Based on Equation 9, steep gradient slopes and small k_1 values result in highest solvent-based gradient compression.[214] Therefore, TASF has the greatest impact when used with a shallow gradient, which is pertinent to the separation of complex mixtures since these mixtures are commonly analyzed using long, shallow gradients.[217] This is consistent with peptide studies using end-of-the-column focusing, wherein solute trapping time was highest for long gradients.[206] While the greatest advantage of TASF is realized with the shallowest gradient, there is still considerable decrease in peak width for polar solutes with the steepest gradient. This demonstrates the ability of TASF to focus beyond what can be achieved with gradient compression alone due to the complimentary nature of these focusing techniques.

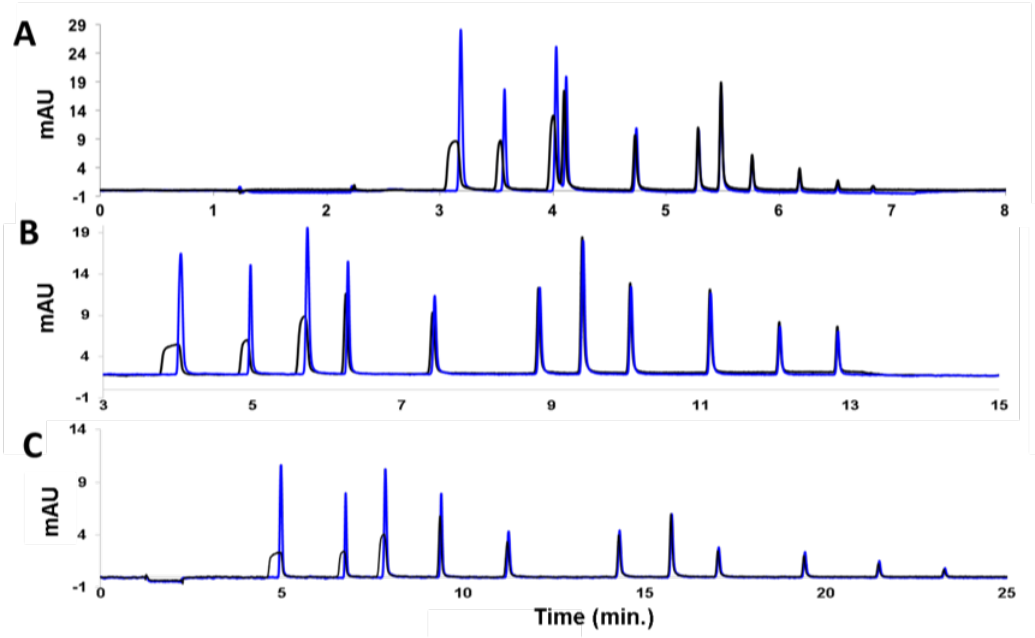

Figure 6 Chromatograms of a 1000 nL injection of the small molecule mixture under isothermal (black line) and TASF (blue line) conditions with varying gradient steepness. A: 5-90% ACN over 6 minutes (14.2% ACN/ min.). B: 5-75% ACN over 12 minutes (5.8% ACN/ min.). C: 5-70% over 24 minutes (2.7% ACN/ min.). Chromatograms are representative of n = 3 replicates.

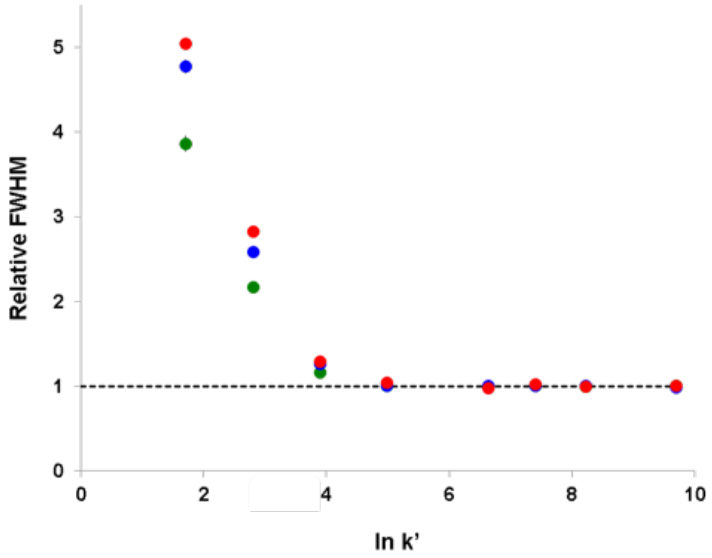

Figure 7 Comparison of relative peak widths ($FWHM_{iso}$ / $FWHM_{TASF}$) at varying gradient steepness depicted in Figure 5. The green dots indicate the 14.2% ACN/ min. gradient, blue dots indicate the 5.8% ACN/ min. gradient, and red dots indicate the 2.7% ACN/ min. gradient. The black dashed line indicates $FWHM_{TASF}$/ $FWHM_{TASF}$.

2.3.6 Predictability

Rearrangement of Equations 2 and 3 models the influence of TASF with gradient elution, which can be used to predict experimental results and determine the critical values that characterize the usefulness of this technique.

Equation 14

$$k_1 = \frac{1}{\sqrt{\gamma^2 - 1}} \left[\frac{V_{inj}}{\sqrt{12}\,\pi\, r_c^2 \varepsilon_{Tot}}\right] \left[\frac{(1 + k_e)}{u_{av}\,\sigma_{col,t}}\right] - 1$$

Equation 15

$$k_1 = \frac{1}{\sqrt{\gamma^2 - 1}} \left[\frac{V_{inj}}{V_{col}\,\sigma_{col,l}}\right] - 1$$

Replacing the denominator of the first bracketed term with its physical definition of the column volume, V_{col}, and substitution of the second bracketed term with the inverse of the column broadening term in length units, $\sigma_{col,l}$, leads to Eq. 15. The square of the ratio of the column length, L, and the latter quantity is the number of theoretical plates, N. This leads to Equation 16 where we indicate that N is an "observed" quantity, in this case including gradient compression.

Equation 16

$$k_1 = \frac{1}{\sqrt{\gamma^2 - 1}} \frac{V_{inj} N_{obs}^{1/2}}{V_{col} \sqrt{12}} - 1$$

γ represents a tolerance term, indicating the acceptable increase in peak width one is willing to tolerate in making large-volume injections. Although the definition of N in terms of a peak width in units of time in gradient elution differs from that in isocratic elution,[214] in units of length on column, they are the same. Equation 16 can be used easily to estimate the potential effectiveness of TASF for a particular separation. Using Equation 16 it was determined that the minimum k_1 required to achieve an observed variance equal to 1.1 times the column variance (γ = 1.1) with a 1000 nL injection is 170. This is consistent with the experimental results seen in Figure 3. For reference, the predicted k_1 under TASF conditions for acetanilide is 21.3, acetophenone is 59.8, and propiophenone is 410. Those solutes with $k_1 < 170$ show dramatic improvement in peak width with TASF while the peaks with $k_1 > 170$ had widths that are relatively close under TASF and isothermal conditions.

Eq. 16 can be rearranged to show the largest injection volume that can be used under given conditions, Eq. 17.

Equation 17

$$\frac{V_{inj}}{V_{col}} = \frac{(k_1+1)\sqrt{12(\gamma^2 - 1)}}{\sqrt{N_{obs}}}$$

Here it can be clearly seen that the effect of gradient compression as expressed in N_{obs} is to increase the allowable volume injected. Using Equations 7 and 17, the combined effects of gradient elution and TASF can be reasonably estimated, allowing prediction of TASF utility for a particular solute prior to experimentation.

2.3.7 Peptide Mixture Studies

In general the effect of changing ϕ on retention is more dramatic for larger molecular weight solutes such as peptides, resulting in greater gradient compression.[187] We have shown that TASF is able to focus large injections of small molecules beyond gradient compression alone so it seems reasonable that biological samples could also benefit from this effect. Indeed, Eghbali et al. focused targeted proteins at the end of the column by lowering the temperature of the end of the column during select portions of a gradient elution run.[206] Figure 8A shows chromatograms of a BSA tryptic digest from injections of over 290% of the column volume, 2 µL. Focusing time was increased to 125 s to accommodate the additional injection time. With TASF, peak shapes for early eluting solutes are significantly improved as is resolution, particularly up to the 6-minute mark. Most noticeable are the four additional peaks detected between 3.5 and 4.5 minutes. We can infer the effect of TASF by considering the total peak area over time, shown in Figure 7. From 6 min to the end of the chromatogram, the areas of the two chromatograms are virtually identical. This is consistent with TASF having little influence over solute behavior for those solutes that would have

focused effectively without TASF. In the earliest part of the chromatogram following the injection transient, the areas of the two chromatograms have different trajectories. The isothermal trace increases rapidly near 3.5 min as poorly retained solutes elute. This shows that while early eluting solutes are detected, they are not resolved. Conversely, with TASF, there is a slow, stepwise increase in area corresponding to the well-resolved peaks in the 4-6 minute region. This highlights the ability to resolve early eluting solute peaks using TASF that were otherwise.

The appearance of the additional *unknown* early eluting peaks and improvement in peak shape for multiple solutes highlights the benefit of placing the focusing segment at the column inlet. In this configuration the approach is general, applicable to all solutes in the mixture with negative retention enthalpies not just beneficial for a few specific solutes in select regions of the chromatogram. This feature has obvious implications for the determination of multiple solutes in complex mixtures where elution times for target analytes may not accommodate multiple focusing, release and thermal re-equilibrations of the focusing segment.

In the example just described, the sample was prepared in 5% acetonitrile to facilitate dissolution of the peptides but this limits solvent focusing. Biological samples are often prepared in pure aqueous solvents, which improves solvent focusing but may exclude less soluble peptides from detection. TASF could therefore be useful when the sample must contain some organic solvent by providing additional focusing without sacrificing solubility.

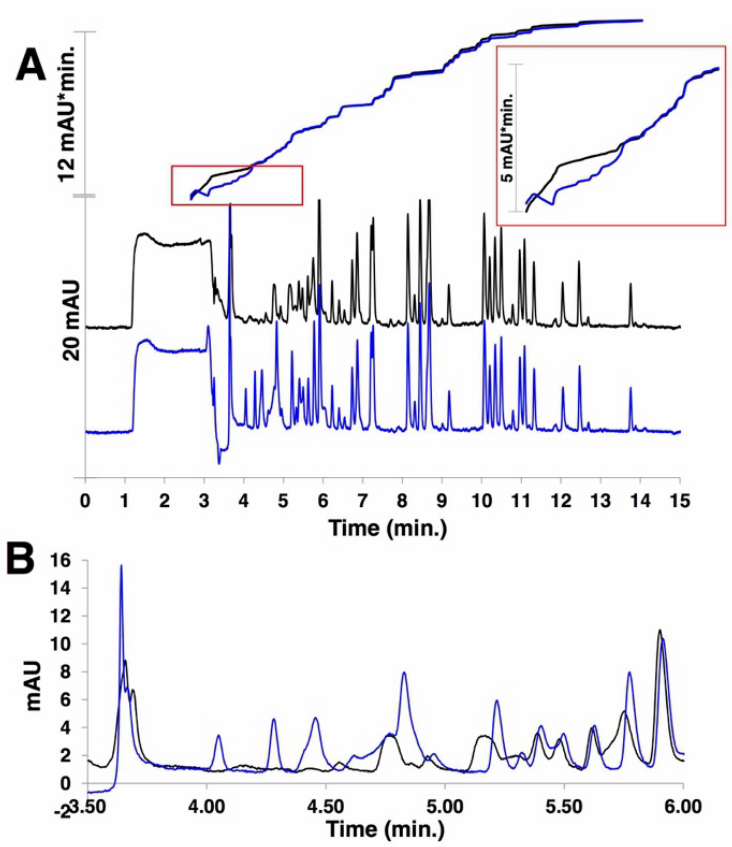

Figure 8 Separation of a 2 µL injection of BSA tryptic digest under isothermal (black line) and TASF (blue line) conditions. Panel A has four traces. The bottom two are the chromatograms and the top two are integrations of the chromatograms. The inset shows an enlargement of the peak area trace from the start of integration (2.5 min.) to 6 min. Panel B is an enlargement of the first 6 minutes of the chromatogram, illustrating the increased sensitivity and resolution of poorly retained solutes. A gradient of 5-40% ACN over 15 minutes was used for these experiments. Chromatograms are representative of n = 2 replicates.

2.4 Conclusions

These results clearly illustrate the effectiveness of TASF for increasing sensitivity for volume-overloaded solutes beyond what can be achieved with solvent gradient elution alone. This is not only applicable for complex mixtures of small molecules, but also for biological samples.

Additionally, this completely instrumental technique offers an automated method to improved sensitivity, peak capacity, and resolution over a range of injection volumes and gradient conditions. Furthermore, using our double extrapolation method for predicting retention factors at extremes of temperature and mobile phase composition, can be modeled successfully using simple equations, allowing prediction of the utility of TASF for a particular application.

It should be noted that in theory, TASF is capable of focusing even more polar compounds than those used here. Stationary and mobile phase conditions can be tailored to a particular sample mixture. As long as the solutes of interest have negative enthalpies under those conditions, increased separation performance with TASF is a possibility. As this is often the case for stationary phases such as HILIC,[218-221] mixed mode,[222] and carbon phases,[223-229] it is clear that the benefits of TASF can be widely applied to a range of applications beyond conventional reversed phase.

2.5 Supporting Information for Gradient Elution Temperature-Assisted On-column Solute Focusing

2.5.1 Flow Rate Calibration

To verify the flow of solvent delivered by the system, varying injection volumes of 1 mM uracil were delivered into a 55 cm x 25 µm ID open capillary spanning the injection valve and the UV detector flow cell. The mobile phase was 50:50 0.1% TFA ACN/ 0.1% TFA H_2O and the flow rate was set to 1.00 µL/min. Uracil absorbance was measured at 254 nm. Timed injections were used to deliver injection volumes of 0.05, 0.1, 0.2, 0.4, 0.6, and 0.8 µL in random order. Each sample was repeated at least three times. Under these conditions, all peaks had flat tops so the half-

width, $w_{1/2}$, of the peak should be equivalent to the width in time units of the injection, t_{inj}, as seen in Equation 18.

Equation 18

$$t_{inj} = w_{1/2} = \frac{1}{F} V_{inj}$$

Thus, a plot of width vs. injection time should yield a line with a slope of one, as seen in Figure 9. The equation of this plot was y=0.9989 (±0.0012)x + 0.00252 (±0.00054) with 95% confidence. This resulted in a calculated flow rate of 1.001 ±0.002 µL/min, which is tolerable in the scope of this work.

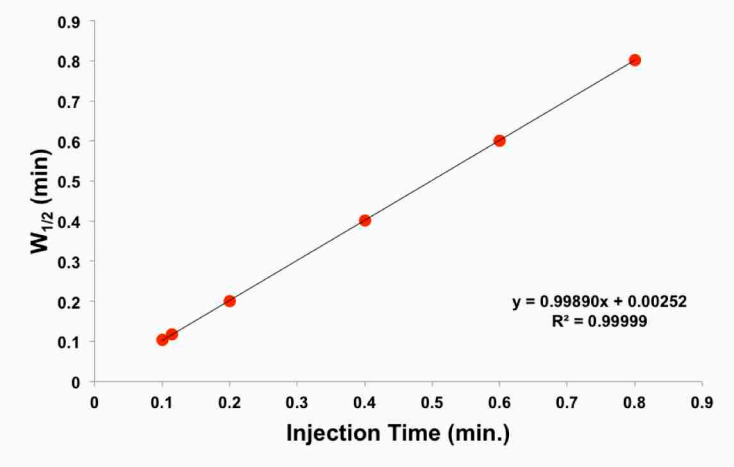

Figure 9 Peak half-widths for varying injection volumes into an open tube for the flow rate validation. Each point represents n = 3 replicates.

2.5.2 Dwell Time Determination

The dwell time of the system was measured using a method described elsewhere.[230] The mobile phase consisted of pure water in channel A and 0.1% acetone in water in channel B. The

injection valve was connected to the flow cell by the same 55 cm x 25 µm ID open capillary used throughout the work reported here. A gradient of 10-90% B was delivered over ten minutes using flow rates of 1.00 µL/min and 1.20 µL/min. Runs were repeated at each flow rate in triplicate. One such chromatogram can be found in Figure 10.

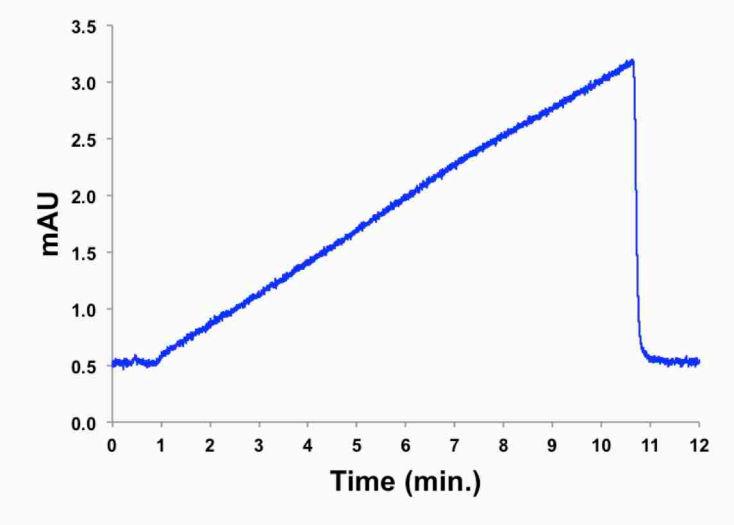

Figure 10 Chromatogram of 10-90% 0.1% acetone/ H_2O gradient over 10 minutes for the determination of the dwell volume. Chromatogram is representative of n = 3 replicates.

To determine the dwell time, a baseline was drawn at the beginning and end of the gradient and the time at which the detector response is at the half point of the gradient, $t_{1/2}$, was determined. The dwell time, t_d, was then calculated using Equation 19 where t_g is the gradient time. This was calculated to be 0.907 ±0.025 minutes.

Equation 19

$$t_d = t_{1/2} - \frac{1}{2} t_g$$

2.5.3 TASF Hardware

The TEC temperature was controlled via a feedback loop in which the voltage at the desired temperature was 'stored' allowing set temperatures to be achieved quickly and reproducibly following several training runs prior to the start of the experiments. The feedback loop operated by slowly increasing or decreasing the current depending on the overall difference between the actual temperature and desired temperature. For example, following a cooling cycle, the voltage was raised rapidly to 95% of the maximum voltage then the increment by which the voltage was raised further slowed until the desired temperature was reached. This is demonstrated in the temperature trace shown in Figure 11A. This trace was reproducible for all experiments and once the desired temperature was reached, temperatures did not fluctuate more than ±0.1 °C from the set point (Figure 12).

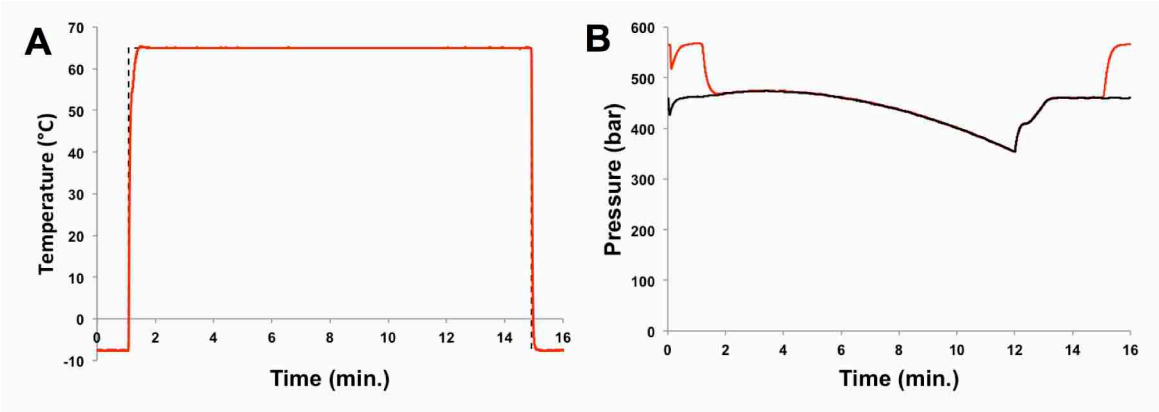

Figure 11 Panel A is the TEC temperature profile of the small molecule mixture separation (Fig. 3). Panel B is the corresponding pressure trace under isothermal (black line) and TASF (red line) conditions.

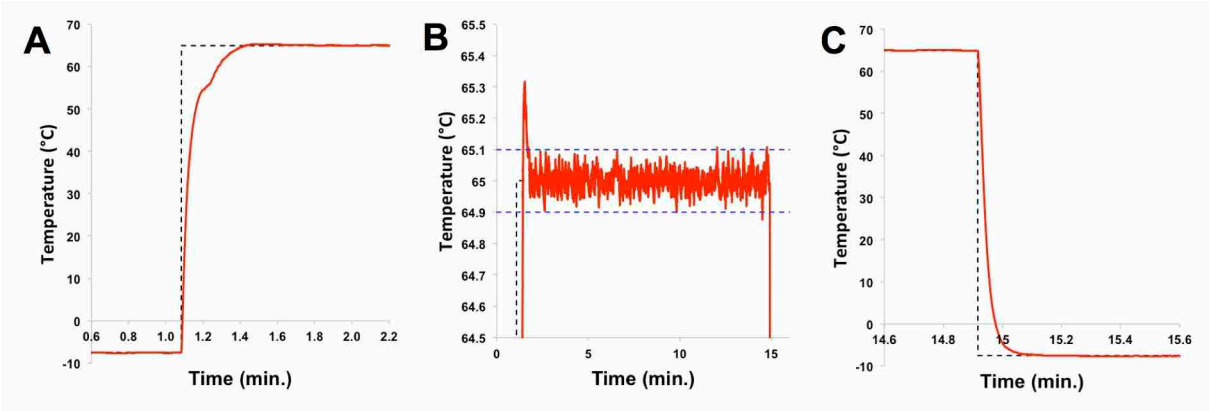

Figure 12 Demonstration of the programmed control of the TEC. Panel A shows the TEC transition from focusing to separation. Panel B shows the temperature trace during the separation phase. Panel C shows cooling of the TEC from the separation to the focusing temperature.

As expected, changing temperatures are also reflected in changing pressures due to the change in viscosity of the mobile phase. Figure 11B demonstrates the pressure cost of TASF (red line) over isothermal separation of the small molecule mixture (black line). It is seen for both traces that valve actuation causes a pressure drop during injection and then pressure decreases accordingly with the increase of organic modifier in the mobile phase. Pressure then increases again during mobile phase re-equilibration. This is consistent with what has been described previously.[231] The focusing temperature used resulted in approximately 100 bar greater pressures during injection and is well within the capabilities of most HPLC pumps and a reasonable compromise for improved peak shapes and separation efficiencies. The pressure increase at the end of the run corresponds to cooling the TEC prior to the start of the next run. These pressure traces were consistent over all runs and sample types (Figure 13).

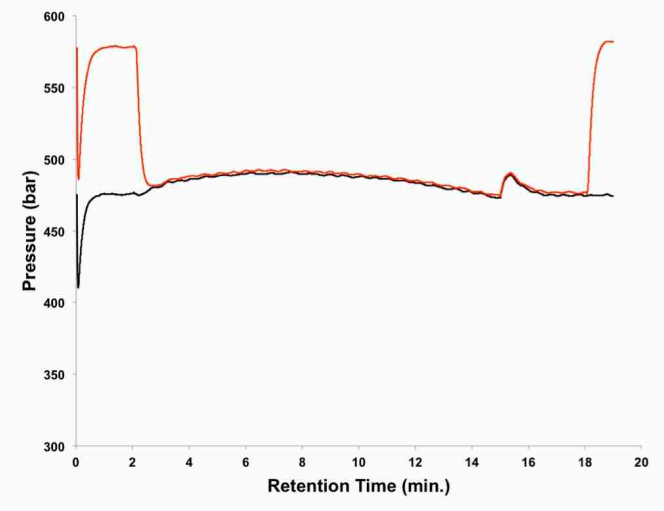

Figure 13 The pressure trace of the separation of the BSA tryptic digest (Figure 8) under isothermal (black line) and TASF (red line) conditions.

2.5.4 Determination of Retention Factors

Table 1 Mobile Phase Compositions[a]

[a] Retention times were measured on a 100 µm ID x 5.5 cm. column packed as described in the experimental section with a flow rate of 1 µL/ min. Parabens and phenones were analyzed separately to avoid cross-over.

	% ACN										
Solute	**5**	**10**	**15**	**20**	**25**	**30**	**35**	**40**	**45**	**50**	**55**
Acetanilide	X	X	X	X							
Methylparaben	X	X	X	X	X						
Ethylparaben		X	X	X	X	X					
Acetophenone	X	X	X	X	X						
Propylphenone	X	X	X	X	X						
Butylphenone			X	X	X	X	X				
Benzophenone					X	X	X	X	X		
Valerophenone						X	X	X	X	X	
Hexanophenone						X	X	X	X	X	X
Heptanophenone								X	X	X	X
Octanophenone								X	X	X	X

Table 2 Calculated Retention Factors at ϕ=0.05[b]

[b]Retention factors were calculated based on the experimental data from Table 1 and Equation 9.

	k'	
Solute	**-7.5 °C**	**65 °C**
Acetanilide	21.3	5.46
Methylparaben	107	13.5
Acetophenone	59.8	16.4
Ethylparaben	410	42.4
Propiophenone	210	49.3
Butylphenone	851	147
Benzophenone	2251	565
Valerophenone	3134	761
Hexanophenone	11800	1640
Heptanophenone	44600	3710
Octanophenone	168000	16200

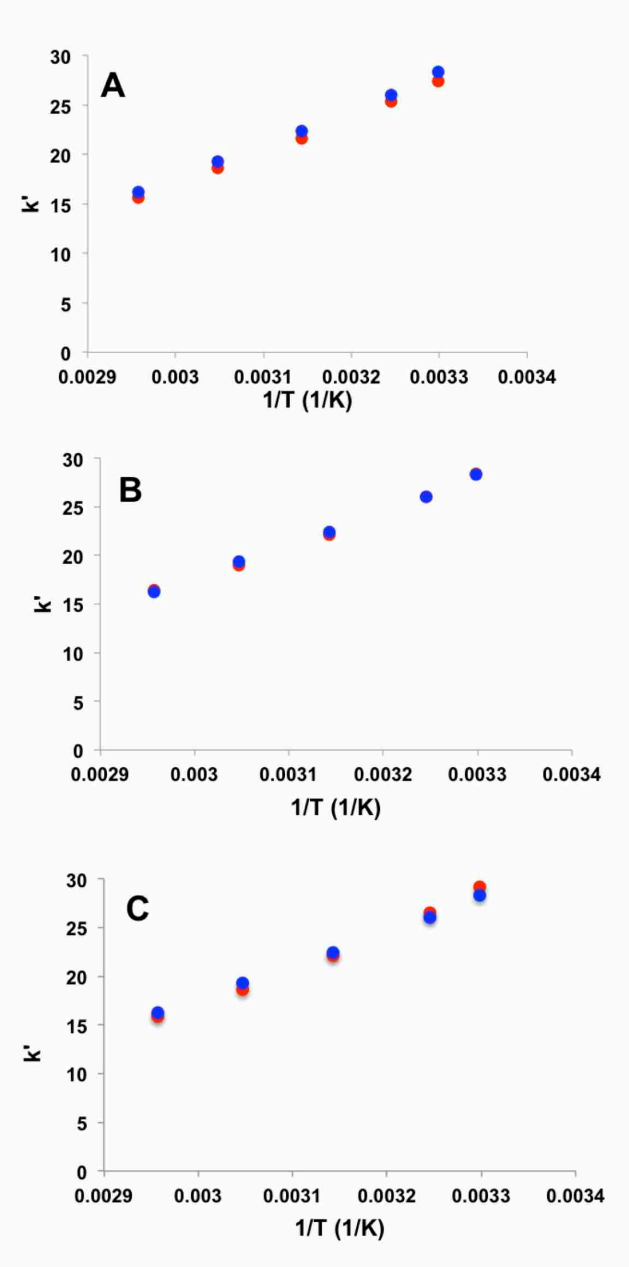

Figure 14 Comparison of van't Hoff plots using extrapolated retention factors (red dots) and experimental data (blue dots) for acetophenone at 30 °C and Φ = 0.05. The extrapolated retention factors were calculated using Equation 8 for Panel A, Equation 9 for Panel B, and Equation 10 for Panel C.

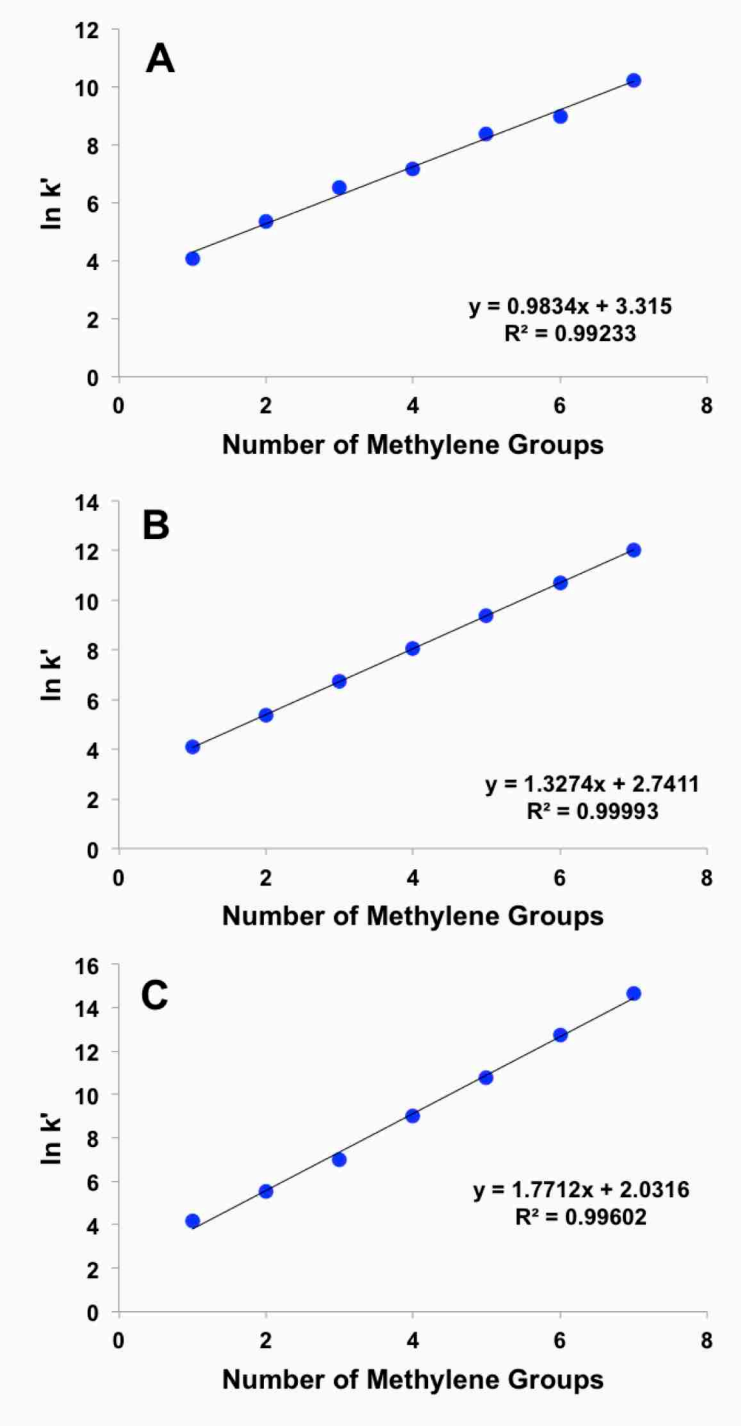

Figure 15 Determination of ln (α_{CH2}) using extrapolated retention factors at -7.5°C and Φ = 0.05. The values in Panel A were calculated using Equation 8, Equation 9 was used for Panel B, and Equation 10 was used for Panel C.

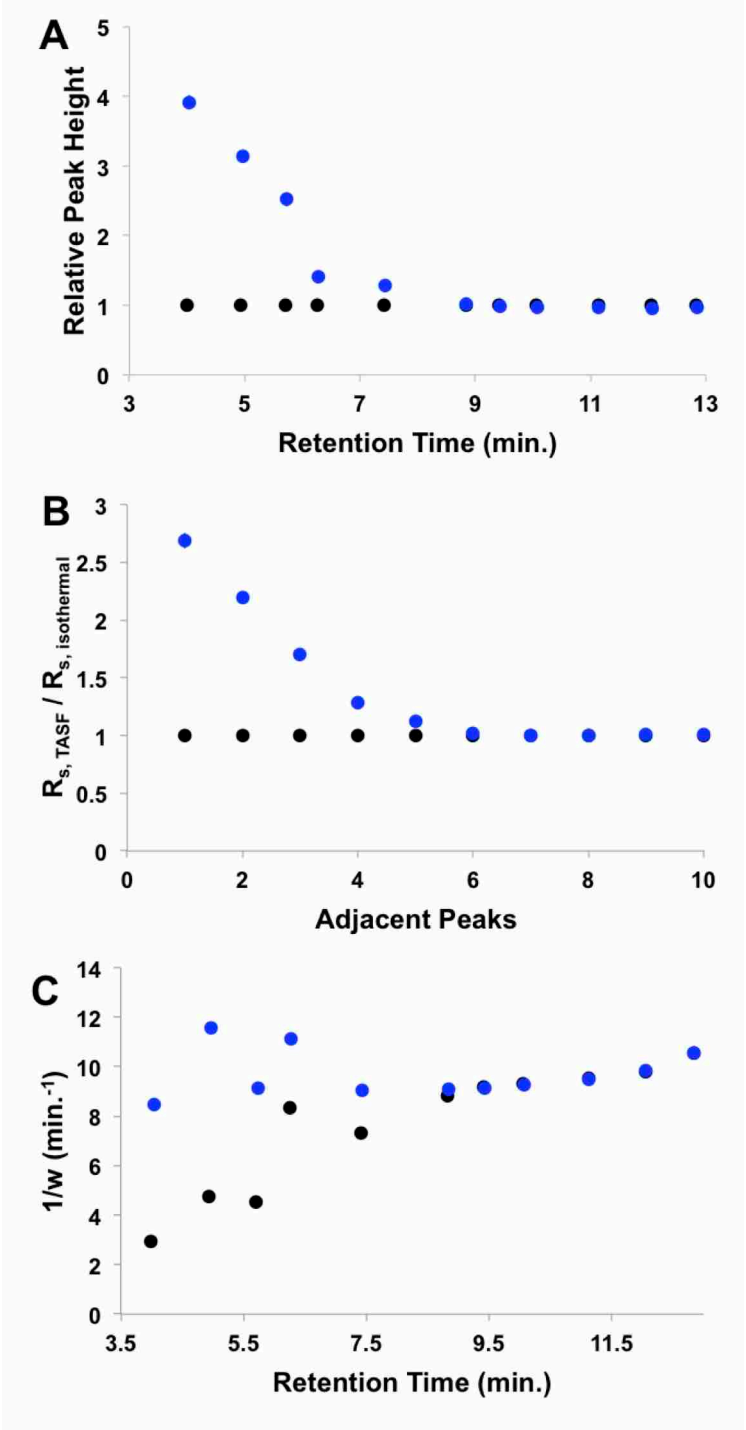

Figure 16 Comparison of peak height (Panel A), resolution (Panel B), and peak capacity (Panel C) of isothermal (black dots) and TASF (blue dots) separations of the small molecule mixture depicted in Figure 3.

3.0 On-column Dimethylation with Capillary Liquid Chromatography-Tandem Mass Spectrometry for Online Determination of Neuropeptides in Rat Brain Microdialysate

We have developed a method for online collection and quantitation of neuropeptides in rat brain microdialysates using on-column dimethylation with capillary liquid chromatography - tandem mass spectrometry (cLC – MS^2). This method addresses a number of the challenges of quantifying neuropeptides with cLC - MS. It is also a completely automated and robust method for the preparation of stable isotope labeled - peptide internal standards to correct for matrix effects and thus ensure accurate quantitation. Originally developed for tissue-derived proteomics samples (Raijmakers, et al., 2008), the efficacy of on-column dimethylation for native peptides in microdialysate has not been demonstrated until now. We have modified the process to make it more amenable to the time scale of microdialysis sampling and to reduce the accumulation of non-volatile contaminants on the column and thus, loss of sensitivity. By decreasing labeling time, we have a temporal resolution of one hour from sample loading to elution and our peptide detection limits are in the low pM range for 5 µL injections of microdialysate. We have demonstrated the effectiveness of this method by quantifying basal and potassium stimulated concentrations of the neuropeptides leu-enkephalin and met-enkephalin in the rat hippocampus. To our knowledge, this is the first report of quantitation of these peptides in the hippocampus using MS.

3.1 Introduction

Neuropeptides are heavily involved in cell signaling in the brain, with roles in neurotransmitter modulation[232-234], reward behaviors[6], and cognition[8, 235]. Unsurprisingly, they are implicated in a number of central nervous system disorders including addiction[7, 236] and depression[10]. Despite their importance, the details of the distance- and time- scales over which they function are largely unknown.[5] *In vivo* investigations of extracellular peptides, typically by microdialysis,[13, 70] are challenging due to the neuropeptides' low extracellular concentrations (pM[96, 237-241]) and the potential for loss of peptides due to sample handling[96], enzymatic hydrolysis,[80, 242] and adsorption[81, 243].

Ideally, online measurements of peptides in microdialysate by capillary liquid chromatography-mass spectrometry (cLC-MS) should be well-suited for the analysis of extracellular processes involving peptides. Online measurements reduce sample handling and cLC-MS is suited to the small volumes and low concentrations expected[96, 239] of peptides in dialysate[244]. As far as we are aware, only Haskins, et al. have used *in vivo* microdialysis with online LC-MS for the analysis of neuropeptides.[95-96] While one of these works focused on the discovery of novel peptides[95], the other involved the quantification of basal and potassium stimulated levels of the neuropeptides met-enkephalin (ME, YGGFM) and leu-enkephalin (LE, YGGFL) in the anesthetized rat globus pallidus.[96] The authors reported higher peptide levels compared to offline studies, which they hypothesized could be due in part to the effectiveness of the online process to minimize sample loss.[96] Thus, online collection and analysis is preferable to offline methods. However, the authors injected dialysate directly on the analytical column, which resulted in rapid column degradation and necessitated daily replacement. In addition, isotopically labeled standards were not included for quantitation. This is essential[80] because ionization efficiencies depend on

the analyte as well as the ionic and solvent composition of the medium. Thus, quantitation cannot be based on detector response alone.[70] While some stable isotope-labeled peptide internal standards are available, it would be expensive and impractical to use them in multi-peptide analyses. An online labeling scheme is preferred.

*Off*line amine labeling has been used in measurements of polar, low-molecular weight neurotransmitters in microdialysate.[244] The benzoyl chloride work of the Kennedy group[245] used $^{12}C_6$-benzoyl, to label analytes in dialysate *off*line while internal standards were labeled with a "heavy" $^{13}C_6$-benzoyl group. This method improved quantitative analysis of microdialysate for 70 small molecule neurotransmitters and metabolites, including dipeptides.[246] An *off*line but *on-column* approach used for quantitative proteomics is the dimethylation of primary amines using formaldehyde and cyanoborohydride.[247] Raijmakers, et al. have shown this to be an effective method for protein quantification in tissue-based samples, with higher efficiency and comparable sensitivity as in-solution methods.[247-248] We theorized that the on-column method could be adapted to the online collection of microdialysate. The potential advantages of this approach are that stable isotope labeled – internal standards (SIL-ISs) for multiple analytes can be generated simultaneously and the labeling reaction rates are compatible with online analysis. Until now, the efficacy of this method has not been demonstrated with native peptides, or with microdialysate[244], or with online *in vivo* sampling.

We made a number of modifications to convert the Raijmakers method from tissue-based samples to the online analysis of microdialysate. Here, we demonstrate the effectiveness of this method by measuring basal and potassium-stimulated levels of LE and ME in the rat hippocampus. These endogenous opioids are involved in learning and memory formation in the hippocampus.[8]

Our method is able to achieve peptide detection limits in the low pM range for 5 μL injections and has a temporal resolution of one hour. While certainly this needs to be decreased, it is faster than the previous on-column dimethylation work with tissue-based samples[248] and comparable to the online microdialysis work of Haskins, et al.[96] This method also improves the robustness of online collection, significantly increasing the number of samples that can be analyzed without human intervention. To our knowledge, this is the first report of online collection, labeling, and analysis of neuropeptides in *in vivo* microdialysis samples and the first report of enkephalin quantitation in the hippocampal extracellular space using cLC - MS.

3.2 Experimental

3.2.1 Peptide Standards

Stock solutions of LE (American Peptide, Sunnyvale, CA), ME (Sigma-Aldrich, St. Louis, MO), and yaGfl (GL Biochem, Shanghai, China) standards were prepared by dissolving the solid as received from the manufacturer in water, which was obtained from a Millipore Milli-Q Synthesis A10 purification system (Billerca, MA), to a concentration of 1 mM. Serial dilutions were then used to prepare 5 nM standards of each peptide. LE, ME, yaGfl standard mixtures were then further diluted to the desired concentrated (usually 100 pM) in either water or a modified Ringer's solution consisting of 148 mM NaCl (EMD-Millipore, Darmstadt, Germany), 1.2 mM $CaCl_2$ (EMD-Millipore), 2.7 mM KCl (Sigma-Aldrich), and 0.85 mM $MgCl_2$ (Fisher Scientific, Fair Lawn, NJ) at pH 7.4. All standards were made fresh daily.

3.2.2 Labeling Reagents

The labeling reagents were prepared in the following way. Triethylammonium acetate (TEAA) buffer was prepared by adding 100 mM acetic acid (Fisher Chemical) to 100 mM triethylamine (Sigma) to achieve a pH of 7.40. A volume of 350 µL of the TEAA buffer was placed into an autosampler vial (Thermo Scientific, Rockwood, TN) followed by 3.50 µL of 0.6 M sodium cyanoborohydride (Sigma) and 3.50 µL of 4% formaldehyde (J.T. Baker, Phillipsburg, NJ). Due to the toxicity of formaldehyde vapors, the labeling reagent components should be prepared in a fume hood. The mixture was then vortexed and placed in the refrigerated autosampler at 5 °C. The heavy labeling reagent was prepared using the same procedure but with formaldehyde-d_2 (Sigma). TEAA, cyanoborohydride, and formaldehyde solutions were made fresh daily.

3.2.3 HPLC Setup and Conditions

A Dionex Ultimate 3000 HPLC system (NCS-3500RS, Thermo Scientific, Germering, Germany) was used for cLC. The system consisted of an online degasser, a low-flow loading pump, a nanoflow analytical pump, an integrated column oven housing two 10-port Cheminert high-pressure 1/16” valves (VICI, Valco, Houston, TX), and a WPS-3000 RS autosampler. For the analytical pump, channel A contained 0.5% acetic acid in DI water and channel B contained 0.5% acetic acid in Optima-grade methanol (MeOH, Fisher Scientific). The loading pump mobile phase consisted of 0.5% acetic acid in a 98:2 water: methanol mixture. Peptide standards and labeling reagents were housed in the temperature-controlled autosampler at 5 °C.

Capillary columns of 50 µm ID were prepared in-house using polyimide coated fused silica (Polymicro, Phoenix, AZ) that was packed at 6000 psi using the downward slurry method as

described previously[152]. The packing material consisted of Acquity BEH 5 μm C18 stationary phase (Waters, Milford, MA) suspended in HPLC-grade isopropanol (Fisher Chemical). Methanol was the packing solvent. The outlet was fritted prior to packing by mixing a 25% formamide (Acros, NJ) solution with KASIL® 1 potassium silicate (Kasil, PQ Corporation, Valley Forge, PA), which was then used to moisten a glass microfiber filter (Whatman, UK).[249] The capillary was dipped onto the filter paper and placed in an oven at 300 °C for 12 hours. After packing, columns were trimmed to 4.5 cm and connected to a pulled silica tip using a PTFE sleeve. Pulled tips were also prepared in-house using a laser puller (P-2000, Sutter Instruments, Novatao, CA) and 25 μm ID capillaries, which were trimmed to a final tip ID of approximately 10 μm and length of 2 cm. The pre-column consisted of an Acclaim PepMap 100 C_{18} column (Thermo Scientific) packed with 3 μm particles and dimensions of 75 μm ID x 2 cm length.

Peptides were eluted at 0.3 μL/min using the following gradient: a step of 2-20% B (nominally in 0.1 minutes) then 20-40% B in 5 minutes with a hold at 40% B for 2 minutes. A ramp of 40-95% B over 1 minute was then used to remove any highly-retained analytes present in the dialysate. The mobile phase was returned to 2% B (nominally in 0.1 minutes) and re-equilibrated for 7 minutes. A 3-minute column wash with 95% B was then performed to prevent carryover. The total analysis time was one hour.

3.2.4 Mass Spectrometry

The cLC was coupled to a Thermo Scientific LTQ XL linear ion trap MS using nanospray in positive ion mode. A locally constructed stage housed a 6-port 1/16” VICI high-pressure Cheminert valve (Valco) connected to a liquid junction tee (Idex, Oak Harbor, WA) by a 25 μm

ID x 10 cm long fused silica capillary. Voltage was applied to the tee at the head of the column. The selected precursor ions used for MS^2 fragmentation and daughter ions used for generating extracted ion chromatograms (EIC) and determining peak area can be found in Table 7 (SI)

The precursor and daughter ions were chosen for each peptide based on information from direct infusions of 5 μM standards into the MS at 0.1 μL/min. Peaks were identified based on MS^2 fragmentation patterns and retention times of the standard peptides as well as comparisons to expected fragmentations based on sequence (prospector.ucsf.edu/prospector/cgi-bin/mssearch). The LC was operated using Chromeleon Xpress with DCMS link to Xcalibur for MS operation and chromatograms were analyzed using Xcalibur Qual Browser.

3.2.5 On-Column Labeling Procedure

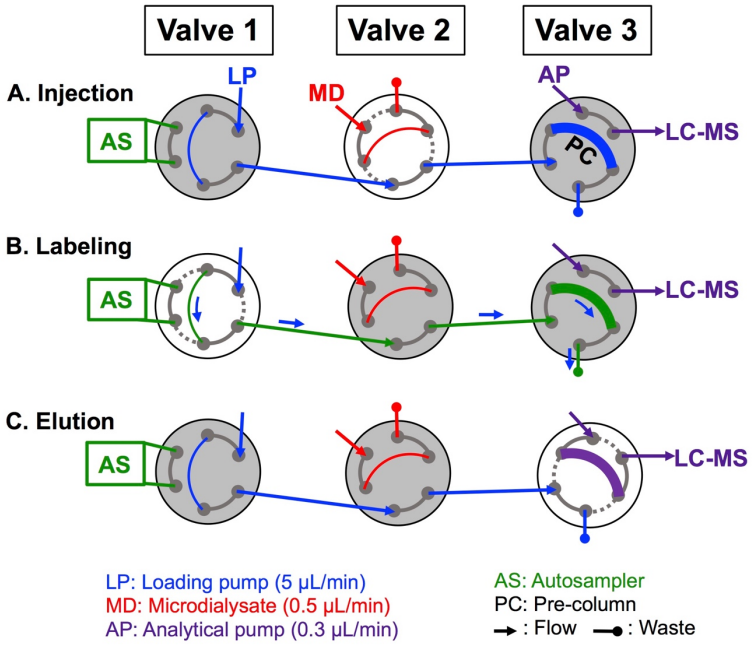

Figure 17 Schematic for two-column labeling setup. Valve 1 is housed on the autosampler, Valve 2 is housed in the LC column oven, and Valve 3 is an external valve housed on the MS stage. Valve 2 is a 10-port valve but is depicted with 6-ports for clarity. White indicates a valve that is switching. Labeling is performed in the following way: (A) A 5-µL sample loop on Valve 2 is filled with microdialysate (MD) and upon switching, the sample is directed onto the pre-column (PC) by the loading pump (LP); (B) A series of five autosampler (AS) injections delivers reagents from vials (In sequential order: light labeling reagent, formic acid, 100 pM peptide aqueous standards, heavy labeling reagent, and formic acid) onto the PC, which react with peptides that have adsorbed onto the PC; and (C) Valve 3 switches, directing flow from the analytical pump (AP) through the PC, eluting peptides off the PC and onto the analytical column-mass spectrometer (LC-MS) by gradient elution.

There are three stages in the online method (Fig. 17): pre-concentration of peptides in the sample (Fig. 17A), reaction of peptides adsorbed to the pre-column with light reagent followed by introduction of unlabeled peptide as internal standards and then reaction of peptides adsorbed to the pre-column with heavy reagent (Fig. 17B), and finally injection of the isotopically labeled

analytes and standards onto the analytical column. The total cycle time is one hour. In more detail, Fig. 17A shows perfusate from the probe continuously filling a 5 μL sample loop on Valve 2. Once per hour Valve 2 is switched allowing peptides to adsorb at the head of the pre-column. We have given this step four minutes at 5 μL/min to ensure complete emptying of the sample loop and sufficient de-salting. Valve 2 is reset to the "fill" position. The second stage has three steps (Fig. 1B) that use the autosampler. The autosampler has five vials as follows: vials 1 and 2 contain light labeling reagent and 5% formic acid, respectively. Vial 3 contains the sought-for peptides (100 pM) that will, when labeled, act as isotopically labeled internal standards. Vials 4 and 5 contain the heavy labeling reagent and 5% formic acid, respectively. The sequence represented in Fig. 17B is thus, first, labeling of the adsorbed analyte peptides with light reagent followed by quenching, injection of the sought-for peptides, then labeling them with heavy reagent following by quenching. Each of the five solutions was loaded into a 5 μL loop and then introduced to the pre-column at 5 μL/min for three minutes. The result is on-column reaction of adsorbed peptides with the injected reagents. The third stage is simpler (Fig. 17C). Valve 3 was switched so that the pre-column is in line with the analytical pump and the analytical column for separation.

3.2.6 One-column Approach versus Two-column Approach

Labeling was performed using a one-column setup and a two-column setup. In the one-column setup, pre-concentration and separation occurred on a single column. For the two-column setup, pre-concentration occurred on a pre-column while the separation occurred on a separate analytical column. Figure 17 illustrates the two-column setup. The valve configuration for the one-column setup was identical except the column was positioned between the loading pump and the

analytical pump on Valve 3, taking the place of the pre-column. The sequence of events was also the same for the one- and two-column approach, except that for the one-column approach, all samples and reagents were injected directly onto the analytical column, with the eluate going into the inlet of the MS rather than to waste.

3.2.7 Labeling Tests

For *in vitro* labeling tests, the Ringer's standard consisted of either 50, 100, or 200 pM mixtures of LE, ME, and yaGfl in Ringer's solution, which was injected via syringe pump in the exact manner used for an animal experiment. The aqueous standard consisted of either 50, 100, or 200 pM mixtures of LE, ME, and yaGfl in water, which were injected using the autosampler in the same way described for the animal experiments. The concentrations and labeling conditions were randomized and repeated for n = 3 replicates. Samples were randomized to prevent bias due to carryover effects at higher concentrations and to demonstrate that the method is reproducible when going from high to low concentrations and vice versa. Table 8 (SI) shows the ion transitions used.

3.2.8 Microdialysis and Surgery

All procedures involving animals were carried out with the approval of the Institutional Animal Care and Use Committee of the University of Pittsburgh. Male Sprague-Dawley rats (250–375g, Charles River, Wilminton, MA) were intubated and anesthetized with isoflurane (S-3 Baxter Healthcare, Deerfield, IL) at 0.5 % by volume and wrapped in a homoeothermic blanket (EKEG Electronics; Vancouver, BC, Canada), (n=4). Body temperature was maintained at 37.5 ^{o}C using a heating pad. The rats were placed in a stereotaxic frame (David Kopf Instruments; Tujunga, CA).

Microdialysis probes (216 μm o.d., 2 mm in length) were constructed with hollow fiber dialysis membrane (Spectra-Por RC Hollow Fiber; MWCO: 13,000 Da, 200 μm i.d., Spectrum Laboratories, Inc.; Rancho Dominguez, CA) and fused silica outlet lines (150 μm o.d., 75 μm i.d., Polymicro Technologies; Phoenix, AZ) as described elsewhere.[250] The scalp was shaved and the skull was exposed. A craniotomy was performed and the dura was carefully removed away to expose the brain. The incisor bar was adjusted so that the dorsal-ventral measurements at lambda and bregma were no more than 0.01 mm apart (flat skull). Microdialysis probes were lowered into the hippocampus to a final position of 5.6 mm anterior to bregma, 4.6 mm lateral from midline and 5.0 mm below dura[251] over a 30-minute period. The probes were perfused throughout all implants with Ringer's at 0.500 μL/min using a syringe pump (Harvard Apparatus, Holliston, MA). Potassium stimulation was conducted using a Ringer's solution containing 100 mM KCl. The concentration of NaCl was adjusted to maintain ionic strength. The high potassium Ringer's was administered via a VICI Valco 10-port valve housed in the LC column oven. After 10 minutes of high potassium stimulation the valve was switched to resume perfusion with the standard Ringer's solution. On completion of testing, the rats underwent intracardial perfusion and the brains were removed for verification of the probe location [Fig. 22 (SI)].

3.2.9 Microdialysis Probe Recovery

The microdialysis probe recovery was tested *in vitro* by placing a probe in a solution of 100 pM LE and ME in Ringer's after removal of the probe from the rat brain. 100 pM yaGfl in Ringer's was perfused through the probe at 0.5 μL/ min and the outlet of the probe was connected directly to the cLC sample loop as shown in Figure 17. At least three replicates were obtained for each measurement.

3.2.10 Data Analysis

Peak integration was automated using the Xcalibur Qual Browser. Each peak was manually inspected prior to area calculation. Relative areas were obtained by dividing the peak area of the light peptide by that of its heavy analog. An analysis of variance (ANOVA) was used to compare basal relative areas for LE for each of the four rats with the null hypothesis being that the mean relative area is the same for each rat (with 95% confidence). A p-value of 0.0004 indicated that the null hypothesis should be rejected and a *post hoc* Tukey test revealed that the measured relative areas for Rat 1 were significantly different from those of Rats 2, 3, and 4. For this reason, the measured values for each rat are presented individually. The ANOVA was repeated in the same way for ME. Although it indicated that there was no significant difference in measurements for each rat ($p = 0.18$), in most cases we were only able to measure ME once in each rat. Thus, we have chosen to report ME values for each rat individually. All statistics were performed using StatPlus in Excel. Values are stated as the mean ± the standard error of the mean (SEM).

3.3 Results and Discussion

3.3.1 On-column Dimethylation

While the efficacy of the on-column dimethylation procedure has been shown elsewhere,[247] this technique was originally developed for proteomics applications, which have a few significant differences compared to online microdialysis applications. First, proteomics samples typically consist of tryptic digests derived from tissue homogenates. Samples go through several purification

and pre-concentration steps, which also enable higher ion counts. The microdialysis probe typically excludes large proteins, resulting in relatively clean samples, but dialysate still contains a high concentration of salts which must be separated from analytes to achieve efficient ionization and detection. Thus, a de-salting step was added following sample loading. Low endogenous concentrations (pM-nM) in the extracellular space combined with limited microdialysis recoveries result in significantly less analyte mass on-column than tryptic digests, so while the previous work utilized larger volumes of labeling reagents (40 μL), we have reduced these volumes to 5 μL, which also reduces labeling time. We note that each labeling step only required three minutes. This reduction in time was necessary to achieve a practical temporal resolution for online microdialysis sample collection and near real-time measurements. Previous work utilized a sodium phosphate buffer for the labeling reagents. We have chosen to use triethylammonium acetate instead to reduce the accumulation of non-volatile salts on the column, which result in decreased sensitivity and column lifetime, particularly for the one-column setup.

3.3.2 Labeling Tests

It is imperative to establish the completeness of the labeling procedure and to confirm the absence of cross-labeling and mixed-labeling which would occur if the first of the two labeling reactions was not effectively complete. Recall that the autosampler contains five vials: light reagent and quench solution (vials 1 and 2), aqueous peptide standards (vial 3), and heavy reagent and quench solution (vials 4 and 5). We determined completeness using two tests: 1) The Ringer's standard (a surrogate for the sample) was injected followed by the sequence of labeling steps (Fig. 17B) *except* the introduction of the aqueous standards, *i.e.,* vials 1, 2, 4, 5 were injected in series; and 2) The Ringer's standard was *not* injected. All steps in Fig. 17B, including the introduction of

the aqueous standard, were injected in sequence. In the first case, the peptide is exposed to both light and heavy reagents but should only be light labeled. The presence of the heavy labeled peptides would indicate incomplete reaction. In the second case, only heavy labeled peptides should be present. The presence of light labeled peptide would indicate carryover of the light labeling reagent. In addition, if we observed differences in the amount of light and heavy label between the two tests, we would infer an effect of incomplete removal of salt on the reactions.

We did not detect unlabeled peptide, cross-labeling, or mixed products over a set of concentrations of peptides (Figs. S23-25). Ions were present in the expected ratios based on relative concentration (1:1). Thus, any amount of unlabeled peptide is below our detection limit and thus the labeling is apparently complete at these concentrations. Given that the ratios between light and heavy peptides were as expected, we conclude that the presence of salts in the Ringer's solution did not affect the labeling efficiency or ionization efficiency compared to the aqueous standard. Thus, we conclude that this is an effective method for labeling. Previous reports[247, 252-253] have investigated the labeling efficiency of the dimethylation reaction at varying concentrations and for various applications and have had similar findings.

3.3.3 One-column Setup

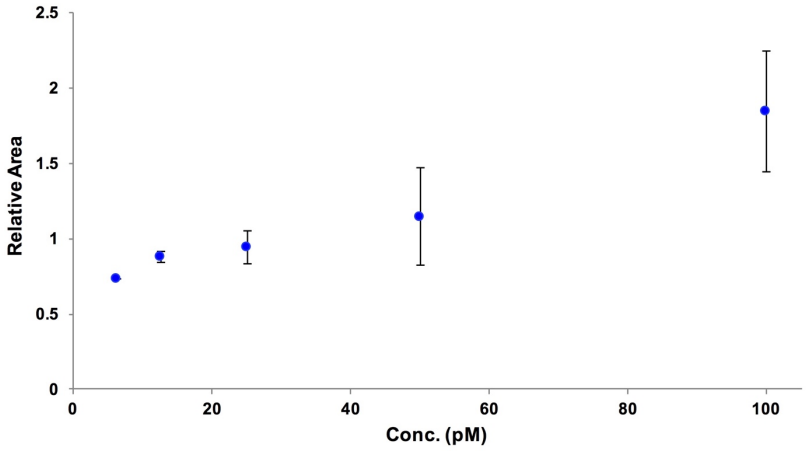

Figure 18 Calibration curve for LE using the one-column setup. The relative area is defined as the area of the light peptide (in Ringer's) divided by the area of the heavy peptide (100 pM LE in water). Error bars represent the SEM for n = 2 replicates.

Initially, we investigated the use of online labeling using a single column. With this approach, the loading pump directs all sample and reagents onto the analytical column and waste is directed into the MS source. This method can be easily adapted to existing LC-MS setups and does not necessarily require additional equipment, such as valves. Fig. 18 depicts a calibration curve of LE generated using the one-column setup, where the relative area was determined by dividing the peak area of the light peptide (prepared in Ringer's) by the peak area of the heavy peptide (100 pM LE in water). The plot should be linear with an intercept equal to approximately zero, yet by eye the points do not describe a good straight line (slope (± SEM) is 0.01130 ± 0.00092) and the intercept (± SEM) is 0.671 ± 0.047. Reproducibility was also a challenge, as indicated by large SEMs for replicate measurements. A significant contribution to this poor calibration is the decrease in MS sensitivity after several hours of repeat injections. This was likely due to the accumulation of non-volatile salts from the Ringer's solution at the MS inlet. This

problem could be prevented if one has a method for preventing eluate from entering the MS source, such as diverting the liquid stream from the glass emitter tip using N_2.[96] Another issue was rapid column degradation, which has been reported by others in similar applications[96, 254-255]. Interestingly, this was not an issue with aqueous standards, only those prepared in Ringer's. Larger-bore columns may minimize this effect[241] but trade-offs in sensitivity must be considered. We found the one-column method useful for method development, especially since it requires minimal changes to existing setups and procedures. It could also be utilized for short-term studies occurring over a few hours but longer studies require a more robust setup. Thus, we pursued a two-column approach.

3.3.4 Two-column Setup

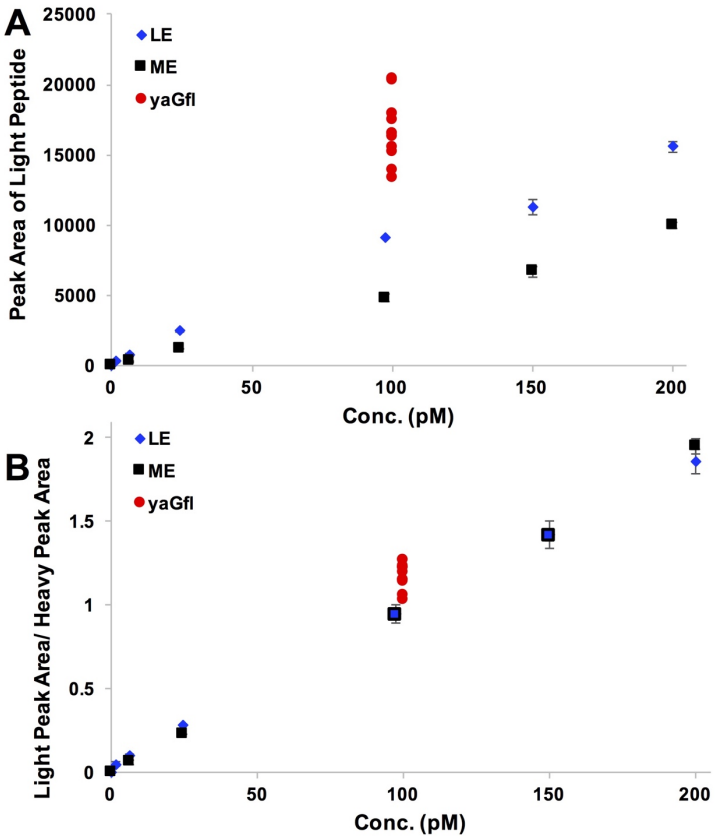

Figure 19 Quantitation of LE (blue), ME (black), and yaGfl (100 pM, red) (A) based on the peak area of the light labeled peptide and (B) based on the relative area, in which the peak area of the light peptide (in Ringer's) is divided by the peak area of the heavy peptide (100 pM in water). Black squares with blue centers indicate overlapping data points. Error bars represent the SEM of n = 2 replicates.

It is well-known that internal standards are necessary for MS^2 quantitation to correct for matrix effects.[80] This is particularly true for dialysate samples (Fig. 19). Fig. 19A depicts the peak areas of Ringer's standards that were labeled using the light reagent. In comparison, Fig. 19B shows the same data, but expressed as the ratio of the peak area of the light labeled peptide to that of the heavy labeled peptide (100 pM in water). The addition of the isotopic standard resulted in

improved reproducibility and linearity (Table 3). These results further demonstrate the efficacy of this method, as ratios of light to heavy are as expected based on relative concentrations. In Fig. 3, yaGfl was present at a concentration of 100 pM in both the Ringer's and the aqueous standards. Though both are normally distributed, the relative standard deviation of the distribution of yaGfl relative areas is considerably smaller than that for the peak area of yaGfl alone (Table 4). Thus, inclusion of the heavy peptide improves reproducibility of dialysate measurements.

Table 3 Slope and Intercept of the Calibration Curve Obtained using the Peak Area of the Light Peptide (Fig. 19A) and the Relative Peak Area[a] (Fig. 19B)

[a]Defined as the peak area of light peptide divided by the peak area of its heavy analog
[b]Units of Peak Area
[c]SEM = standard error of the mean
[d]Units of (Peak Area)(Conc.)$^{-1}$
[e]Units of Relative Area
[f]Units of (Relative Area)(Conc.)$^{-1}$

	Peak Area of Light Peptide		Relative Peak Area	
Peptide	**Intercept[b] (± SEM[c])**	**Slope[d] (± SEM)**	**Intercept[e] (± SEM) x 10^4**	**Slope[f] (± SEM) x 10^4**
LE	399 ± 337	76 ± 3	373 ± 115	91.7 ± 1.1
ME	-23 ± 194	48 ± 2	-26 ± 96	96.47 ± 0.98

Table 4 Mean and Standard Deviation[a] of Light yaGfl Peak Areas (Fig. 3A) and Relative yaGfl Peak Areas[b] (Fig. 3B)

[a]Statistics are based on n = 12 measurements.
[b]Defined as the peak area of light yaGfl divided by the peak area of heavy yaGfl
[c]Units of Peak Area
[d]Unitless

Parameter	Peak Area of Light yaGfl[c]	Relative Peak Area[d]
Mean	16700	1.18
Standard Deviation	2200	0.078
Relative SD	0.13	0.066
Median	16400	1.21

3.3.5 In Vivo Microdialysis

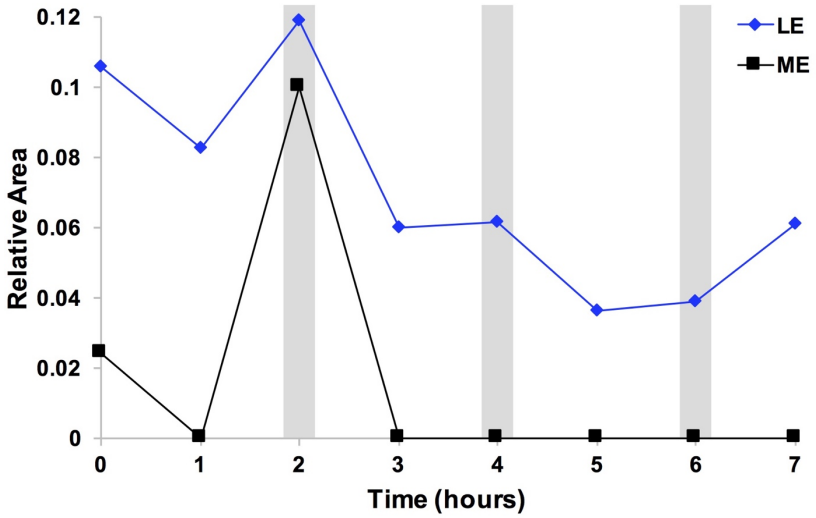

Figure 20 Profile of LE (blue) and ME (black) levels during sampling of a single rat. The first point (t=0 hours) was collected 15 minutes after probe implantation. Shaded areas represent points collected during 10-minute potassium stimulation. The relative area is defined as the peak area of the light peptide divided by the peak area of the heavy peptide.

To demonstrate the utility of this method for studying dynamic changes in endogenous neuropeptides *in vivo*, we monitored LE and ME concentrations in the rat hippocampus. Fig. 20 depicts recorded LE and ME levels throughout the sampling time for a single rat. This was a typical profile obtained for each of the rats (Fig. 26). Interestingly, with each rat we saw an initial high peptide level immediately after probe implantation. This phenomenon has been observed in other neuropeptide microdialysis studies.[93, 238] The calibration curves in Fig. 3B were used to convert the relative areas, such as those shown in Fig. 20, to concentrations for each rat. Estimated dialysate concentrations of LE and ME can be found in Table 5. ANOVA revealed that basal concentrations of Rat 1 were statistically different from the others (see Experimental). This could be because the

probe for Rat 1 was slightly outside the targeted area where the other probes were located (Fig. S1).

Table 5 Estimated Concentrations[a,b,c] of LE and ME in Dialysate

[a]Values are not corrected for probe recovery.
[b]Levels were quantified using the regression statistics in Table 3
[c]Concentrations are expressed as the mean ± SEM, where the value in parenthesis indicates the number of measurements in which the peptide was detected
[d]Based on the first potassium stimulation
[e]Potassium stimulation was not performed on Rat 2
[f]Measurements that do not have SEM values were only measured once (n = 1)

	LE		ME	
Rat	**Basal Conc. (pM)[c]**	**K^+ Stimulated[d] Conc. (pM)**	**Basal Conc. (pM)[c]**	**K^+ Stimulated[d] Conc. (pM)**
1	67 ± 12 (n = 3)	126[f]	49 ± 8 (n = 3)	84[f]
2	5.6 ± 1.2 (n = 2)	Not Performed[e]	3.7[f]	Not Performed[e]
3	4.4 ± 1.2 (n = 4)	8.9[f]	2.8[f]	11[f]
4	2.0[f]	7.5[f]	9.0[f]	14 ± 2 (n = 2)

Potassium stimulation is a commonly employed method used to verify the presence of a neuropeptide.[256-258] Fig. 21 shows the typical EIC and MS spectra for peptides following stimulation with potassium. Each peptide was easily identifiable under these conditions. Thus, we are observing endogenous neuropeptide release. Peptide response decreased with repeated potassium stimulation. This has been observed elsewhere.[240] We observed a statistically significant 2.8-fold increase in LE during potassium stimulation compared to basal levels (Fig. 26). We did

not detect a significant increase (defined as $p < 0.05$) in ME during potassium stimulation (9). This was because basal levels were often below the detection limit.

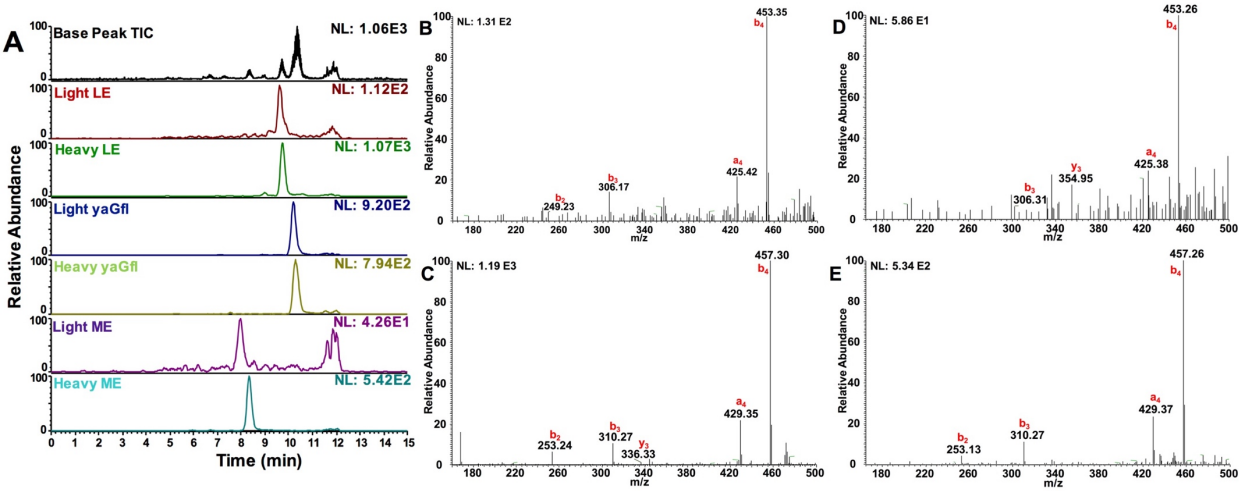

Figure 21 Peptide detection during potassium stimulation. A) Chromatograms and corresponding mass spectra at the point of elution of B) light LE, C) heavy LE, D) light ME, and E) heavy ME during 10-minute stimulation with 100 mM KCl Ringer's. Light and heavy yaGfl spectra can be found in Figure 27 (SI).

At the end of the sampling time, the microdialysis probe was removed to test for *in vitro* recovery. The recoveries ± SEM were 14.9 ± 1.1% for LE and 13.3 ± 2.4% for ME (n = 3). Probe recovery was determined after *in vivo* use to prevent carryover of standards prior to rat experiments and to show that the probe was properly functioning throughout the course of the experiment. Thus, we conclude that this method is useful for observing dynamic changes in neuropeptide concentrations in the extracellular space.

Since this is the first report of online labeling and MS quantitation of neuropeptides in rat brain microdialysates and the first study quantifying enkephalin levels in the hippocampal extracellular space using MS, there is a lack of literature with which to compare our results. The closest work consists of two reports, both conducted by Rocha, et al., in which microdialysis followed by radioimmunoassay (RIA) was used to compare total opioid peptide (defined as

peptides with YGGFM… or YGGFL… N-terminal sequences) levels in the hippocampus of control rats to those with induced seizures. They reported total opioid concentrations in control animals of 11.2 ± 2.5 pM[259] and 24.5 ± 2 pM,[260] without correction for probe recovery. These values are similar to ours. They also observed approximately 1.5-[259] and 4-fold[260] increases in total opioid levels when stimulating with 100 mM potassium for 10 minutes. These values are similar to the relative changes in LE levels that we observed under the same stimulation conditions.

Extracellular neuropeptide concentrations are region-dependent.[13] Our measured LE and ME concentrations were near and at times below our detection limits. Three of our probe locations were primarily in the CA1 region of the hippocampus, which has lower enkephalin levels than the nearby dentate gyrus and the CA3.[49,50] More broadly, RIA and immunohistochemistry measurements have shown that LE and ME levels vary considerably among regions of the brain and are higher in other brain regions, such as the striatum, compared to the hippocampus.[261-266] Although immunoreactivity is not directly related to extracellular concentrations of the pentapeptides, we speculate that the detection limits of this technique will allow for measurements in many other brain regions.

3.3.6 Use of yaGfl as a Quality Control Indicator

Given the complexity of the experimental setup, we found it useful to include the D-amino acid-containing peptide yaGfl in the perfusate to aid in troubleshooting and as a semi-quantitative measure of the data quality. This synthetic amino acid was chosen because it is similar in length and composition to our analytes of interest and is not hydrolyzed to any detectable extent in the extracellular space.[267] If a peptide that is hydrolyzed in the extracellular space were used, it would not be a suitable control because it would not be known if decreases in signal observed at the

detector were due to instrumental issues or enzymatic hydrolysis. The yaGfl present in the perfusate was light labeled along with the other peptides in the microdialysate. In order to generate a SIL-IS, yaGfl was also contained in the aqueous standard. By pooling data from all four rats, we found that the relative area of yaGfl (ratio of light to heavy peak area) was normally distributed, with a mean of 0.989 and a standard deviation of 0.067 (n = 23, Table 6). Using this value, we can quickly assess the quality of an injection. If we obtain a relative area outside the range of 0.85 to 1.13, we suspect (with 95% confidence based on 22 degrees of freedom) that there is some problematic issue, such as a leak. It is especially important to have a control such as this when doing online analysis, which requires rapid troubleshooting to avoid sample loss. Additionally, by comparing the SEM of yaGfl measurements to that for a peptide, we can determine if variations in peptide levels are due to physiological variations or procedural errors. Thus, yaGfl is a useful internal standard to assess point-to-point and rat-to-rat reproducibility.

Retrodialysis of yaGfl is also useful for determining microdialysis probe extraction fraction, which is important for accurate quantitation. This is typically determined *in vitro* but it is helpful to have an *in vivo* method since the environment of the brain is much different than that of a beaker. By comparing the mean relative area ± SEM of yaGfl in the absence of the microdialysis membrane (Table 2, 1.180 ± 0.022) to the mean in Table 6, the extraction fraction is 16.19 ± 0.03% (1-(0.989/1.180) expressed as a percent). Assuming there is no degradation of yaGfl in the extracellular space, the extraction fraction is equal to the probe recovery. This value is within reasonable agreement with the LE and ME recoveries and indicates that yaGfl is useful for determining probe recovery *in vivo*.

Table 6 Descriptive Statistics[a] for the Relative Area[b] of yaGfl

[a]Statistics are based on n = 23 measurements.
[b]The relative area was calculated by dividing the peak area of light yaGfl (from the perfusate) by the peak area of heavy yaGfl (100 pM aqueous standard).

Parameter	Value
Mean	0.989
Standard Deviation	0.067
Standard Error	0.014
Median	0.982

3.4 Conclusion

We have developed an online, automated method for labeling endogenous neuropeptides in microdialysate and corresponding isotopic standards. This allows quantitation of dynamic processes occurring in the extracellular space. We have demonstrated this by quantifying LE and ME in the anesthetized rat hippocampus under basal and potassium-stimulated conditions. To our knowledge this is the first report of online collection and labeling for microdialysis applications and the first quantitative study of endogenous LE and ME in the hippocampus using MS^2. One drawback of this technique is the time required for labeling. In this study we did not optimize the labeling procedure for maximum time efficiency. We anticipate improving this for future work, both by optimizing labeling steps to achieve complete labeling in the least amount of time and by increasing loading flow rates.

3.5 Supporting Information for On-column Dimethylation of Neuropeptides in Microdialysate

3.5.1 Mass Spectrometry

Table 7 Selected Ions for Fragmentation and Quantitation of Neuropeptides

[a]Isolation widths were 3 m/z
[b]Tolerance was ± 0.5 m/z.

Peptide	Abbreviation	Precursor m/z[a]	Daughter m/z[b]
Dimethyl leu-enkephalin	Light LE	584.30	425 + 453
$^{2}H_4$ Dimethyl leu-enkephalin	Heavy LE	588.30	429 + 457
Dimethyl yaGfl	Light yaGfl	598.30	439 + 467
$^{2}H_4$ Dimethyl yaGfl	Heavy yaGfl	602.30	443 + 471
Dimethyl met-enkephalin	Light ME	602.30	425 + 453
$^{2}H_4$ Dimethyl met-enkephalin	Heavy ME	606.30	429 + 457

Table 8 Selected Ions for Fragmentation and Quantitation in Labeling Tests

[a]Isolation widths were chosen so that multiple analytes, including potential cross-labeled products, could be detected in a single fragmentation step.

Peptide	Center m/z	Isolation[a] Width (m/z)	Daughter m/z
Leu-enkephalin (LE)	556.60	3	397 + 425
yaGfl	570.25	3	411 + 439
Met-enkephalin (ME)	574.20	3	397 + 425
Light LE	588.30	8	425 + 453
Heavy LE	588.30	8	429 + 457
Light yaGfl	602.30	10	439 + 467
Heavy yaGfl	602.30	10	443 + 471
Light ME	602.30	10	425 + 453
Heavy ME	602.30	10	429 + 457

3.5.2 Microdialysis Probe Location

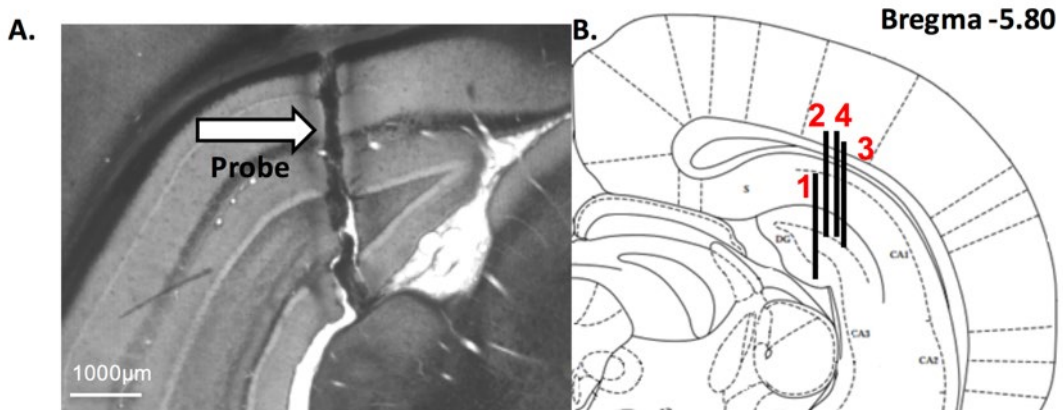

Figure 22 Localization of microdialysis probes in the rat brain. (A) Representative microdialysis probe track. (B) Schematic reconstructions of positions of the four microdialysis probes (adapted from Paxinos and Watson[251]). Coordinates were chosen to sample from the CA1 region. Note that probe 1 is in the dentate gyrus. Numbers in red correspond to the rat numbers in Table 5 of the text.

3.5.3 Labeling Tests

To confirm the absence of unlabeled or cross-labeled peptides, we performed a series of tests in which labeling was conducted as described in the text but: 1) The Ringer's standard was injected prior to treatment with labeling reagents and no aqueous standard was injected and 2) The aqueous standard was injected after quenching of the light label but before treatment with the heavy label. In this test, no Ringer's standard was injected. For each test the Ringer's standard consisted of 50 pM (Fig. 23), 100 pM (Fig. 24), or 200 pM (Fig. 25) LE, yaGfl, and ME in Ringer's and the aqueous standard consisted of matching concentrations (either 50, 100, or 200 pM) of LE, yaGfl, and ME in water. As expected, for the first test we observed only light product in the mass spectra and for the second test we saw only heavy product, indicating complete labeling.

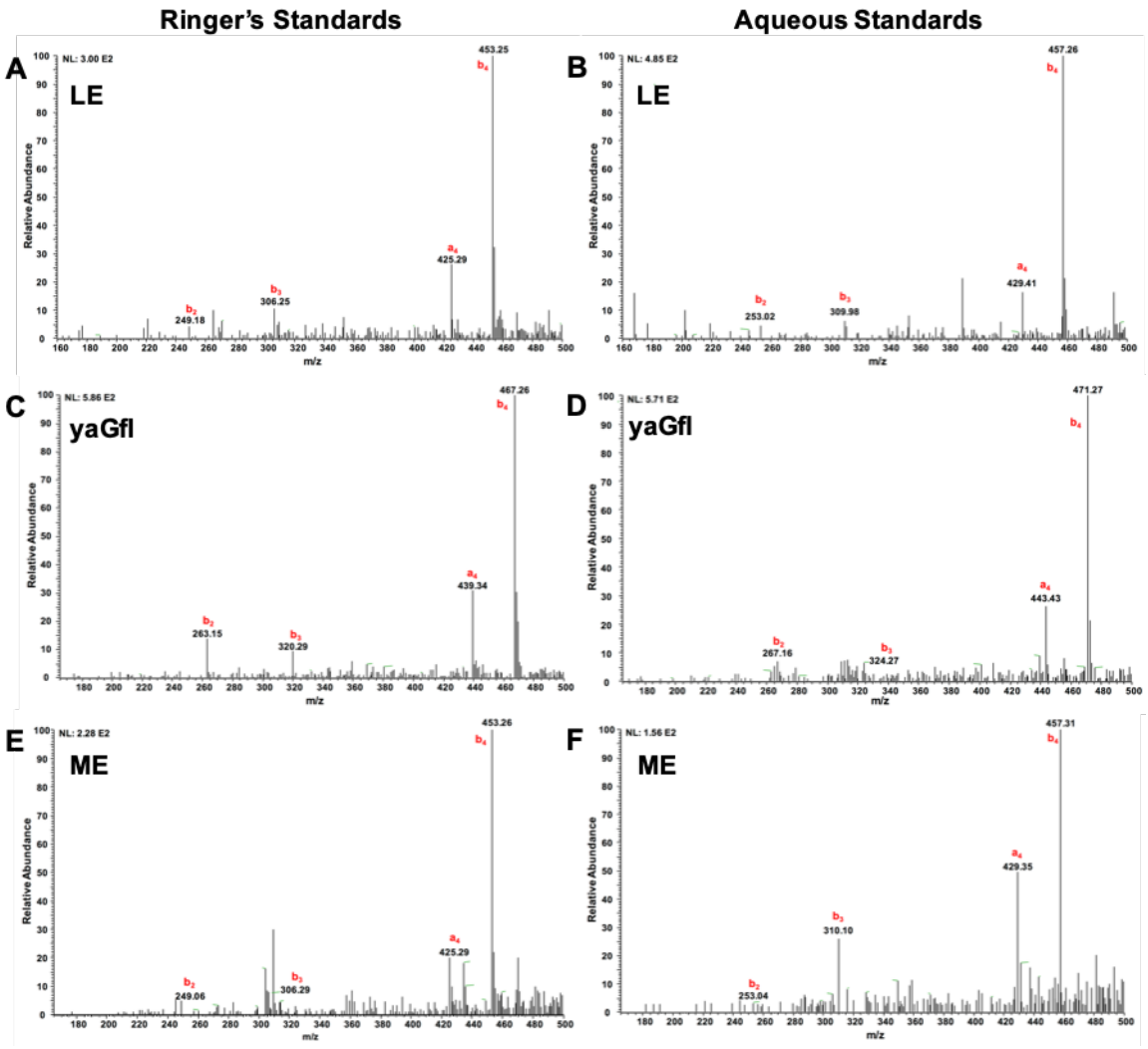

Figure 23 Labeling test results for 50 pM Ringer's standards (left column) and 50 pM aqueous standards (right column) for A-B) LE, C-D) yaGfl, and E-F) ME. Peak identifications were made using prospector.ucsf.edu/prospector/cgi-bin/mssearch.cgi.

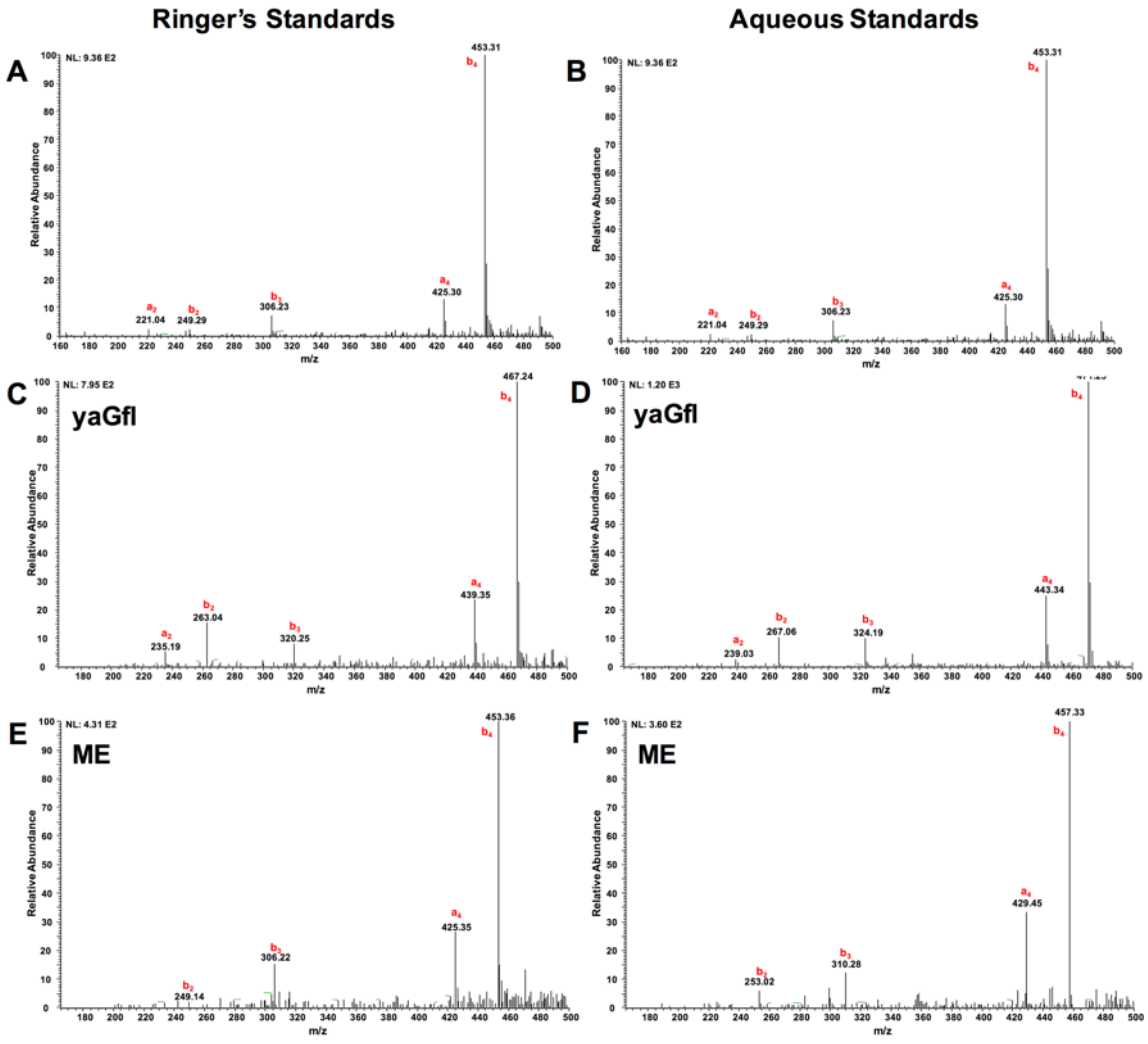

Figure 24 Labeling test results for 100 pM Ringer's standards (left column) and 100 pM aqueous standards (right column) for A-B) LE, C-D) yaGfl, and E-F) ME.

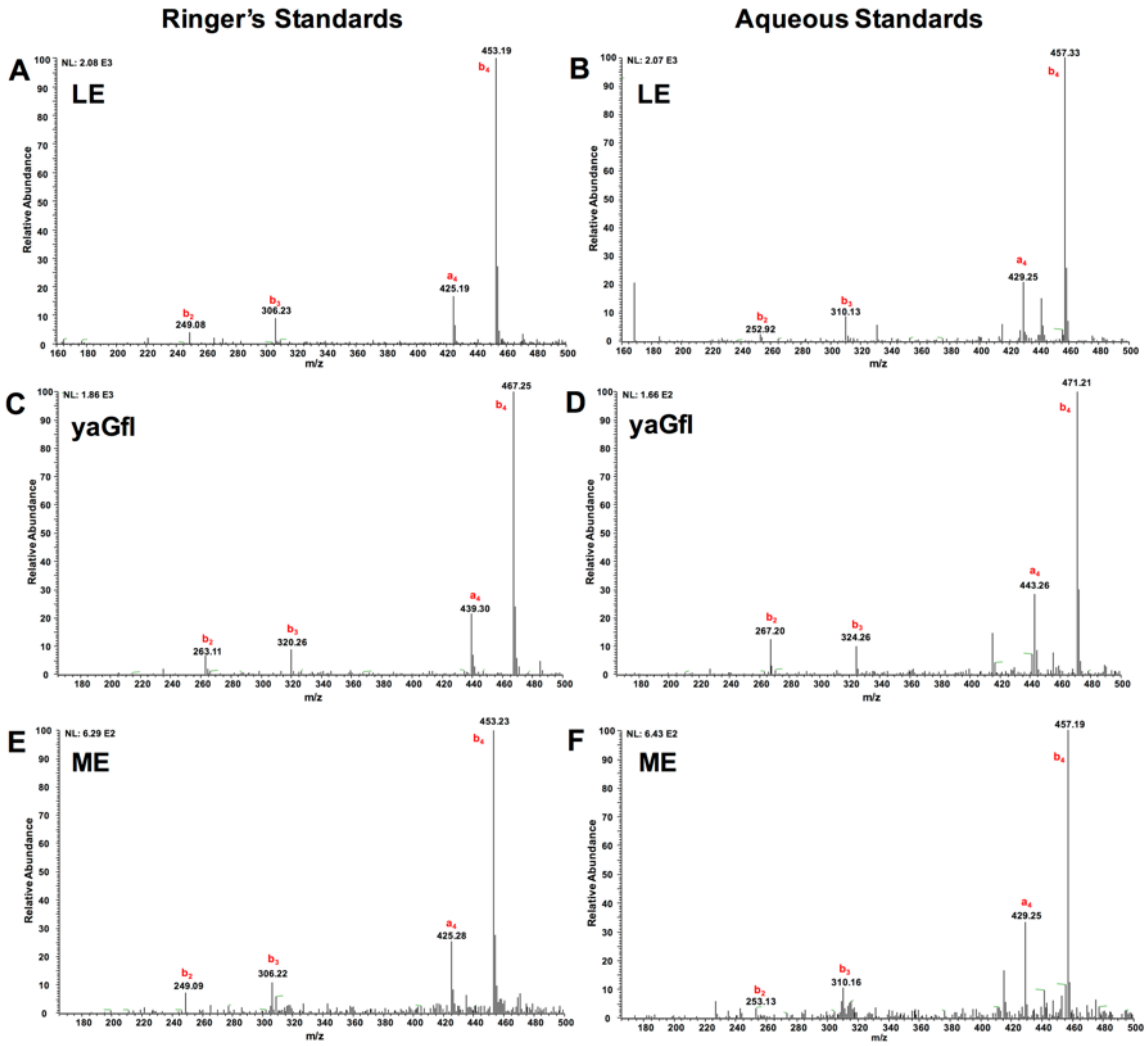

Figure 25 Labeling test results for 200 pM Ringer's standards (left column) and 200 pM aqueous standards (right column) for A-B) LE, C-D) yaGfl, and E-F) ME.

3.5.4 In Vivo Microdialysis Data

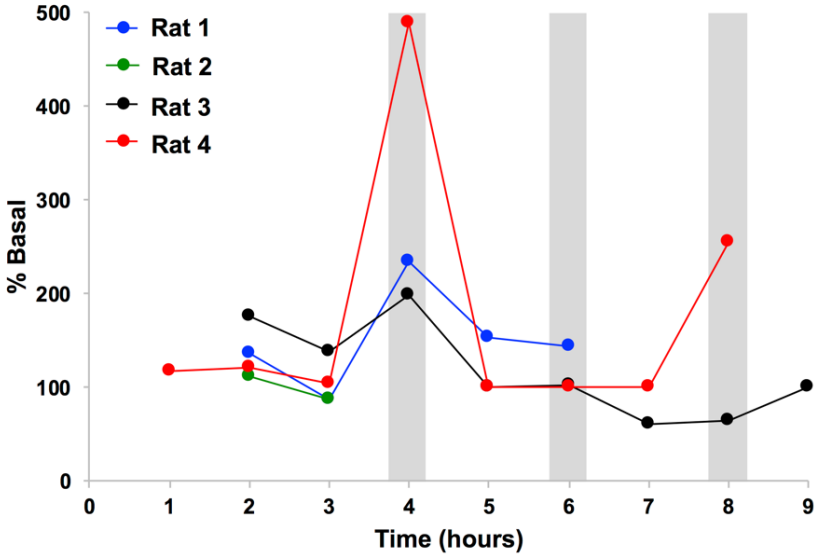

Figure 26 Measured LE Levels for Each Rat. To determine the percent basal, all detectable basal light LE peak areas were divided by the corresponding heavy peak area to obtain the relative area. The basal relative areas for each individual rat were averaged. Each time point was divided by the mean basal relative area and expressed as a percentage. Gray shaded areas indicate points that were collected during potassium stimulation. The time axis of each rat has been adjusted so that the potassium stimulated points are aligned.

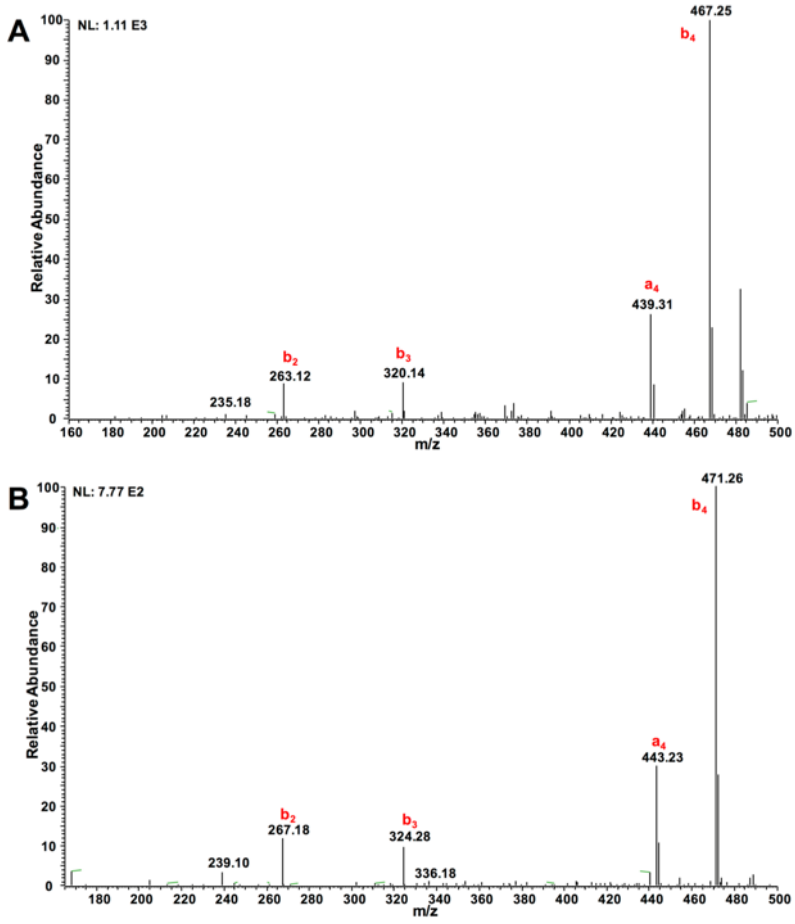

Figure 27 Mass spectra at the point of elution for A) light yaGfl and B) heavy yaGfl during 10-minute stimulation with 100 mM KCl Ringer's. Corresponding chromatograms can be found in Figure 21.

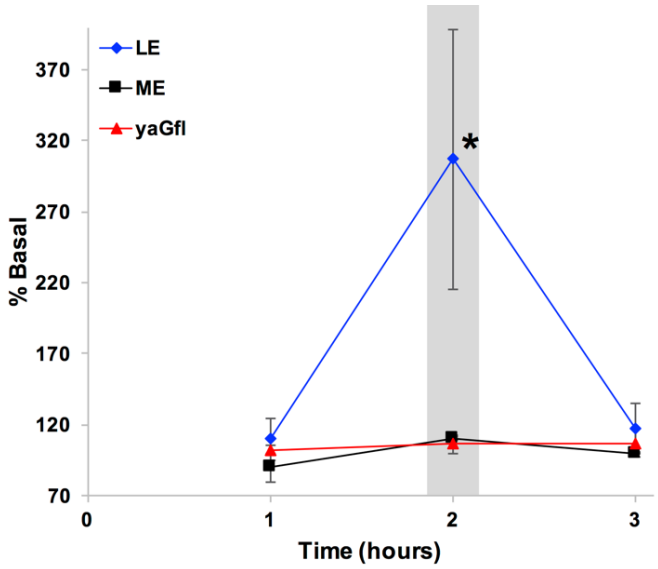

Figure 28 Comparison of LE, ME, and yaGfl Potassium Stimulated Levels to Basal Levels. Percent basal levels were determined by dividing the relative area (light peak area/ heavy peak area) at each time point by the mean basal relative area for each rat, which was then expressed as a percentage. The shaded gray area indicates points that were collected during potassium stimulation. The time axes have been adjusted so that the potassium stimulated points are aligned. The asterisk indicates a statistically significant (p=0.03) increase in LE levels during potassium stimulation as determined using a one-tailed t-test (with 95% confidence). The error bars represent the SEM of n = 3 rats.

Table 9 Comparison of Basal[a] Levels of ME with Potassium Stimulated[b] Levels

[a]The mean of pooled basal levels (± SEM) was 0.260 ± 0.062 for n = 6 measurements.
[b]The mean of pooled potassium stimulated levels (± SEM) was 0.33 ± 0.10 for n = 5 measurements.
[c]Comparisons were made using a one-tailed t-test with 95% confidence.

Source of Variation	Sum of Squares	Degrees of Freedom	Mean Square	F	P-value
Between Groups	0.015	1	0.015	0.20	0.67
Within Groups	0.71	9	0.079		
Total	0.72	10			

4.0 The Development of Electroosmotic Perfusion-Microdialysis for *In vivo* Measurement of Ectopeptidase Activity

Neuropeptides are a diverse set of chemical messengers that are involved in a number of cognitive processes including learning and memory. Their effects in the extracellular space are modulated, in part, by ectopeptidases, membrane-bound enzymes with active sites facing the extracellular space. When neuropeptides are degraded by ectopeptidases, their effects are altered or ceased and resulting hydrolysis products can have effects different from the parent peptide. Thus, release of a particular peptide can initiate a cascade of events throughout the central nervous system. Understanding of the fate of neuropeptides in the extracellular space is limited by the lack of available methods for quantifying ectopeptidase activity with natural substrates *in vivo*, especially at spatial resolutions relevant to the brain.

We have developed a technique called electroosmotic perfusion-microdialysis, in which substrate peptides are perfused into the brain of an anesthetized rat using current. The substrate peptide interacts with ectopeptidases in the extracellular space and hydrolysis products along with unhydrolyzed substrate are collected using microdialysis. Using current allows us to control the volume of substrate perfused and the residence time in the tissue. Thus, we can make quantitative measurements of ectopeptidase activity. We have demonstrated this technique by measuring leucine enkephalin (LE, YGGFL) degradation to the product GGFL in the prefrontal cortex of the anesthetized rat with a spatial resolution of 100 μm. We also observed a dose-dependent effect on LE hydrolysis using an insulin regulated aminopeptidase (IRAP, EC 3.4.11.3) inhibitor. This is the first report of a sampling method capable of performing such measurements in the extracellular space of the rat brain *in vivo*.

4.1 Introduction

Ectopeptidases, membrane-bound enzymes with active sites facing the extracellular space[2], modulate the effects of neuropeptides, a diverse class of signaling molecules.[236] Hydrolysis products produced by ectopeptidases can have effects that are different from the parent peptide.[5] Thus, at the very least, ectopeptidases can control the local activity of a neuropeptide. The release of a particular neuropeptide can sometimes result in a series of effects throughout the central nervous system as a result of ectopeptidase activity. The understanding of such processes is limited by the lack of suitable methods.[1] Making quantitative measurements of ectopeptidase are especially challenging in the brain where the role of a peptidase can be tied to its specific location[2, 236], requiring spatially-resolved but minimally-invasive methods for probing the extracellular space. *In vitro* assays[128, 268-270] and *in situ* histological studies[120, 271-274] provide important information but it is unknown how activities implied by these methods translate to *in vivo* conditions.[103, 275] There exists a need for a sampling-based method for measuring membrane-bound ectopeptidase activity using natural substrates in an *in vivo* model, particularly in the brain.

Microdialysis (MD) is the most commonly used method for sampling the extracellular space [78] and has been used to study enzyme activity qualitatively *in vitro*[128-129] and *in vivo* in the brain[50-51, 94, 122-125, 276-278] and other tissues[130, 132, 279-283]. Substrate introduction through the membrane (retrodialysis) and collection of substrate and products through the membrane of the probe depends on diffusion, probe characteristics and chemical processes in the tissue.[131, 135-137] Thus, there is no experimental parameter to directly control substrate residence time.[134] In work outside the brain, the Stenken group has explored using extraction fraction, the ratio of the concentration of substrate collected at the probe outlet compared to that introduced at the inlet, as a measure of enzymatic activity.[127-130, 132, 134] They concluded that because the extraction fraction

is more affected by mass transport processes than hydrolysis in tissue, it cannot be used to quantitatively study enzymatic activity *in vivo*.[134]

Electroosmotic flow is the basis of a method that has been used to study ectopeptidase activity in organotypic hippocampal slice cultures (OHSCs).[139-140, 148, 150-151, 284] . Electroosmotic flow results from a current passing through an electrolyte solution in a matrix with charged walls such as a fused silica capillary or tissue.[133, 285-287] In tissue, the cell membranes and extracellular matrix are negatively charged, and a fused silica capillary naturally has negatively charged-walls. Bulk fluid flow is due to the movement of the surface's counterions in the diffuse layer.[285-286] The main advantage of using electroosmotic flow is that the current path, and thus spatial resolution, is dependent on the positioning of the current source and sink in relation to one another.[149] The velocity of an ectoenzyme substrate introduced through the tissue, and thus the residence time, can be controlled by changing the magnitude of the applied current.[139, 148-149] In electroosmotic push-pull perfusion (EOPPP) as applied in OHSCs a substrate-containing pulled capillary inserted into the tissue provides substrate near a collection capillary that is placed perpendicular to the top surface of the OHSC[140]. The collection capillary contains substrate and products of enzymatic reactions. EOPPP has been used to identify differential hydrolysis rates of galanin[140] and LE[151] in different regions (CA1 and CA3) of OHSCs. The latter work recently resulted in the first report of spatially resolved, quantitative ectoenzyme activity using natural substrates in live tissue.[151] The CA1 region, which is more vulnerable to oxygen and glucose deprivation than the CA3 region, had a greater activity (V_{max}) of a bestatin-sensitive ectopeptidase than the CA3 region. This difference was correlated with neuronal damage during oxygen and glucose deprivation and was abolished by the δ-opioid receptor antagonist naltrindole at which LE acts[151].

The work described above represents a major technological step in quantitative evaluation of ectopeptidase activity in intact tissue using natural substrates. However, it is obviously preferable to perform these measurements *in vivo*. This is especially important for peptide substrates that are regulated based on physiological changes like blood flow, such as the angiotensins [288]. However, transitioning to *in vivo* models is not as simple as performing the same steps *in vivo* as were done *ex vivo*. There are several technical issues that must be addressed. The most significant problem is flow rate. EOPPP operates in nL/ min flow rates.[148] This is advantageous for achieving a desirable analyte residence time but results in small sample volumes. This is not practical for obtaining multiple samples from a single animal over time. The second challenge is reproducibly implanting the two probes at a distance of ~100 μm, the spatial resolution at which our previous work was done.[140, 151]

Using direct laser writing[289-299], we have fabricated a dual-channel electroosmotic perfusion – microdialysis (EOP-MD) probe that allows perfusion of a natural substrate into the extracellular space where it interacts with ectopeptidases. Hydrolysis products along with any unhydrolyzed substrate are collected using the integrated MD probe. Dialysate is analyzed online using high-performance capillary liquid chromatography-tandem mass spectrometry (cLC-MS^2). This allows the monitoring of ectopeptidase activity in near-real time with a spatial resolution of approximately 100 μm. Because substrate perfusion velocity is dictated by current, we can control the substrate residence time in the ECS of the tissue by changing the magnitude of the current.[148, 151] The dual-channel perfusion tip permits sampling under a pair of matched conditions (± inhibitor) without disturbing the probe.

We have demonstrated that this technique is capable of measuring dose-dependent effects of the inhibitor HFI-419[66] on LE hydrolysis. HFI-419 is a specific inhibitor of insulin-regulated

aminopeptidase (IRAP, EC 3.4.11.3), an ectopeptidase known to hydrolyze neuroprotective peptides including the enkephalins[17-18], arginine-vasopressin[17, 20-21], and oxytocin[17, 21] *in vitro.* These measurements were performed in the rat cortex, an area of the brain in which both IRAP[300-301] and LE[263, 302] are found.

This work is novel both technologically and biochemically in that: (1) it is the first account of using direct laser writing to fabricate a perfusion/ sampling device for use in the brain, (2) it is the first method capable of controlling substrate residence time in the extracellular space of the anesthetized rat brain, and (3) it is the first demonstration of IRAP hydrolysis of a natural peptide substrate in the presence and absence of a specific IRAP inhibitor *in vivo*.

4.2 Results

4.2.1 Development of the EOP-MD Probe

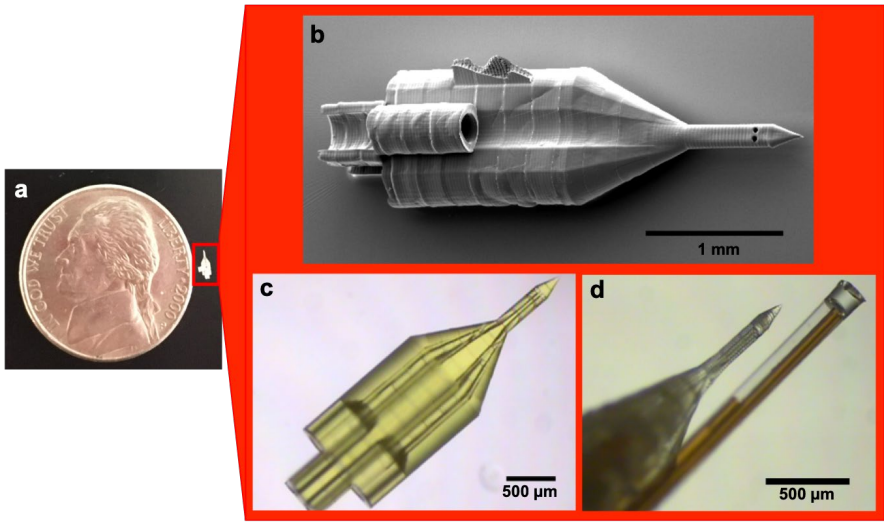

Figure 29 (a) Relative size of EOP-MD perfusion tip compared to a nickel. The tip is outlined in red. A 48x SEM image is shown in (b) and a 3x stereoscopic photo is shown in (c). Temporary "wings" on the device allow the device to be manipulated during probe assembly. They are were removed prior to insertion in the animal. A remnant of one wing can be seen in Fig 29b. The wing-free device, suitable for implanting, is seen in Fig 29c. The fully assembled EOP-MD probe is shown in (d).

We created a device that integrates a source probe, which provides substrate solution, and a MD probe, which collects unreacted substrate and products, with the Nanoscribe direct laser writing system (Fig 29). The source probe contains two independent microfluidic channels so that different perfusion solutions can be used alternately in the same experiment. Aside from the initial designing of the probe and a few steps after fabrication to rinse out any unreacted photoresist, direct laser writing is a relatively hands-off process. The distance between the source tip and the nearest surface of the microdialysis probe as measured using a stereoscope was 90 ± 5 µm (mean ± SEM, n = 3).

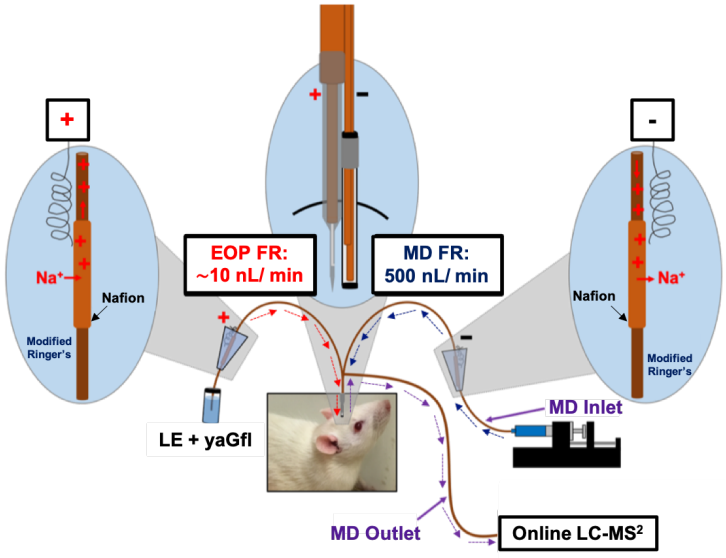

Figure 30 Schematic drawing of the general procedure of EOP-MD sampling. An electrode is placed in the reservoir surrounding the Nafion wall of the channel containing the perfusion solution. When a positive voltage is applied to the electrode, cations carry the current across the Nafion. This current generates electroosmotic flow through the capillaries and into the tissue. The current passes through the microdialysis membrane to a second Nafion wall in the microdialysis inlet capillary. Analytes, in this case LE plus hydrolysis products and the D-amino acid internal standard yaGfl, are collected at the MD probe. The outlet of the MD probe is connected to the LC-MS, resulting in online collection and analysis.

Electroosmotic delivery was achieved (Fig 30) using a constant current. The positive current passes through the source capillary, out the source tip, through the medium (tissue or gel), through the microdialysis membrane, and up the inlet microdialysis capillary. A short length of Nafion tubing is integrated with the current-carrying capillaries. Current flows through the Nafion into an electrolyte bath and a Ag electrode.

4.2.2 *In vitro* Fluorescence Studies

To visualize solute transport from the perfusion tip to the MD probe, we infused fluorescent dyes into a hydrogel and monitored the fluorescence intensity over time. The hydrogels have a similar zeta potential as that of brain tissue[303] and have been used as an *in vitro* model for electrokinetic transport in the brain.[287, 304] We used 3 kDa Texas Red (TR3), which is neutral, and tris(bipyridyl)Ru(II) ($Ru(bpy)_3^{2+}$) as the solutes[151].

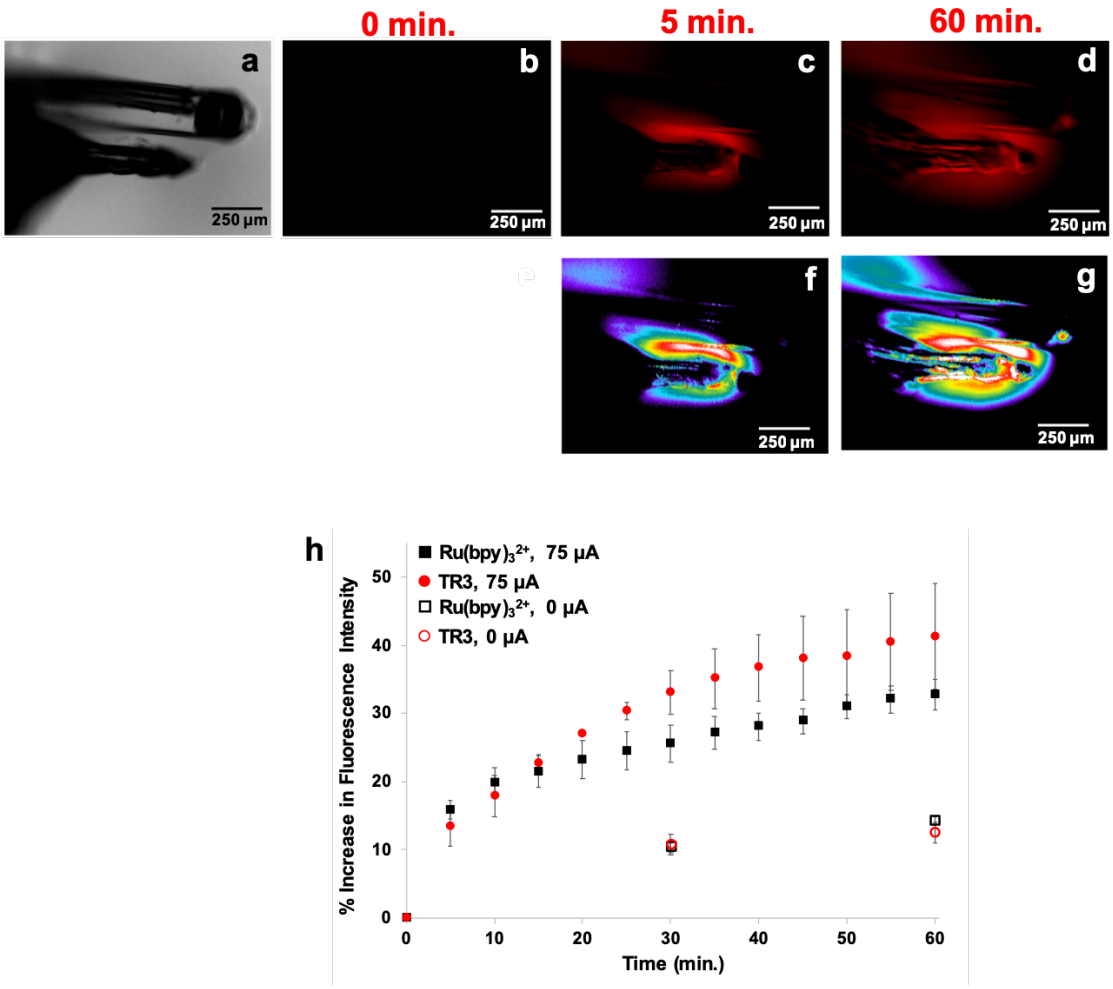

Figure 31 Measuring fluorescence intensity in a hydrogel over time. (a) A 4x brightfield image of the perfusion tip and MD probe placement in the gel. TR3 was infused into the hydrogel using a current of 75 µA. The intensity of fluorescence was measured (b) prior to turning on current (0 minutes) and after (c) 5 minutes and (d) 60 minutes of perfusion at 75 µA. The corresponding false color plots are shown in e-g. Figure h depicts the percent increase in fluorescence intensity for TR3 (●) and $Ru(bpy)_3^{2+}$ (■) at 75 µA and 0 µA (○ for TR3, □ for $Ru(bpy)_3^{2+}$). The error bars represent the SEM of n = 3 replicates for Texas Red and n = 4 replicates for $Ru(bpy)_3^{2+}$.

Fig 31a illustrates the brightfield image of the EOP-MD probe positioned in the gel. Prior to current flow, there is no apparent fluorescence (Fig 31b). After five minutes of perfusion, Fig 31c, there a is detectable increase in fluorescence in the hydrogel. Transport of the dye through the gel is biased towards the MD probe. This is especially clear in the false color plots (Fig 31e-g).

The highest concentration of dye (red) is confined between the EOP tip and the MD probe. This indicates that the dye is being carried by the EO flow from the perfusion tip, through the hydrogel, and to the MD probe.

To illustrate the ability of EOP to move molecules of various sizes and charges, we repeated the experiments described above with $Ru(bpy)_3^{2+}$, a cationic dye with a formula weight of 748.63 g/ mol (images not shown). We compared the percent increase in fluorescence over the entire image over time (Fig 31h). For both dyes we saw an increase in fluorescence intensity over the EOP sampling time. $Ru(bpy)_3^{2+}$ had a lower increase in fluorescence compared to TR3. $Ru(bpy)_3^{2+}$ is smaller, and cationic, in contrast to the larger and neutral TR3. Thus, it likely crosses the MD membrane more readily than the larger TR3. For both dyes we saw a minor increase in fluorescence after 60 minutes in the absence of current. This is due to diffusion. We see slightly more diffusion for $Ru(bpy)_3^{2+}$ compared to TR3, as we would expect due to the smaller size of $Ru(bpy)_3^{2+}$.

4.2.3 Assessing Mass Transport with yaGfl

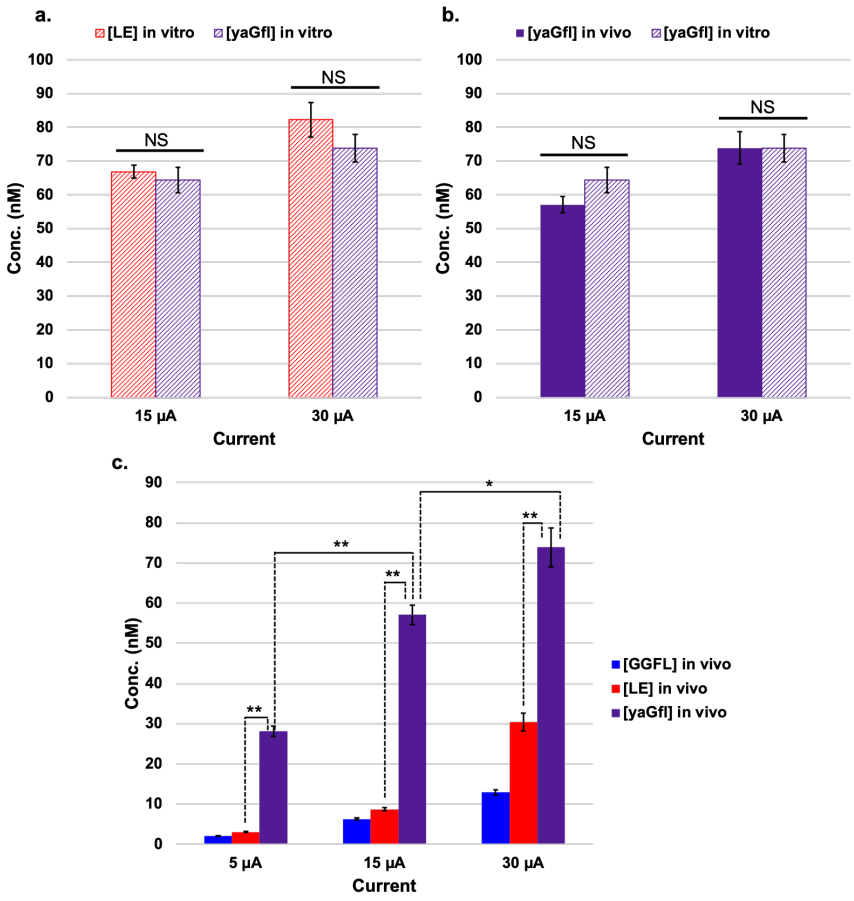

Figure 32 (a) Concentration of leu-enkephalin (LE, red diagonal lines) and yaGfl (purple diagonal lines) in dialysate during the electroosmotic perfusion of 10 µM LE and yaGfl into a hydrogel at 15 µA and 30 µA using the EOP-MD device. The concentration of yaGfl in the dialysate *in vivo* (solid purple bar) is compared to that obtained *in vitro* (from Fig 32a) in (b). Fig 4c depicts the concentrations of GGFL (solid blue bar), LE (solid red bar), and yaGfl measured in the dialysate in in vivo experiments. 'NS' indicates that the values shown under the bar were not significantly different as determined by ANOVA ($p > 0.05$) with post hoc Tukey test. The single asterisk (*) and double asterisk (**) represent $p < 0.05$ and $p < 0.01$, respectively. The error bars indicate the SEM for n = 3 replicates for in vitro data and n = 4 replicates for in vivo data.

In the assessment of enzymatic degradation of a peptide traversing the extracellular space, it is helpful to have an internal standard representing what would be observed in the absence of

enzymatic activity. Therefore, we use yaGfl as an internal transport standard. It is similar in size to LE and has not shown any measurable hydrolysis in the tissue in work with OHSCs.[139-140, 148, 151] We assessed its suitability for use with our EOP-MD device *in vitro* and *in vivo*., We performed an *in vitro* experiment in which we perfused a solution of 10 μM LE and yaGfl into a hydrogel and measured the concentrations of the recovered peptides in the dialysate at multiple currents. The range of currents was appropriate for *in vivo* use. They were lower than that shown in Fig. 31 and in the range of those dictated by our previous work done at approximately the same spatial resolution[151] and consistent with conditions that minimize cell death[305]. As seen in Fig 32a, for both currents used, there was no significant difference between the concentrations of LE and yaGfl in the dialysate. This confirms that yaGfl is a suitable standard for assessing mass transport in the absence of hydrolysis and can be used as an estimate of the initial substrate concentration. To further validate our use of yaGfl as a mass transport standard, we repeated the experiment *in vivo* in an anesthetized rat. There was no statistical difference ($p < 0.05$) between the yaGfl concentrations in the dialysate *in vivo* compared to *in vitro* (Fig 32b). Since there is no hydrolysis in the hydrogel and no difference between the yaGfl recoveries in the gel and the tissue, we can confirm that there is no significant uptake or hydrolysis of the internal standard in the tissue.

4.2.4 Effect of Current In Vivo

An important distinction of EOP-MD compared to other *in vivo* sampling techniques is the ability to control solute velocity and thus residence time. This is achieved by changing the magnitude of the applied current. To demonstrate this effect, we performed an *in vivo* experiment in which we perfused a peptide solution with the same concentration as was used *in vitro* (10 μM LE and yaGfl). We observed a statistically significant increase in the dialysate concentration of

yaGfl from 5 μA to 15 μA ($p < 0.01$) as well as from 15 μA to 30 μA ($p < 0.05$) (Fig 32C). This increase is due to higher solute velocity at higher currents leading to a larger volume containing substrate at steady state[287]. There was also a statistically significant difference between [LE] in the dialysate compared to [yaGfl] at each current. We attribute this difference to LE hydrolysis. Accordingly, the product GGFL was also detected in the dialysate.

We can calculate a steady-state collection efficiency based on the ratio of the mass flow rate (mole/s) of yaGfl out of the microdialysis probe to the same quantity infused by electroosmotic flow. Note that the mass flow rate is just the concentration multiplied by the volume flow rate of the solution. Given the electroosmotic mobility and conductivity of the extracellular fluid in brain, the ratio of electroosmotic flow rate to current is 1.45×10^{-8} $m^3/A*s$ in SI units and 0.87 nL/min per μA in more practical terms[148, 287]. The flux into the brain is the product of this flow rate (at a particular current) and the concentration of yaGfl in the source. The volume flow rate in the microdialysis probe exit is set and the concentration of yaGfl is determined by LC-MS. Fig 33 shows the ratios of the mass-flow rate out of the MD probe to the mass-flow rate infused. For yaGfl, the increase is not linear. This is because the solute electroosmotic velocity is relatively low, so diffusion also contributes significantly to mass flux in the tissue, and more so for lower currents[287]. The reactive LE, on the other hand, demonstrated the effect of a longer residence time in the tissue causing a greater extent of hydrolysis. In order to have the dynamic range to reliably detect changes in both LE and GGFL, we used the intermediate current, 15 μA, for subsequent inhibitor experiments.

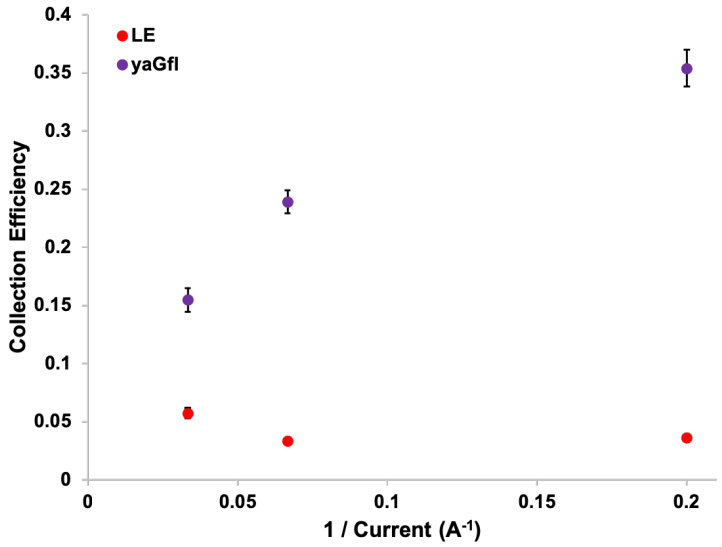

Figure 33 Effect of current on collection efficiency in vivo for LE (●) and yaGfl (●). The collection efficiency was calculated by dividing the moles per minute perfused (measured by LC-MS^2) divided by the moles per minute collected at the MD probe (based on laboratory concentrations). The error bars represent the SEM for n = 3 replicates.

4.2.5 LE Hydrolysis in the Presence and Absence of HFI-419

Our goal was to determine if we could observe an effect of HFI-419[66], a specific IRAP inhibitor, on the hydrolysis of LE. To be consistent with our EOP-MD experiments described above, we perfused 10 μM LE and yaGfl in the presence and absence of 10, 25, and 50 μM HFI-419. The product, GGFL is itself subject to hydrolysis by ectopeptidases. Thus, we use as a measure of the extent of reaction the loss of substrate as a ratio to initial substrate concentration, ($[S_0]$-$[S]$) / $[S_0]$. Recall that the initial substrate concentration is taken to be the concentration of the internal standard, yaGfl. Fig 34 is a plot of the resulting data. We observed a statistically significant ($p < 0.01$) decrease in product formation at 25 μM and 50 μM inhibitor concentrations compared to perfusing the substrate in the absence of inhibitor (0 μM).

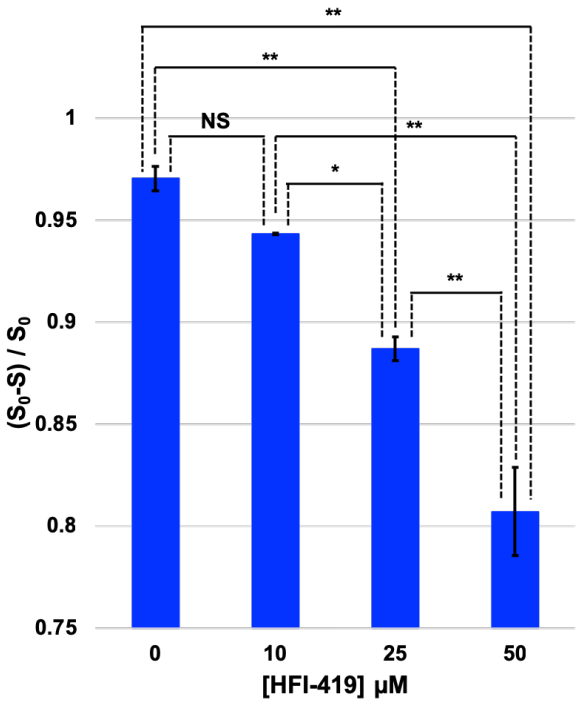

Figure 34 Effect of HFI-419 concentration on product formation. Statistical significance was determined using ANOVA followed by a Tukey test. The single asterisk (*) indicates p<0.05 and the double asterisk (**) indicates p<0.01. 'NS' indicates the differences were not significant (p>0.05). The error bars indicate the SEM of n = 9 replicates for 0 µM inhibitor (3 replicates from each rat) and n = 3 replicates for the 10, 25, and 50 µM inhibitor concentrations.

4.3 Discussion

4.3.1 Using yaGfl as a Mass Transport Standard

To determine the relative amount of peptide substrate that is hydrolyzed in the tissue, we must know the initial substrate concentration. The laboratory concentration of the substrate in the source probe is known but becomes lower due to dilution upon introduction to the tissue.[148] Thus,

we do not know the concentration of the substrate in the tissue through which we are sampling. A standard that has similar diffusion characteristics as the substrate but is resistant to hydrolysis is necessary as a surrogate for the bioactive peptide. We use this to infer the amount of substrate that would have been recovered in the absence of hydrolysis.

Fig 32 shows that the collected yaGfl concentration was similar to that of LE *in vitro*. Thus, yaGfl has similar electroosmotic transport through the hydrogel as LE and can be used as a mass transport standard. The concentration of yaGfl collected in the *in vivo* experiments was not significantly different from that in the *in vitro* experiment, suggesting that yaGfl is not hydrolyzed to a measurable extent in the tissue. We can use the collected yaGfl levels as a substitute for the concentration of LE that would be recovered in the absence of hydrolysis.

The concentrations of LE and yaGfl in Fig 32c are significantly different at each current used *in vivo*. We attribute this difference to LE hydrolysis in the tissue. Accordingly, we detected the major product, GGFL. The sum of the concentrations of LE and GGFL do not equal that of yaGfl, suggesting that GGFL is further hydrolyzed.

4.3.2 Solute Collection Efficiency Depends on Current

Fig 33 shows increasing collection efficiency with decreasing current for the internal standard yaGfl. We can make qualitative observations about solute transport with EOP-MD using this plot. The fluorescence experiments shown in Fig 31 suggest that solute is transported around the MD probe due to low membrane permeability. The MD probe is not a perfect sink for solute. Thus, collection efficiency is dictated both by electroosmotic transport through the tissue and transport processes within the MD probe. Simulations of our two-probe EOPPP work in tissue cultures showed that, with similar current to that used here, solute transport is both by

electroosmosis and diffusion.[148] Increased currents resulted in increased recovery of analyte due to a greater contribution of convection compared to diffusion.[148] Fluid flow through the MD probe adds additional transport processes that result in the collection efficiency trend that we observed with EOP-MD.

Fluid flow through the MD probe augments the diffusion-dominated mass transport, not by pushing solute where it needs to go, but by replenishing the solute within the diffusion layer in the fluid near the inner membrane wall.[131] Increasing the flow velocity through the MD probe increases mass transport by a power less than one. [131] The flow velocity through the probe also controls the residence time of the solute in the membrane area of the probe. This time is linearly related to flow rate.[131, 306] The result is that the total mass collected within the probe per unit time *decreases* per unit time. It increases by a fractional power due to faster mass transport but decreases by the power -1 due to the residence time.[306] For a steady concentration outside the probe, the collection efficiency *decreases* with increasing flow rate.

The combination of solute transport through the tissue and the MD probe results in the observed changes in yaGfl collection efficiency with changing current. For LE, we observed decreasing collection efficiency with decreasing current. This is due to lower solute velocity through the tissue at lower currents and thus higher residence time. In-depth simulations are required to quantitatively understand the relationship between current and collection efficiency.

Qualitatively, we can use Fig 33 to determine the appropriate current to use for a particular application. The optimum current depends on the application. We chose to perfuse substrate using 15 μA. In our case of looking at enzyme inhibition, we expect an increase in substrate concentration. Thus, low substrate recoveries as a result of a low current are not detrimental. In observing at a process that would decrease the substrate concentration, such as upregulation of the

ectopeptidase, a higher current, and thus higher substrate recovery, would be beneficial so that a decrease could be detected.

At 15 μA the sum of the concentrations of LE and GGFL was less than the concentration of yaGfl (Fig 32c). This suggests that GGFL is further hydrolyzed in the tissue. For this reason, we cannot make conclusions about product formation based on measured GGFL levels. By subtracting the ratio of hydrolyzed substrate ([LE] = [S]) to substrate concentration in the absence of hydrolysis ([yaGfl] = [S_0]) from 1, we have a measure of the concentration of product formed from LE hydrolysis ([P]).

4.3.3 Observing Changes in LE Hydrolysis in the Extracellular Space

To demonstrate the utility of the dual probe EOP-MD technique, we perfused the tissue in the presence and absence of the IRAP inhibitor HFI-419 within the same rat. Initially, we perfused the inhibitor at a concentration of 50 μM and, as shown in Fig 33, we observed a statistically significant ($p < 0.01$) decrease in product formation at that concentration compared to perfusing the same concentration of substrate without inhibitor. This shows that we can sample the tissue under two different conditions (with and without inhibitor in our case) and observe differing effects as a result. We then wanted to see if the EOP-MD technique is sensitive to changes in inhibitor concentration, so we repeated the experiment at 10 μM and 25 μM inhibitor concentrations. The results in Fig 33 show that our technique is capable of detecting differences in product formation with different inhibitor concentrations. More replicates and a wider range of inhibitor concentrations would be required to draw biological conclusions pertaining to IRAP activity in this region, but these results demonstrate that EOP-MD could be used to gain insight into this

ectopeptidase with further studies. This technique could also be used with a variety of inhibitors as well as other exogenous substances for the study of ectopeptidases.

4.3.4 Tissue Perturbation with EOP-MD

Though the purpose of this study was primarily technical and not biological in nature, it is important to assess the extent of tissue perturbation when sampling the extracellular space. Prior work in our lab has shown that electric fields used in this work should result in minimal cell death [284, 305] and we did not observe any visible defects in the tissue post-mortem, aside from the probe track (Fig S36). Electric fields have been used in the brain in other *in vivo* work, such as to guide stem cells[307] and deliver drugs electrokinetically[304]. Fekete, et al. performed iontophoretic injections of a biotinylated dextran amine tracer using 3-5 μA pulses and recorded neural activity with an integrated microelectrode array.[308] They found that tissue damage appeared to occur from insertion of the probe itself but delivery of the tracer was not affected by this.

A histological study assessing damage from pressure-driven low-flow push-pull perfusion at 50 nL/ min saw 20-30% of cell damage surrounding the probe [309] compared to 10% seen in our past EOPPP histological work [305]. Based on the applied current of 15 μA used in this work, the electroosmotic flow rate was calculated to be approximately 9 nL/ min. [148] Nonetheless, a rigorous assessment of tissue damage resulting from this EOP-MD technique is necessary to fully understand it's effect on sampling and for comparison to other techniques.

4.4 Conclusion

We have developed a sampling method known as EOP-MD that allows quantitative study of ectopeptidases *in vivo* using natural substrates. To our knowledge, this is the first report of such a technique. We have described the development of this technique and demonstrated that it is capable of measuring dose-dependent changes in LE hydrolysis with the IRAP inhibitor HFI-419. Simulations of solute transport and histological studies assessing tissue damage as a result of this technique will aid in the application of EOP-MD for biological studies concerning ectopeptidase activity.

4.5 Methods

4.5.1 Direct Laser Writing

The perfusion probe consisted of three main parts: two inlet ports through which capillaries are inserted, two outlet ports through which fluid exits the probe, and a tube for microdialysis probe mounting and alignment. The overall dimensions of the probe were 2023 μm (W) x 1015 μm (L) x 3650 μm (H). The inlet ports were 150 μm in diameter and the outlet ports were 50 μm in diameter. The narrow shaft of the probe (containing the outlet ports) was 150 μm wide and 850 μm long. The microdialysis probe holder had a diameter of 310 μm.

The pattern for perfusion probe was designed in Solidworks and printed by 3D direct laser writer (Nanoscribe Photonic Professional, GT) with IP-S photopolymetric resist. The printing was done through two-photon polymerization of IP-S resist by a femtosecond pulsed laser at 780 nm.

The Nanoscribe direct laser writer uses a Gaussian laser beam and a unique deep-in-liquid mode to print large-height patterns, as well as minimize optical aberration.

To fabricate the perfusion probe, the 3D model of the pattern was saved in STL file then converted into GWL (General Writing Lithography) file through DeScribe conversion software. During file conversion, the pattern was sliced and hatched, with a slicing distance of 1 μm and a hatching distance of 0.5 μm. The pattern was hatched with the shell and scaffold mode which creates a hollow structure to reduce the printing time significantly. Subsequently, the whole pattern was split into blocks of 220 μm × 220 μm × 200 μm, with a stitching overlap of 2μm. After conversion, the GWL file was loaded into the printing software, Nanowrite, for printing. In the printing, a 25x objective lens and ITO-coated glass substrate were used. The laser power was set to 100 mW and writing speed was set to 100 mm/s.

After printing was done, the structure was developed in a propylene glycol monomethyl ether acetate (PGMEA) bath overnight to wash out unpolymerized photoresist in the channels inside the structure. After the structure was naturally dried in the air, it was placed under UV lamp for 30 min with 16 mW/cm^2 intensity. This polymerizes the photoresist trapped in the shell/scaffold structure to make the whole structure more rigid and robust.

To inspect the printed structure, it was sputter-coated with about 10 nm AuPd for scanning electron microscopy (SEM).

4.5.2 EOP-MD Probe Assembly

The steps of the EOP-MD probe assembly are shown in Figure 37. Prior to assembly (Fig 37a), the EOP tip was fixed to a piece of tape using a small dot of 5-minute epoxy (Devcon, Danvers, MA). This permitted handling of the tip during assembly and allowed easy removal from

the tape once finished. Two sections of 75 μm ID x 150 μm OD capillary (Polymicro) were cut, each 1 cm in length. Each capillary was then pushed into one of the channels of the EOP tip until it could go no further (Fig 37b). Then, a 15 cm length of 200 μm ID x 360 μm OD capillary was threaded over the top of the 75 μm ID capillary to a distance approximately 0.5 cm from the start of the EOP tip, leaving a 0.5 cm portion of the 75 μm ID capillary exposed. A drop of 2-ton epoxy (Devcon) was placed onto the exposed portion of the 75 μm ID capillary and the 200 μm ID capillary was immediately pushed over the glue and into the EOP probe channel. The EOP probe channel is tapered so that the 200 μm ID capillary can only advance 1 mm into the channel. Applying the glue in this way serves to seal the junction between the 75 μm ID capillary and the 200 μm ID capillary and to seal the area between the 200 μm ID capillary and the channel of the EOP tip. Attaching the 200 μm ID/ 360 μm OD capillary to the 75 μm ID/ 150 μm OD capillary allows easier handling, as the 75 μm ID/ 150 μm OD capillary is rather fragile. This allows easy assembly with the Nafion tubing. After the epoxy has cured completely, each channel is tested for leaks by flushing the capillaries with water via a syringe.

Microdialysis probes were assembled by first cutting two 5-cm lengths of 40 μm ID/ 100 μm OD fused silica capillary (Polymicro). The capillaries were placed side-by-side with the ends staggered by 1 mm. The “longer” end was the microdialysis outlet while the “shorter” end was the inlet. A 13 kDa Spectra/ Por hollow fiber microdialysis membrane (Spectrum, Los Angeles, CA) 3 mm in length was then placed over the two capillaries and the open end of the membrane sealed with 2-ton epoxy. After the epoxy was completely cured, the membrane was pushed down so that it was as close to the outlet capillary as possible without touching it. The probe was then threaded through the 250 μm tube integrated on the EOP tip. The membrane was sealed around the capillaries by placing a drop of epoxy at the end of the tube furthest from the tip. This also served

to fix the microdialysis probe in position, approximately 100 μm from the EOP tip. The probe was positioned so that the inlet capillary was closest to the EOP tip.

Nafion tubing was used to allow the movement of ions through the channels of the EOP tip, into the tissue or hydrogel, and to the microdialysis probes. An 8-cm length of 200 μm ID/ 360 μm OD capillary was threaded approximately 0.5 cm into one end of a 2-cm length of a 0.014 (± 0.002, tolerance) in. ID x 0.021 (± 0.003, tolerance) in. OD Nafion tubing (Perma Pure, Lakewood, NJ). A 5-cm length of 200 μm ID capillary was threaded in the same way on the other end. Both Nafion-capillary junctions were sealed with 2-ton epoxy and cured overnight. A small hole was punctured in the bottom of a 3-cm plastic centrifuge tube (Fisher) and the capillary was threaded through the tube until the tube was surrounding the Nafion membrane with the 5-cm length capillary at the bottom of the tube. The area between the tube and the capillary was then sealed with epoxy. The 8-cm length of capillary was connected to a channel on the EOP tip using a PTFE sleeve while the distal end of the capillary-Nafion apparatus was placed through a hole in the top of a microcentrifuge tube (Fisher). This tube acted as the sample reservoir and also had a hole in the bottom of the tube through which a 1-cm length of polyethylene tubing (0.38 mm ID x 1.09 mm OD, Becton Dickinson, Sparks, MD) was threaded. Each channel of the EOP tip was connected to a separate Nafion apparatus.

4.5.3 Electroosmotic Perfusion

To fill the channels, an insulin syringe (Becton Dickinson) was filled with the perfusion solution and inserted into the polyethylene tubing contained in the sample reservoir. The capillary corresponding to a particular channel was threaded into the other end of the polyethylene tubing

and the microcentrifuge tube filled with the remaining perfusion solution using a pipette. The channel was filled with the insulin syringe until several drops were observed coming out of the EOP tip. At that point, the distal end of the capillary (furthest from the animal) was removed from the polyethylene tubing, followed by the syringe. This ensured that the end of the capillary remained in contact with the perfusion solution at all times and prevented bubbles from entering the system.

After each channel was filled with the desired solution, each centrifuge tube surrounding the Nafion was filled with the modified Ringer's solution. The inlet of the microdialysis probe was also connected to a Nafion apparatus and the centrifuge tube contained on it was similarly filled. To perfuse the solution of a particular channel, a silver electrode was placed in that channel's centrifuge tube surrounding the Nafion. The electrode was connected to the positive terminal of the high voltage power supply via an alligator clip. A silver electrode was also connected to the negative terminal and placed in the centrifuge tube contained on the inlet of the microdialysis probe. The desired current was set on the power supply and the voltage continually adjusted to maintain that current. A schematic of the sampling procedure in the context of a rat can be found in Figure 30.

4.5.4 Hydrogels

Hydrogel pieces were synthesized as previously described by Faraji et al.[303] Poly(acrylamide-*co*-acrylic acid) hydrogels were prepared by a thermally-initiated radical polymerization reaction. The gel had an acrylic acid percentage of 25%; weight of acrylic acid (69.0 mg)/weight of all monomer species (206.0mg). The bisacrylamide cross-linker was maintained at a fixed weight percentage of approximately 1.4% (4.0mg). Reagents were weighed

and dissolved in 4.5 mL of ultrapure water (Cayman Chemical, Ann Arbor, MI) and stirred for 5 minutes. The pH was adjusted to a range between 7-8 using 1 M NaOH solution. Ultra-pure water was used to adjust the final volume to 5 ml. The solutions were then deaerated with nitrogen for 20 minutes at room temperature and 5.0 mg of ammonium persulfate (0.02 mmol) and 5.2 µL of tetramethylethylenediamine (TEMED, 0.03 mmol) were added to each solution. After vigorously stirring at room temperature, the solution was poured in a 50 mm x 16 mm Pyrex glass dishes and placed inside an oven at 100 ± 5 °C for 2 hours. The Pyrex dishes were removed from the oven and allowed to cool for 10 minutes. Next, each gel was individually placed in a covered plastic dish filled with approximately 25 mL Glucose Free-Hank's Balanced Salt Solution (GF-HBSS) solution and shaken lightly at 10°C overnight. The buffer solution was exchanged the following day with fresh GF-HBSS, placed back in the shaker at 10 °C for another 24 hours. To end, the GF-HBSS was exchanged once more, and the gels were placed in the refrigerator to complete the equilibration. The pH was checked to assure the gels were pH 7.40.

4.5.5 Fluorescent Dyes

To observe EOP of fluorescent dyes *in vitro*, a 3 kDa dextran Texas Red dye (Molecular Probes, Eugene, OR) was prepared at a concentration of 166 µM in Modified Ringer's. A 1 mM tris(2,2'-bipyridyl)dichlororuthenium(II) hexahydrate (abbreviated $Ru(bpy)_3^{2+}$, Aldrich, Milwaukee, WI) solution in Modified Ringer's was also used. The Modified Ringer's solution consisted of 148 mM NaCl (EMD-Millipore, Darmstadt, Germany), 2.7 mM KCl (Sigma-Aldrich), and 0.85 mM $MgCl_2$ (Fisher Scientific) adjusted to a pH of 7.4. All dye solutions were filtered with a 0.20 µm PES syringe filter (Corning Inc., Corning, NY) prior to use.

4.5.6 Fluorescent Studies

All fluorescent studies were conducted using an Olympus IX-81 fluorescent microscope equipped with an inverted stage and an ORCA-ER high-resolution charged-coupled device camera. The MetaMorph 7.6.2.0 software (MDS Analytical Technologies, Sunnyvale, CA) was used to capture the images along with an Olympus 4x objective lens. Images were analyzed using NIS Elements Advanced Research software version 4.0 (Nikon Instruments, Inc.). The threshold function within the NIS Elements software was used to remove the background then the percent fluorescence of the image was recorded. Surface intensity plots were also generated using the NIS Elements software, where intensities range from 0 (black) to 365 (white).

To conduct the fluorescent experiments, a small section of hydrogel (approximately 2 cm x 2 cm x 5 mm thick) was placed on the microscope stage and the EOP-MD tip was inserted about 1 mm into the hydrogel. The tip was inserted at an angle to minimize the impact of the background fluorescence of the tip. The desired current was induced using a Stanford Research Systems model PS350 high-voltage source in which the positive terminal was connected to a silver wire placed in the buffer surrounding the Nafion on the EOP capillary using an alligator clip and the negative terminal was connected to the MD probe in the same way. The power supply was operated by specifying the desired current and the applied voltage was continually adjusted to achieve that current. Each dye was perfused for 1 hour and images were acquired every 5 minutes. The emission/ excitation wavelengths for each dye were 535/ 610 for Texas Red and 475/ 602 for $Ru(bpy)_3^{2+}$. Only one channel of the EOP-MD probe contained dye at a time due to overlapping wavelengths between Texas Red and $Ru(bpy)_3^{2+}$.

4.5.7 Offline Labeling

To minimize analysis time, heavy peptide standards were prepared using an offline dimethylation procedure described previously[310] with a few modifications. Stock solutions of LE (American Peptide, Sunnyvale, CA), GGFL (American Peptide), yaGfl (GL Biochem, Shanghai, China), and yasfl (Shanghai Royobiotech, Shanghai, China) were prepared by diluting each solid to a concentration of 1 mM in water purified using a Millipore Milli-Q Synthesis A10 filtration system (Billerca, MA). Serial dilutions were then performed until a concentration of 5.3 nM was obtained for each peptide. An aliquot of 49.6 μL of each peptide was then added to an autosampler vial (Thermo Scientific, Rockwood, TN) along with 2 μL of glacial acetic acid (Fisher Chemical, Fair Lawn, NJ). Multiple vials were prepared simultaneously then frozen at -20 °C until needed. On the day of an experiment, a vial was thawed and a volume of 8 μL of 4% formaldehyde-d_2 (Sigma-Aldrich, St. Louis, MO) was added and the mixture vortexed. Next, 8 μL of 600 mM sodium cyanoborohydride (Sigma-Aldrich) was added to the autosampler vial, vortexed, and allowed to react for 5 minutes. The reaction was then quenched with the addition of 32 μL of 1% ammonium hydroxide (Sigma-Aldrich), vortexed again, and allowed to react for 1 minute. Finally, 16 μL of 5% formic acid (Sigma-Aldrich) was added to the autosampler vial, after which the mixture was vortexed a final time and placed in the refrigerated autosampler at 5 °C. The final concentration of each peptide in the sample was approximately 1 nM.

4.5.8 Online Labeling

Primary amines in the dialysate were "light" labeled using an on-column procedure described previously.[97] Briefly, at the start of each analysis, 1.1 μL of the heavy labeled standard (prepared as described in the previous section) was injected onto the column via the autosampler. Next, 1.1 μL of dialysate was injected onto the column via the "sample valve" housed in the LC oven. The light labeling reagent, consisting of 350 μL of triethylammonium acetate (100 mM triethyl amine (Sigma-Aldrich) titrated with 100 mM acetic acid to a pH of 7.4), 3.50 μL of 0.6 M sodium cyanoborohydride, and 3.50 μL of 4% formaldehyde (J. T. Baker, Phillipsburg, NJ), was then injected onto the column followed by 5% formic acid. Each reagent was injected at a volume of 1.1 μL.

4.5.9 HPLC Instrumentation

The cLC separation was achieved using a Dionex Ultimate 3000 HPLC system (NCS-3500RS, Thermo Scientific, Germering, Germany), which consisted of a low-flow loading pump, a high-pressure analytical pump fitted with a nanoflow selector, and a column oven in which a 10-port Cheminert high-pressure 1/16 in. valve (VICI, Valco, Houston, TX) was housed. The column oven valve was fitted with a 1.1 μL sample loop through which dialysate was collected and injected. The Dionex WPS-3000 RS autosampler was used for heavy standard and reagent injections at a volume of 1.1 μL. The autosampler was maintained at 5 °C.

4.5.10 Chromatography Columns

Reversed phase capillary columns were packed in-house as described previously[152]. Briefly, a 20-cm length of 50 μm ID fused silica capillary (Polymicro, Phoenix, AZ) was fritted by sintering 2 μm borosilicate spheres (Thermo Scientific, Fremont, CA) in one end of the capillary using an electrical arc. A 65 mg/ mL slurry of Acquity 5 μm BEH C18 particles (Waters, Milford, MA) was prepared in isopropanol (Fisher Chemical) and packed into the capillary at 18000 PSI using methanol as the packing solvent. The column was trimmed to 15 cm and connected to a 25 μm ID x 15 cm length of fused silica capillary (Polymicro) via a liquid junction tee (Idex, Oak Harbor, WA). The 25 μm ID capillary was then connected to a 6-port 1/16 in. Cheminert high-pressure valve (VICI, Valco) that was housed on the MS stage. The valve was plumbed so that flow could be directed through the capillary and into the column from either the loading pump (during labeling) or the analytical pump (during elution). The column was housed on a resistive heater held at 50 °C. The fritted end of the column was connected to a fused silica PicoTip emitter (New Objective, Woburn, MA) with a tip ID of approximately 10 μm via a PTFE sleeve.

4.5.11 Mobile Phases

The loading pump solvent consisted of 0.5% acetic acid, 2% Optima LC-MS grade methanol (Fisher Chemical, Fair Lawn, NJ), and 97.5% Optima LC-MS grade water (Fisher Chemical) mixed v/v. For the analytical pump, channel A contained 0.5% acetic acid in water while channel B consisted of 0.5% acetic acid in methanol. All solvents were used as received from the manufacturer.

4.5.12 Chromatography

The dialysate sample and labeling reagents were delivered onto the column using the loading pump (containing 0.5% acetic acid/ 2% methanol/ 97.5% water) at a flow rate of 1 μL/ min. After the labeling steps were completed, a valve was switched, and 45% B was delivered onto the column via the analytical pump at 0.5 μL/min. This effectively created a step gradient. This mobile phase composition was maintained for 5.5 minutes, after which it was increased to 85% B (nominally in 0.1 minutes) for 0.2 minutes to elute highly hydrophobic contaminants then decreased to 2% B (in 0.1 minutes) to allow the column to re-equilibrate for 1 minute prior to the start of the next run. The analysis time for a single run including labeling steps was 19 minutes. To prevent build-up of salts and contaminants on the MS inlet, the column was manually moved out of line with the inlet using the micromanipulators equipped on the MS stage then placed back in line with the inlet immediately prior to the elution step.

4.5.13 Mass Spectrometry

LC-MS^2 analysis was performed using positive ion mode nanospray ionization with an LTQ XL linear ion trap mass spectrometer (Thermo Scientific). A spray voltage of 2.3 kV was applied at the head of the column via the liquid junction tee. MS^2 was performed using collision induced dissociation with a normalized collision energy of 35 and an activation time of 30 ms. Precursor and daughter ions were chosen based on a method described previously and were analyzed in the same way[97]. The ions used for MS^2 fragmentation and extracted ion chromatograms can be found in Table 10. To confirm that the method was capable of detecting relevant concentrations of peptides, we constructed a calibration curve (Fig 35) using a serial

dilution of peptide standards in Modified Ringer's from 6.25 nM to 0.019 nM. Based on the standard deviation of replicates (n = 3) for the lowest concentration used and the slope of the calibration curve (Table 11), it was determined that the detection limit was approximately 3.2 ± 0.1 pM for yaGfl, 7.2 ± 0.8 pM for LE, and 22 ± 3 pM for GGFL.

4.5.14 Animal Surgeries

All procedures involving animals were approved by the Institutional Animal Care and Use of Committee of the University of Pittsburgh. Male Sprague-Dawley rats (250-350 g, Hilltop, Scottsdale, PA) were anesthetized with isoflurane (5% induction, 2.5% maintenance), placed in a stereotaxic frame (David Kopf Instruments, Tujunga, CA, USA) and adjusted to flat skull for probe insertion. The incisor bar was adjusted so the dorsal ventral measurements at lambda and bregma were no more than 0.01 mm apart. Rats were wrapped in a heating blanket (37°C) and placed in a stereotaxic frame. A small craniotomy was made over the PFC. Probes were lowered slowly (10 μm/sec) into the PFC (2.3 mm anterior and 3.0 mm lateral from bregma) to final position of 3 mm below dura. Aseptic technique was used throughout.

4.5.15 In Vivo Sampling

The EOP-MD probe was soaked in 70% ethanol (Decon, King of Prussia, PA) for 20 minutes. A solution of 100 nM yasfl in Modified Ringer's was then perfused through the microdialysis probe at a flow rate of 0.5 μL/ min using a Harvard Apparatus PHD 4400 programmable syringe pump (Holliston, MA). The inclusion of yasfl in the perfusate served as a control to ensure the MD probes were working as expected.[97] One channel of the EOP portion of

the probe was filled with a solution of 10 μM LE and yaGfl in Modified Ringer's while the other channel was filled with a Modified Ringer's solution also containing 10 μM LE and yaGfl as well as the HFI-419 IRAP inhibitor (a gift from Dr. Philip Thompson at Monash University). The HFI-419 concentration (10, 25, and 50 μM) was varied between each rat (n = 3). To check for the presence of bubbles, the probe was lowered into a 1-dram vial containing Modified Ringer's and current was applied for 5 minutes for each channel. Absence of current as voltage is applied is indicative of a bubble. Once it was apparent that the current was sufficiently stable, the current was turned off and the probe lowered into the PFC. Flow was continuous through the microdialysis probe during insertion. After 1.5 hours, the current from the high voltage power supply was induced and sampling of the peptide solution not containing inhibitor began. The waiting period was necessary to achieve steady-state between the tissue and the microdialysis probe as well as a stable baseline. Sampling occurred for 35 minutes prior to the first injection and was continuous for 2 hours after which the current was stopped, and the electrode moved to the second (peptide + inhibitor) channel. Current was then applied for another 2 hours, after which the electrode was moved back to the peptide channel. Sampling then continued for another hour.

4.5.16 Data Analysis

For each rat, 6 baseline measurements (no inhibitor) were recorded followed by 6 measurements in the presence of inhibitor (at either 10, 25, or 50 μM). The final 3 measurements for each condition (with or without inhibitor) were used for analysis. The relative area for each peptide was determined by taking the peak area of the light peptide (from dialysate) and dividing it by the peak area of the 1 nM heavy peptide standard. The relative area was then converted to a

concentration using the regression in Table 11. Data were analyzed using Minitab Express (State College, PA). Significance was determined using one-way ANOVA followed by Tukey tests.

4.6 Supporting Information for Electroosmotic Perfusion-Microdialysis

Table 10 Selected Ions for Fragmentation and Quantitation of Neuropeptides

[a]Isolation widths were 3 m/z
[b]Tolerance was ± 0.5 m/z

Peptide	Abbreviation	Precursor m/z[a]	Daughter m/z[b]
Dimethyl GGFL	Light GGFL	421.20	143 + 290
$^{2}H_4$ Dimethyl GGFL	Heavy GGFL	425.20	147 + 294
Dimethyl LE	Light LE	584.30	425 + 453
$^{2}H_4$ Dimethyl LE	Heavy LE	588.30	429 + 457
Dimethyl yaGfl	Light yaGfl	598.30	439 + 467
$^{2}H_4$ Dimethyl yaGfl	Heavy yaGfl	602.30	443 + 471
Dimethyl yasfl	Light yasfl	628.30	479 + 497
$^{2}H_4$ Dimethyl yasfl	Heavy yasfl	632.30	483 + 501

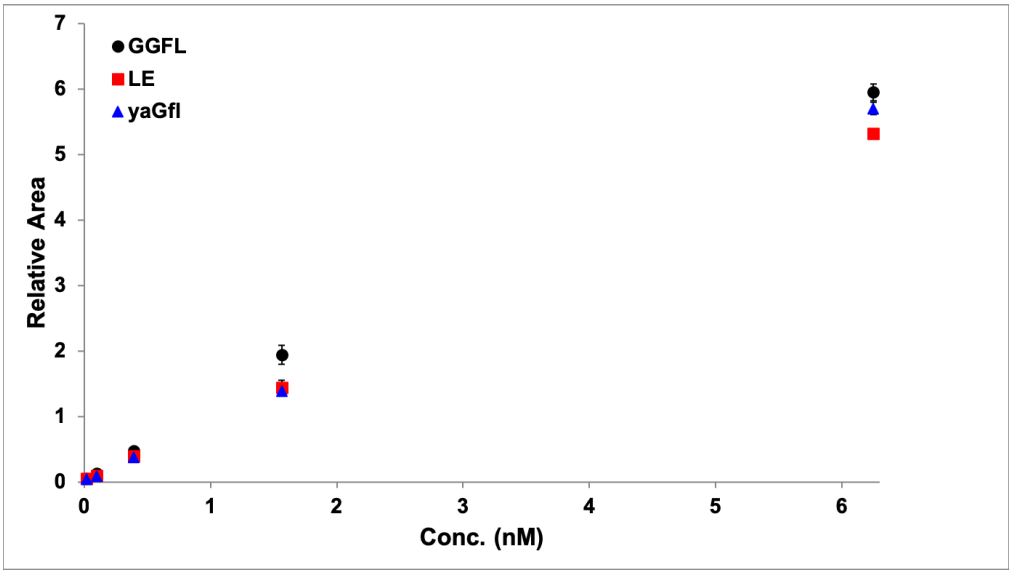

Figure 35 Calibration curve obtained using a serial dilution of GGFL (black circles), LE (red squares), and yaGfl (blue triangles) in Modified Ringer's. The relative area refers to the area of the light-labeled standard prepared in varying concentrations divided by that of the heavy-labeled standard (1 nM). Error bars represent the SEM of n = 3 replicates.

Table 11 Regression Statistics for Figure 35

[a]Unitless

Peptide	Slope ± SEM (nM^{-1})	Intercept ± SEM[a]
GGFL	0.94 ± 0.04	0.1 ± 0.1
LE	0.846 ± 0.008	0.05 ± 0.02
yaGfl	0.911 ± 0.005	0.00 ± 0.01

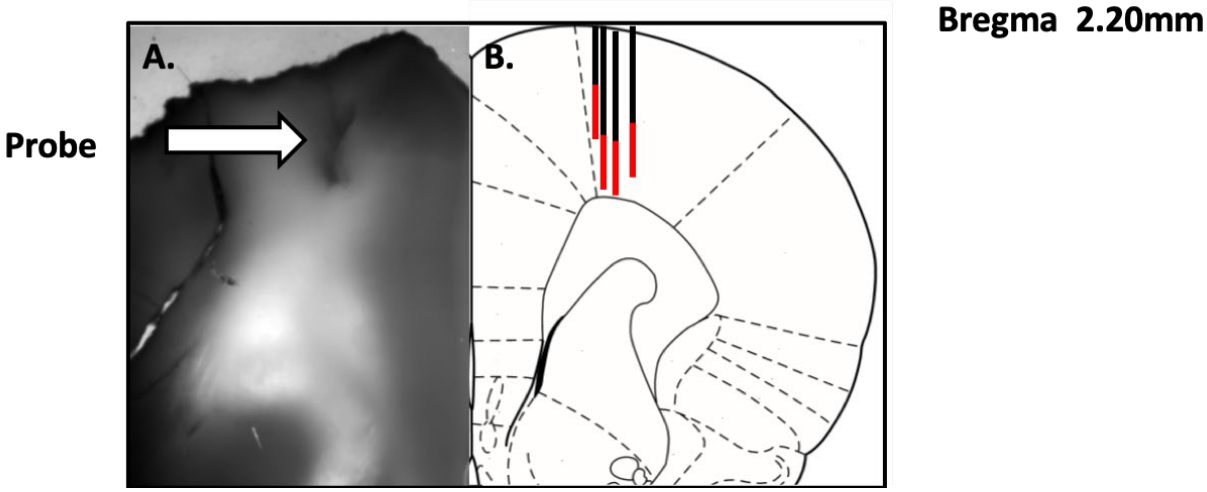

Figure 36 Localization of microdialysis probes in the rat brain. (A) Representative microdialysis probe track. (B) Schematic reconstructions of positions of the electroosmotic perfusion – microdialysis (EOP-MD) probe in the rat brain. One millimeter coronal slices demonstrate that microdialysis membranes are located in the PFC region. Arrow represents the probe location. The red color represents the active area of the probe.

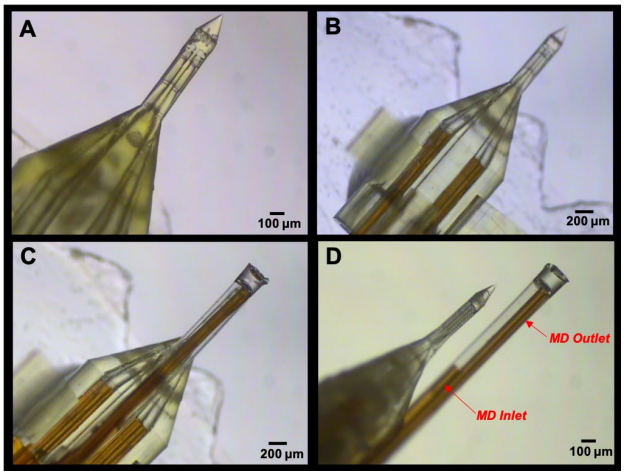

Figure 37 EOP-MD probe assembly. Fig 37a depicts the probe following printing. It is temporarily affixed to a piece of tape using epoxy so that the 150 µm OD/ 75 µm ID capillaries could be inserted into each channel (Fig 37b). The MD probe is then inserted through the integrated microdialysis probe holder. Fig 37c depicts the assembled EOP-MD probe looking down from the MD probe and Fig 37d shows the space between the EOP tip and the MD probe. For more details see the Methods section.

5.0 Concluding Remarks

This dissertation described the development of analytical tools for quantitatively studying the fate of neuropeptides in the extracellular space. We have approached the challenges of studying neuropeptides *in vivo*, including low analyte concentration and sample loss upon collection, by applying novel approaches to improve capillary liquid chromatograpy (cLC) separation and detection and by designing sampling probes for the study of ectopeptidases. Using temperature-assisted solute focusing (TASF), in which sub-ambient temperature transients resulted in improved peak shape for early-eluting analytes, we demonstrated improved detection limits for the reversed phase gradient elution of small molecules and peptides with cLC. We also applied the proteomics strategy of duplex dimethyl labeling of primary amines to the analysis of neuropeptides in microdialysate for a completely online approach to sample collection and analysis with cLC and tandem mass spectrometry (MS^2). Translating this approach to microdialysis required optimization for the analytes, buffers, and time scales necessary for online *in vivo* analyses and resulted in the first quantitative estimates of the neuropeptides leu-enkephalin and met-enkephalin in the rat hippocampus using cLC-MS^2. Finally, using direct laser lithography, we designed and produced an integrated dual-channel electroosmotic perfusion-microdialysis (EOP-MD) probe for the study of ectopeptidases, membrane-bound enzymes which hydrolyze neuropeptides, under matched conditions (± inhibitor). While further studies of solute transport and tissue damage are required for application of EOP-MD to biological questions, we have demonstrated that this is a promising technique for the quantitative study of ectopeptidases.

Acknowledgements

Funding for this work was provided by an Arts and Sciences Fellowship from the Kenneth P. Dietrich School of Arts and Sciences as well as the National Institutes of Health (R01 GM044842). Dr. Ed Bouvier and Dr. Moon Chul Jung, both of Waters Corporation, generously provided Acquity packing material used in all work described here. For the TASF and on-column dimethylation work, we would like to thank Anthony Horner (University of Pittsburgh) for assistance with the development of Matlab programs for the analysis of chromatograms as well as Bart Degreef (Vrije Universiteit Brussel) and the Dietrich School of Arts and Sciences Machine and Electronics Shops (Tom Gasmire, Josh Byler, and Jim McNerney) for help in designing and constructing TASF instrumentation and a custom MS stage. For the EOP-MD work, Dr. Philip Thompson (Monash University) provided us with the HFI-419 inhibitor and Dr. Amir Faraji (University of Pittsburgh Medical Center) provided helpful guidance for animal surgeries. Dr. Andrea Jacquins-Gerstl performed the animal surgeries and histology and provided expertise for *in vivo* experiments. Dr. Jun Chen provided expertise on direct laser lithography and fabricated the EOP-MD probes.

Bibliography

1. Antczak, C.; De Meester, I.; Bauvois, B., *BioEssays* **2001,** *23*, 251-260.

2. Konkoy, C. S.; Davis, T. P., *Trends in Pharmacological Sciences* **1996,** *17*, 288-294.

3. Iversen, L. L.; Lee, C. M.; Gilbert, R. F.; Hunt, S.; Emson, P. C., *Proc R Soc Lond B Biol Sci* **1980,** *210*, 91-111.

4. Pow, D. V.; Morris, J. F., *Neuroscience* **1989,** *32*, 435-439.

5. van den Pol, A. N., *Neuron* **2012,** *76*, 98-115.

6. Bodnar, R. J., *Peptides* **2014,** *62*, 67-136.

7. Klenowski, P.; Morgan, M.; Bartlett, S. E., *Br. J. Pharmacol.* **2015,** *172*, 297-310.

8. Ogren, S. O.; Kuteeva, E.; Elvander-Tottie, E.; Hokfelt, T., *Eur J Pharmacol* **2010,** *626*, 9-17.

9. de Wied, D.; Diamant, M.; Fodor, M., *Front Neuroendocrinol* **1993,** *14*, 251-302.

10. de Wied, D.; Sigling, H. O., *Neurotox Res* **2002,** *4*, 453-468.

11. Hoyer, D.; Bartfai, T., *Chem Biodivers* **2012,** *9*, 2367-87.

12. Albiston, A. L.; Diwakarla, S.; Fernando, R. N.; Mountford, S. J.; Yeatman, H. R.; Morgan, B.; Pham, V.; Holien, J. K.; Parker, M. W.; Thompson, P. E.; Chai, S. Y., *Br J Pharmacol* **2011,** *164*, 37-47.

13. Wotjak, C. T.; Landgraf, R.; Engelmann, M., *Pharmacol Biochem Behav* **2008,** *90*, 125-34.

14. Kandror, K.; Pilch, P. F., *Journal of Biological Chemistry* **1994,** *269*, 138-142.

15. Keller, S. R.; Scott, H. M.; Mastick, C. C.; Aebersold, R.; Lienhard, G. E., *J Biol Chem* **1995,** *270*, 23612-8.

16. Rogi, T.; Tsujimoto, M.; Nakazato, H.; Mizutani, S.; Tomoda, Y., *J Biol Chem* **1996,** *271*, 56-61.

17. Lew, R. A.; Mustafa, T.; Ye, S.; McDowall, S. G.; Chai, S. Y.; Albiston, A. L., *Journal of Neurochemistry* **2004,** *86*, 344-350.

18. Matsumoto, H.; Nagasaka, T.; Hattori, A.; Rogi, T.; Tsuruoka, N.; Mizutani, S.; Tsujimoto, M., *Eur. J. Biochem.* **2001,** *268*, 3259-3266.

19. Noble, F.; Banisadr, G.; Jardinaud, F.; Popovici, T.; Lai-Kuen, R.; Chen, H.; Bischoff, L.; Parsadaniantz, S. M.; Fournie-Zaluski, M. C.; Roques, B. P., *Neuroscience (Oxford, U. K.)* **2001,** *105*, 479-488.

20. Herbst, J. J.; Ross, S. A.; Scott, H. M.; Bobin, S. A.; Morris, N. J.; Lienhard, G. E.; Keller, S. R., *Am J Physiol* **1997,** *272*, E600-6.

21. Wallis, M. G.; Lankford, M. F.; Keller, S. R., *Am J Physiol Endocrinol Metab* **2007,** *293*, E1092-102.

22. Fernando, R. N.; Larm, J.; Albiston, A. L.; Chai, S. Y., *J Comp Neurol* **2005,** *487*, 372-90.

23. Albiston, A. L.; McDowall, S. G.; Matsacos, D.; Sim, P.; Clune, E.; Mustafa, T.; Lee, J.; Mendelsohn, F. A.; Simpson, R. J.; Connolly, L. M.; Chai, S. Y., *J Biol Chem* **2001,** *276*, 48623-6.

24. Mouw, D.; Bonjour, J. P.; Malvin, R. L.; Vander, A., *Am J Physiol* **1971,** *220*, 239-42.

25. Braszko, J.; Wisniewski, K., *Pol J Pharmacol Pharm* **1976,** *28*, 667-72.

26. Braszko, J. J., *J Pharm Pharmacol* **1981,** *33*, 192-3.

27. Köller, M.; Krause, H. P.; Hoffmeister, F.; Ganten, D., *Neuroscience Letters* **1979,** *14*, 71-75.

28. Baranowska, D.; Braszko, J. J.; Wisniewski, K., *Psychopharmacology* **1983,** *81*, 247-251.

29. Braszko, J. J., *Behavioural Brain Research* **2002,** *131*, 79-86.

30. Braszko, J. J., *Clin. Exp. Hypertens.* **2005,** *27*, 635-649.

31. Braszko, J. J.; Wisniewski, K., *Peptides (Fayetteville, N. Y.)* **1988,** *9*, 475-9.

32. Braszko, J. J.; Wisniewski, K.; Kupryszewski, G.; Witczuk, B., *Behav. Brain Res.* **1987,** *25*, 195-203.

33. Braszko, J. J.; Wlasienko, J.; Kupryszewski, G.; Witczuk, B.; Wisniewski, K., *Physiol. Behav.* **1988,** *44*, 327-32.

34. de Souza, F. A. M.; Sanchis-Segura, C.; Fukada, S. Y.; de Bortoli, V. C.; Zangrossi, H.; de Oliveira, A. M., *Neurobiol. Learn. Mem.* **2004,** *81*, 100-103.

35. Georgiev, V.; Yonkov, D., *Methods Find. Exp. Clin. Pharmacol.* **1985,** *7*, 415-18.

36. Yonkov, D.; Georgiev, V.; Kambourova, T.; Opitz, M., *Methods Find Exp Clin Pharmacol* **1987,** *9*, 205-8.

37. Yonkov, D.; Georgiev, V.; Opitz, M., *Methods Find. Exp. Clin. Pharmacol.* **1986,** *8*, 203-6.

38. Winnicka, M. M., *Pharmacol., Biochem. Behav.* **1999,** *62*, 625-630.

39. Albiston, A. L.; Pederson, E. S.; Burns, P.; Purcell, B.; Wright, J. W.; Harding, J. W.; Mendelsohn, F. A.; Weisinger, R. S.; Chai, S. Y., *Behav. Brain Res.* **2004,** *154*, 239-243.

40. Borawska, M.; Kupryszewski, G.; Witczuk, B.; Wisniewski, K., *Pol. J. Pharmacol. Pharm.* **1989,** *41*, 227-30.

41. Olson, M. L.; Olson, E. A.; Qualls, J. H.; Stratton, J. J.; Harding, J. W.; Wright, J. W., *Peptides (N. Y., NY, U. S.)* **2004,** *25*, 233-241.

42. Pederson, E. S.; Harding, J. W.; Wright, J. W., *Regul. Pept.* **1998,** *74*, 97-103.

43. Wright, J. W.; Clemens, J. A.; Panetta, J. A.; Smalstig, E. B.; Stubley Weatherly, L.; Kramar, E. A.; Pederson, E. S.; Mungall, B. H.; Harding, J. W., *Brain Res.* **1996,** *717*, 1-11.

44. Faure, S.; Bureau, A.; Oudart, N.; Javellaud, J.; Fournier, A.; Achard, J.-M., *J. Hypertens.* **2008,** *26*, 2008-2015.

45. Faure, S.; Oudart, N.; Javellaud, J.; Fournier, A.; Warnock, D. G.; Achard, J.-M., *J. Hypertens.* **2006,** *24*, 2255-2261.

46. Braszko, J. J.; Kupryszewski, G.; Witczuk, B.; Wisniewski, K., *Neuroscience* **1988,** *27*, 777-83.

47. Braszko, J. J., *Peptides (N. Y., NY, U. S.)* **2004,** *25*, 1195-1203.

48. Braszko, J. J.; Wlasienko, J.; Koziolkiewicz, W.; Janecka, A.; Wisniewski, K., *Brain Res.* **1991,** *542*, 49-54.

49. Braszko, J. J.; Walesiuk, A.; Wielgat, P., *J Renin Angiotensin Aldosterone Syst* **2006,** *7*, 168-74.

50. Stragier, B.; Sarre, S.; Vanderheyden, P.; Vauquelin, G.; Fournie-Zaluski, M.-C.; Ebinger, G.; Michotte, Y., *J. Neurochem.* **2004,** *90*, 1251-1257.

51. Beyer, C. E.; Dwyer, J. M.; Platt, B. J.; Neal, S.; Luo, B.; Ling, H. P.; Lin, Q.; Mark, R. J.; Rosenzweig-Lipson, S.; Schechter, L. E., *Psychopharmacology (Berl)* **2010,** *209*, 303-11.

52. De Bundel, D.; Demaegdt, H.; Lahoutte, T.; Caveliers, V.; Kersemans, K.; Ceulemans, A.-G.; Vauquelin, G.; Clinckers, R.; Vanderheyden, P.; Michotte, Y.; Smolders, I., *J. Neurochem.* **2010,** *112*, 1223-1234.

53. Stragier, B.; Hristova, I.; Sarre, S.; Ebinger, G.; Michotte, Y., *Eur J Neurosci* **2005,** *22*, 658-64.

54. Wright, J. W.; Miller-Wing, A. V.; Shaffer, M. J.; Higginson, C.; Wright, D. E.; Hanesworth, J. M.; Harding, J. W., *Brain Research Bulletin* **1993,** *32*, 497-502.

55. Wright, J. W.; Stubley, L.; Pederson, E. S.; Kramár, E. A.; Hanesworth, J. M.; Harding, J. W., *The Journal of Neuroscience* **1999,** *19*, 3952-3961.

56. Swanson, G. N.; Hanesworth, J. M.; Sardinia, M. F.; Coleman, J. K. M.; Wright, J. W.; Hall, K. L.; Miller-Wing, A. V.; Stobb, J. W.; Cook, V. I.; Harding, E. C.; Harding, J. W., *Regulatory Peptides* **1992,** *40*, 409-419.

57. Vanderheyden, P. M., *Mol Cell Endocrinol* **2009,** *302*, 159-66.

58. Albiston, A. L.; Fernando, R. N.; Yeatman, H. R.; Burns, P.; Ng, L.; Daswani, D.; Diwakarla, S.; Pham, V.; Chai, S. Y., *Neurobiol. Learn. Mem.* **2010,** *93*, 19-30.

59. Albiston, A. L.; Mustafa, T.; McDowall, S. G.; Mendelsohn, F. A. O.; Lee, J.; Chai, S. Y., *Trends in Endocrinology & Metabolism* **2003,** *14*, 72-77.

60. Chai, S. Y.; Fernando, R.; Peck, G.; Ye, S. Y.; Mendelsohn, F. A.; Jenkins, T. A.; Albiston, A. L., *Cell Mol Life Sci* **2004,** *61*, 2728-37.

61. Wright, J. W.; Harding, J. W., *Prog Neurobiol* **2011,** *95*, 49-67.

62. De Bundel, D.; Fafouri, A.; Csaba, Z.; Loyens, E.; Lebon, S.; El Ghouzzi, V.; Peineau, S.; Vodjdani, G.; Kiagiadaki, F.; Aourz, N.; Coppens, J.; Walrave, L.; Portelli, J.; Vanderheyden, P.; Yeen, C. S.; Thermos, K.; Bernard, V.; Collingridge, G.; Auvin, S.; Gressens, P.; Smolders, I.; Dournaud, P., *J. Neurosci.* **2015,** *35*, 11960-11975.

63. De Bundel, D.; Smolders, I.; Yang, R.; Albiston, A. L.; Michotte, Y.; Chai, S. Y., *Neurobiol Learn Mem* **2009,** *92*, 19-26.

64. Diwakarla, S.; Nylander, E.; Groenbladh, A.; Vanga, S. R.; Khan, Y. S.; Gutierrez-de-Teran, H.; Ng, L.; Pham, V.; Saevmarker, J.; Lundbaeck, T.; Jenmalm-Jensen, A.; Andersson, H.; Engen, K.; Rosenstroem, U.; Larhed, M.; Aaqvist, J.; Chai, S. Y.; Hallberg, M., *Mol. Pharmacol.* **2016,** *89*, 413-424.

65. Diwakarla, S.; Nylander, E.; Groenbladh, A.; Vanga, S. R.; Khan, Y. S.; Gutierrez-de-Teran, H.; Saevmarker, J.; Ng, L.; Pham, V.; Lundbaeck, T.; Jenmalm-Jensen, A.; Svensson, R.; Artursson, P.; Zelleroth, S.; Engen, K.; Rosenstroem, U.; Larhed, M.; Aaqvist, J.; Chai, S. Y.; Hallberg, M., *ACS Chem. Neurosci.* **2016,** *7*, 1383-1392.

66. Albiston, A. L.; Morton, C. J.; Ng, H. L.; Pham, V.; Yeatman, H. R.; Ye, S.; Fernando, R. N.; De Bundel, D.; Ascher, D. B.; Mendelsohn, F. A.; Parker, M. W.; Chai, S. Y., *FASEB J* **2008,** *22*, 4209-17.

67. Stragier, B.; Demaegdt, H.; De Bundel, D.; Smolders, I.; Sarre, S.; Vauquelin, G.; Ebinger, G.; Michotte, Y.; Vanderheyden, P., *Brain Res.* **2007,** *1131*, 97-105.

68. Albiston, A. L.; Peck, G. R.; Yeatman, H. R.; Fernando, R.; Ye, S.; Chai, S. Y., *Pharmacol Ther* **2007,** *116*, 417-27.

69. Andersson, H.; Hallberg, M., *Int. J. Hypertens.* **2012**, 789671, 18 pp.

70. Buchberger, A.; Yu, Q.; Li, L., *Annu. Rev. Anal. Chem.* **2015,** *8*, 485-509.

71. Kohsaka, A.; Watanobe, H.; Kakizaki, Y.; Suda, T., *Neuroendocrinology* **1999,** *69*, 245-53.

72. Mizuno, M.; Gearing, M.; Terasawa, E., *Endocrinology* **2000,** *141*, 1772-9.

73. Kent, P.; Anisman, H.; Merali, Z., *Neuroendocrinology* **2001,** *73*, 203-14.

74. Slaney, T. R.; Nie, J.; Hershey, N. D.; Thwar, P. K.; Linderman, J.; Burns, M. A.; Kennedy, R. T., *Anal. Chem. (Washington, DC, U. S.)* **2011,** *83*, 5207-5213.

75. Redgrave, P., *Pharmacology Biochemistry and Behavior* **1977,** *6*, 471-474.

76. Kottegoda, S.; Shaik, I.; Shippy, S. A., *Journal of Neuroscience Methods* **2002,** *121*, 93-101.

77. Dluzen, D. E.; Ramirez, V. D., *Pharmacology Biochemistry and Behavior* **1986,** *24*, 147-150.

78. Ungerstedt, U.; Hallström, Å., *Life Sciences* **1987,** *41*, 861-864.

79. Watson, C. J. V., B. J.; Kennedy, R. T., *Anal. Chem.* **2006**, 1392-1399.

80. Lanckmans, K.; Sarre, S.; Smolders, I.; Michotte, Y., *Rapid Commun Mass Spectrom* **2007,** *21*, 1187-95.

81. Zhou, Y.; Wong, J. M.; Mabrouk, O. S.; Kennedy, R. T., *Anal Chem* **2015,** *87*, 9802-9.

82. Wilson, S. R.; Vehus, T.; Berg, H. S.; Lundanes, E., *Bioanalysis* **2015,** *7*, 1799-815.

83. Desmet, G.; Eeltink, S., *Analytical chemistry* **2013,** *85*, 543-56.

84. Gilar, M. M., T. S.; Roman, G.; Johnson, J. S.; Murphy, J. P.; Jorgenson, J. W. , *J. Chromatogr. A.* **2015,** *1381*, 110-117.

85. Snyder, L. R. K., J. J; Dolan, J. W., *Introduction to Modern Liquid Chromatography*. Third ed.; John Wiley and Sons, Inc.: Hoboken, N.J., 2010.

86. Heron, S. T., A.; Chervet, J.-P., *Chromatographia* **2000,** *51*, 495-499.

87. Foster, M. D. A., M. A. Nichols, J. A.; Bakalyar, S. R., *J. Chromatogr. A* **2000,** *869*, 231-241.

88. Molander, P. T., S. J.; Bruheim, I. A.; Trones, R.; Greibrokk, T.; Lundanes, E.; Gundersen, T. E. , *J. High Resol. Chromatogr.* **1999,** *22*, 490-494.

89. Leon-Gonzalez, M. E.; Rosales-Conrado, N.; Perez-Arribas, L. V.; Polo-Diez, L. M., *J. Chromatogr. A* **2010,** *1217*, 7507-13.

90. Collins, D.; Nesterenko, E.; Connolly, D.; Vasquez, M.; Macka, M.; Brabazon, D.; Paull, B., *Analytical chemistry* **2011,** *83*, 4307-13.

91. Causon, T. J.; Cortes, H. J.; Shellie, R. A.; Hilder, E. F., *Analytical chemistry* **2012,** *84*, 3362-8.

92. Emmett, M. R.; Andren, P. E.; Caprioli, R. M., *J. Neurosci. Methods* **1995,** *62*, 141-147.

93. Lanckmans, K.; Stragier, B.; Sarre, S.; Smolders, I.; Michotte, Y., *Journal of separation science* **2007,** *30*, 2217-24.

94. André, P. E.; Caprioli, R. M., *Journal of Mass Spectrometry* **1995,** *30*, 817-824.

95. Haskins, W. E.; Watson, C. J.; Cellar, N. A.; Powell, D. H.; Kennedy, R. T., *Anal Chem* **2004,** *76*, 5523-33.

96. Haskins, W. E. W., Z.; Watson, C. J.; Rostand, R. R.; Witowski, S. R.; Powell, D. H.; Kennedy, R. T., *Anal Chem* **2001,** *73*, 5005-5014.

97. Wilson, R. E.; Jaquins-Gerstl, A.; Weber, S. G., *Anal Chem* **2018,** *90*, 4561-4568.

98. Ou, Y.; Wilson, R. E.; Weber, S. G., *Annu Rev Anal Chem (Palo Alto Calif)* **2018,** *11*, 509-533.

99. Frommer, W. B.; Davidson, M. W.; Campbell, R. E., *Chem. Soc. Rev.* **2009,** *38*, 2833-2841.

100. Johansson, M. K.; Cook, R. M., *Chem. - Eur. J.* **2003,** *9*, 3466-3471.

101. Razgulin, A.; Ma, N.; Rao, J., *Chem. Soc. Rev.* **2011,** *40*, 4186-4216.

102. Koretsky, A. P., *Neuroimage* **2012,** *62*, 1208-15.

103. Hingorani, D. V.; Yoo, B.; Bernstein, A. S.; Pagel, M. D., *Chem. - Eur. J.* **2014,** *20*, 9840-9850.

104. Weissleder, R.; Tung, C.-H.; Mahmood, U.; Bogdanov, A., Jr., *Nat. Biotechnol.* **1999,** *17*, 375-378.

105. Tung, C.-H.; Mahmood, U.; Bredow, S.; Weissleder, R., *Cancer Res.* **2000,** *60*, 4953-4958.

106. Lee, J.; Bogyo, M., *ACS Chem. Biol.* **2010,** *5*, 233-243.

107. Gu, K.; Xu, Y.; Li, H.; Guo, Z.; Zhu, S.; Zhu, S.; Shi, P.; James, T. D.; Tian, H.; Zhu, W.-H., *J. Am. Chem. Soc.* **2016,** *138*, 5334-5340.

108. Rosell, A.; Ortega-Aznar, A.; Alvarez-Sabín, J.; Fernández-Cadenas, I.; Ribó, M.; Molina, C. A.; Lo, E. H.; Montaner, J., *Stroke* **2006,** *37*, 1399-1406.

109. Gawlak, M.; Górkiewicz, T.; Gorlewicz, A.; Konopacki, F. A.; Kaczmarek, L.; Wilczynski, G. M., *Neuroscience* **2009,** *158*, 167-176.

110. Gillespie, J. W.; Best, C. J. M.; Bichsel, V. E.; Cole, K. A.; Greenhut, S. F.; Hewitt, S. M.; Ahram, M.; Gathright, Y. B.; Merino, M. J.; Strausberg, R. L., *The American journal of pathology* **2002,** *160*, 449-457.

111. Hadler-Olsen, E.; Kanapathippillai, P.; Berg, E.; Svineng, G.; Winberg, J.-O.; Uhlin-Hansen, L., *J. Histochem. Cytochem.* **2010,** *58*, 29-39.

112. Wiera, G.; Nowak, D.; Van Hove, I.; Dziegiel, P.; Moons, L.; Mozrzymas, J. W., *Journal of Neuroscience* **2017,** *37*, 1240-1256.

113. Jares-Erijman, E. A.; Jovin, T. M., *Nature Biotechnology* **2003,** *21*, 1387-1395.

114. Keow, J. Y.; Herrmann, K. M.; Crawford, B. D., *Matrix Biol.* **2011,** *30*, 169-177.

115. Renema, W. K. J.; Kan, H. E.; Wieringa, B.; Heerschap, A., *NMR Biomed.* **2007,** *20*, 448-467.

116. Choi, C.; Ganji, S. K.; DeBerardinis, R. J.; Hatanpaa, K. J.; Rakheja, D.; Kovacs, Z.; Yang, X. L.; Mashimo, T.; Raisanen, J. M.; Marin-Valencia, I.; Pascual, J. M.; Madden, C. J.; Mickey, B. E.; Malloy, C. R.; Bachoo, R. M.; Maher, E. A., *Nat Med* **2012,** *18*, 624-9.
117. Kanamori, K., *Analytical Biochemistry* **2017,** *529*, 179-192.

118. Kanamori, K.; Ross, B. D., *Biochem. J.* **1993,** *293*, 461-8.

119. Bivehed, E.; Stromvall, R.; Bergquist, J.; Bakalkin, G.; Andersson, M., *Peptides* **2017,** *87*, 20-27.

120. Grobe, N.; Elased, K. M.; Cool, D. R.; Morris, M., *Am. J. Physiol.* **2012,** *302*, E1016-E1024.

121. OuYang, C.; Chen, B.; Li, L., *Journal of The American Society for Mass Spectrometry* **2015,** *26*, 1992-2001.

122. Zhang, H.; Stoeckli, M.; Andren, P. E.; Caprioli, R. M., *J. Mass Spectrom.* **1999,** *34*, 377-383.

123. Reed, B.; Bidlack, J. M.; Chait, B. T.; Kreek, M. J., *J. Neuroendocrinol.* **2008,** *20*, 606-616.

124. Reed, B.; Zhang, Y.; Chait, B. T.; Kreek, M. J., *J. Neurochem.* **2003,** *86*, 815-823.

125. Klintenberg, R.; Andren, P. E., *J. Mass Spectrom.* **2005,** *40*, 261-270.

126. Stenken, J. A.; Holunga, D. M.; Decker, S. A.; Sun, L., *Anal Biochem* **2001,** *290*, 314-23.

127. Steuerwald, A. J.; Villeneuve, J. D.; Sun, L.; Stenken, J. A., *J. Pharm. Biomed. Anal.* **2006,** *40*, 1041-1047.

128. Sun, L.; Stenken, J. A.; Yang, A. Y.; Zhao, J. J.; Musson, D. G., *Anal. Biochem.* **2007,** *370*, 26-37.

129. Wang, Y.; Zagorevski, D. V.; Stenken, J. A., *Anal. Chem. (Washington, DC, U. S.)* **2008,** *80*, 2050-2057.

130. Sun, L.; Stenken, J. A.; Brunner, J. E.; Michel, K. B.; Adelsberger, J. K.; Yang, A. Y.; Zhao, J. J.; Musson, D. G., *Anal. Biochem.* **2008,** *381*, 214-223.

131. Bungay, P. M.; Morrison, P. F.; Dedrick, R. L., *Life Sciences* **1990,** *46*, 105-119.

132. Mou, X.; Stenken, J. A., *Anal. Chem.* **2006,** *78*, 7778-7784.

133. Dubey, S.; Kalia, Y. N., *J. Controlled Release* **2011,** *152*, 356-362.

134. Wang, Y.; Zagorevski, D. V.; Lennartz, M. R.; Loegering, D. J.; Stenken, J. A., *Anal. Chem. (Washington, DC, U. S.)* **2009,** *81*, 9961-9971.

135. Morrison, P. F.; Bungay, P. M.; Hsiao, J. K.; Ball, B. A.; Mefford, I. N.; Dedrick, R. L., *Journal of Neurochemistry* **1991,** *57*, 103-119.

136. Chen, K. C.; Höistad, M.; Kehr, J.; Fuxe, K.; Nicholson, C., *Journal of Neurochemistry* **2002,** *81*, 108-121.

137. Yang, H.; Peters, J. L.; Allen, C.; Chern, S.-S.; Coalson, R. D.; Michael, A. C., *Analytical Chemistry* **2000,** *72*, 2042-2049.

138. Smith, A. D.; Justice, J. B., *Journal of Neuroscience Methods* **1994,** *54*, 75-82.

139. Xu, H.; Guy, Y.; Hamsher, A.; Shi, G.; Sandberg, M.; Weber, S. G., *Anal Chem* **2010,** *82*, 6377-83.

140. Rupert, A. E.; Ou, Y.; Sandberg, M.; Weber, S. G., *ACS Chem Neurosci* **2013,** *4*, 838-48.

141. Rice, C. L.; Whitehead, R., *The Journal of Physical Chemistry* **1965,** *69*, 4017-4024.

142. Probstein, R. F., *Physicochemical Hydrodynamics: An Introduction*. John Wiley & Sons, Inc.: Hoboken, New Jersey, 2003.

143. Kirby, B. J.; Hasselbrink, E. F., Jr., *Electrophoresis* **2004,** *25*, 187-202.

144. Rathore, A. S.; Wen, E.; Horváth, C., *Analytical Chemistry* **1999,** *71*, 2633-2641.

145. Rathore, A. S., *Electrophoresis* **2002,** *23*, 3827-46.

146. Scales, N.; Tait, R. N., *J Chem Phys* **2006,** *125*, 094714.

147. Støverud, K. H.; Darcis, M.; Helmig, R.; Hassanizadeh, S. M., *Transport in Porous Media* **2011,** *92*, 119-143.

148. Ou, Y.; Weber, S. G., *Anal Chem* **2017,** *89*, 5864-5873.

149. Ou, Y.; Wu, J.; Sandberg, M.; Weber, S. G., *Anal Bioanal Chem* **2014,** *406*, 6455-68.

150. Wu, J.; Sandberg, M.; Weber, S. G., *Anal Chem* **2013,** *85*, 12020-7.

151. Ou, Y.; Weber, S. G., *ACS Chem Neurosci* **2018,** *9*, 535-544.

152. Wilson, R. E.; Groskreutz, S. R.; Weber, S. G., *Anal Chem* **2016,** *88*, 5112-21.

153. Granger, J.; Plumb, R.; Castro-Perez, J.; Wilson, I. D., *Chromatographia* **2005,** *61*, 375-380.

154. Desmet, G.; Eeltink, S., *Anal. Chem.* **2013,** *85*, 543-56.
155. Gika, H. G.; Theodoridis, G. A.; Plumb, R. S.; Wilson, I. D., *J. Pharm. Biomed. Anal.* **2014,** *87*, 12-25.

156. Lee, H.; Griffin, T. J.; Gygi, S. P.; Rist, B.; Aebersold, R., *Anal. Chem.* **2002,** *74*, 4353-4360.

157. Lasonder, E.; Ishihama, Y.; Andersen, J. S.; Vermunt, A. M. W.; Pain, A.; Sauerwein, R. W.; Eling, W. M. C.; Hall, N.; Water, A. P.; Stunnenber, H. G.; Mann, M., *Nature* **2002,** *419*, 537-542.

158. Ishihama, Y., *J. Chromatogr. A.* **2005,** *1067*, 73-83.

159. Rogeberg, M.; Vehus, T.; Grutle, L.; Greibrokk, T.; Wilson, S. R.; Lundanes, E., *J. Sep. Sci.* **2013,** *36*, 2838-47.

160. Falkenby, L. G.; Such-Sanmartin, G.; Larsen, M. R.; Vorm, O.; Bache, N.; Jensen, O. N., *Journal of proteome research* **2014,** *13*, 6169-75.

161. Moruz, L.; Pichler, P.; Stranzl, T.; Mechtler, K.; Kall, L., *Anal. Chem.* **2013,** *85*, 7777-85.

162. Theodoridis, G.; Gika, H. G.; Wilson, I. D., *TrAC, Trends Anal. Chem.* **2008,** *27*, 251-260.

163. Filla, L. A.; Yuan, W.; Feldman, E. L.; Li, S.; Edwards, J. L., *Journal of proteome research* **2014,** *13*, 6121-34.

164. Chen, S.; Hoene, M.; Li, J.; Li, Y.; Zhao, X.; Haring, H. U.; Schleicher, E. D.; Weigert, C.; Xu, G.; Lehmann, R., *J. Chromatogr. A* **2013,** *1298*, 9-16.

165. Gao, X.; Zhang, Q.; Meng, D.; Isaac, G.; Zhao, R.; Fillmore, T. L.; Chu, R. K.; Zhou, J.; Tang, K.; Hu, Z.; Moore, R. J.; Smith, R. D.; Katze, M. G.; Metz, T. O., *Analytical and bioanalytical chemistry* **2012,** *402*, 2923-33.

166. Tseng, Y. J.; Kuo, C. T.; Wang, S. Y.; Liao, H. W.; Chen, G. Y.; Ku, Y. L.; Shao, W. C.; Kuo, C. H., *Electrophoresis* **2013,** *34*, 2918-27.

167. Haggarty, J.; Oppermann, M.; Dalby, M. J.; Burchmore, R. J.; Cook, K.; Weidt, S.; Burgess, K. E., *Metabolomics.* **2015,** *11*, 1465-1470.

168. Haskins, W. E.; Wang, Z.; Watson, C. J.; Rostand, R. R.; Witowski, S. R.; Powell, D. H.; Kennedy, R. T., *Anal. Chem.* **2001,** *73*, 5005-5014.

169. Zhou, Y.; Mabrouk, O. S.; Kennedy, R. T., *J. Am. Soc. Mass Spectrom.* **2013,** *24*, 1700-9.

170. Zhang, Z.; Jia, C.; Li, L., *J. Sep. Sci.* **2012,** *35*, 1779-84.

171. Maes, K.; Van Liefferinge, J.; Viaene, J.; Van Schoors, J.; Van Wanseele, Y.; Bechade, G.; Chambers, E. E.; Morren, H.; Michotte, Y.; Vander Heyden, Y.; Claereboudt, J.; Smolders, I.; Van Eeckhaut, A., *J. Chromatogr. A* **2014,** *1360*, 217-28.

172. Mabrouk, O. S.; Kennedy, R. T., *J. Neurosci. Methods.* **2012,** *209*, 127-33.

173. Han, J.; Ye, L.; Xu, L.; Zhou, Z.; Gao, F.; Xiao, Z.; Wang, Q.; Zhang, B., *Anal. Chim. Acta* **2014,** *852*, 267-73.

174. Shen, Y.; Zhang, R.; Moore, R. J.; Kim, J.; Metz, T. O.; Hixson, K. K.; Zhao, R.; Livesay, E. A.; Udseth, H. R.; Smith, R. D., *Anal. Chem.* **2005,** *77*, 3090-3100.

175. Wang, F.; Wei, X.; Zhou, H.; Liu, J.; Figeys, D.; Zou, H., *Proteomics* **2012,** *12*, 3129-37.

176. Grebe, S. K. G.; Singh, R. J., *Clin. Biochem. Rev.* **2011,** *32*.

177. Abbatiello, S. E.; Schilling, B.; Mani, D. R.; Zimmerman, L. J.; Hall, S. C.; MacLean, B.; Albertolle, M.; Allen, S.; Burgess, M.; Cusack, M. P.; Gosh, M.; Hedrick, V.; Held, J. M.; Inerowicz, H. D.; Jackson, A.; Keshishian, H.; Kinsinger, C. R.; Lyssand, J.; Makowski, L.; Mesri, M.; Rodriguez, H.; Rudnick, P.; Sadowski, P.; Sedransk, N.; Shaddox, K.; Skates, S. J.; Kuhn, E.; Smith, D.; Whiteaker, J. R.; Whitwell, C.; Zhang, S.; Borchers, C. H.; Fisher, S. J.; Gibson, B. W.; Liebler, D. C.; MacCoss, M. J.; Neubert, T. A.; Paulovich, A. G.; Regnier, F. E.; Tempst, P.; Carr, S. A., *Mol. Cell. Proteomics.* **2015,** *14*, 2357-74.

178. Rauh, M., *Journal of chromatography. B, Analytical technologies in the biomedical and life sciences* **2012,** *883-884*, 59-67.

179. Alberice, J. V.; Amaral, A. F.; Armitage, E. G.; Lorente, J. A.; Algaba, F.; Carrilho, E.; Marquez, M.; Garcia, A.; Malats, N.; Barbas, C., *J. Chromatogr. A* **2013,** *1318*, 163-70.

180. Bjellaas, T.; Holm, A.; Molander, P.; Tornes, J. A.; Greibrokk, T.; Lundanes, E., *Analytical and bioanalytical chemistry* **2004,** *378*, 1021-30.

181. Novotny, M. V.; Daido, I., *Microcolumn Separations Columns, Instrumentation, and Ancillary Techniques*. Elsevier Science Pub. Co.: Amsterdam, New York; New York, 1985.

182. Moore, A. W.; Jorgenson, J. W., *Anal. Chem.* **1995,** *67*, 3448-3455.

183. Molander, P.; Thommesen, S. J.; Bruheim, I. A.; Trones, R.; Greibrokk, T.; Lundanes, E.; Gundersen, T. E., *J. High Resol. Chromatogr.* **1999,** *22*, 490-494.

184. Trones, R.; Tangen, A.; Lund, W.; Greibrokk, T., *J. Chromatogr. A.* **1999,** *835*, 105-112.

185. Prüß, A.; Kempter, C.; Gysler, J.; Jira, T., *J. Chromatogr. A.* **2004,** *1030*, 167-176.

186. Wei, H.; Nolkrantz, K.; Parkin, M. C.; Chisolm, C. N.; O'Callaghan, J. P.; Kennedy, R. T., *Anal. Chem.* **2006,** *78*, 4342-4351.

187. Gilar, M.; McDonald, T. S.; Roman, G.; Johnson, J. S.; Murphy, J. P.; Jorgenson, J. W., *J. Chromatogr. A.* **2015,** *1381*, 110-117.

188. Snyder, L. R.; Kirkland, J. J.; Dolan, J. W., *Introduction to Modern Liquid Chromatography*. Third ed.; John Wiley and Sons, Inc.: Hoboken, N.J., 2010.

189. Foster, M. D.; Arnold, M. A.; Nichols, J. A.; Bakalyar, S. R., *J. Chromatogr. A* **2000,** *869*, 231-241.

190. Heron, S.; Tchapla, A.; Chervet, J.-P., *Chromatographia* **2000,** *51*, 495-499.

191. Layne, J.; Farcas, T.; Rustamov, I.; Ahmed, F., *J. Chromatogr. A* **2001,** *913*, 233-242.

192. Rezai, M. A.; Famiglini, G.; Cappiello, A., *J. Chromatogr. A* **1996,** *742*, 69-78.

193. Wang, X.; Barber, W. E.; Carr, P. W., *J. Chromatogr. A* **2006,** *1107*, 139-51.

194. Grushka, E., *Anal. Chem.* **1970,** *42*, 1142-1147.

195. Robards, K.; Haddad, P. R.; Jackson, P. E., *Principles and Practice of Modern Chromatographic Methods*. Academic Press, Inc. : San Diego, CA, 1997.

196. Bird, R. B.; Stewart, W. E.; Lightfoot, E. N., *Transport Phenomena*. 2nd ed.; John Wiley and Sons, Inc.: New York, 2002.

197. Poppe, H.; Kraak, J. C.; Huber, J. F. K.; van den Berg, J. H. M., *Chromatographia* **1981,** *14*, 515-523.

198. Bowermaster, J.; McNair, H., *J. of Chromatogr.* **1983,** *279*, 431-438.

199. Zhu, P. L.; Dolan, J. W.; Snyder, L. R., *J. Chromatogr. A* **1996,** *756*, 41-50.

200. Jandera, P.; Blomberg, L. G.; Lundanes, E., *J. Sep. Sci.* **2004,** *27*, 1402-1418.

201. Giddings, J. C., *Unified Separation Science*. Wiley-Interscience: New York, 1991.

202. Greibrokk, T.; Andersen, T., *J. Sep. Sci.* **2001,** *24*, 899-909.

203. Grushka, E.; Colin, H.; Guiochon, G., *J. Chromatogr.* **1982,** *248*, 325-339.

204. Gasslander, U.; Arbin, A.; Albertsson, A.-C., *Polymer* **2007,** *48*, 7523-7530.

205. Holm, A.; Molander, P.; Lundanes, E.; Greibrokk, T., *Journal of Separation Science* **2003,** *26*, 1147-1153.

206. Eghbali, H.; Sandra, K.; Tienpont, B.; Eeltink, S.; Sandra, P.; Desmet, G., *Anal. Chem.* **2012,** *84*, 2031-2037.

207. Groskreutz, S. R.; Weber, S. G., *J. Chromatogr. A* **2014,** *1354*, 65-74.

208. Groskreutz, S. R.; Horner, A. R.; Weber, S. G., *J. Chromatogr. A* **2015,** *1405*, 133-9.

209. Chuman, H.; Mori, A.; Tanaka, H.; Yamagami, C.; Fujita, T., *J. Pharm. Sci.* **2004,** *93*, 2681-97.

210. Schultz, T. W.; Hewitt, M.; Netzeva, T. I.; Cronin, M. T. D., *QSAR & Combinatorial Science* **2007,** *26*, 238-254.

211. Neue, U. D.; Kuss, H. J., *J. Chromatogr. A* **2010,** *1217*, 3794-803.

212. Zhang, J.; Liu, Y.; Jaquins-Gerstl, A.; Shu, Z.; Michael, A. C.; Weber, S. G., *J. Chromatogr. A.* **2012,** *1251*, 54.

213. Colin, H.; Martin, M.; Guiochon, G., *J. Chromatogr.* **1979,** *185*, 79-95.

214. Snyder, L. R.; Dolan, J. W., *High-Performance Gradient Elution: The Practical Application of the Linear-Solvent-Strength Model*. John Wiley and Sons, Inc.: 2007.

215. Gilpin, R. K.; Jaroniec, M.; Lin, S., *Chromatographia* **1990,** *30*, 393-399.

216. Chen, M. H.; Horvath, C., *J. Chromatogr. A* **1997,** *788*, 51-61.

217. Liu, H.; Finch, J. W.; Lavallee, M. J.; Collamati, R. A.; Benevides, C. C.; Gebler, J. C., *J. Chromatogr. A* **2007,** *1147*, 30-6.

218. Jandera, P., *Anal. Chim. Acta* **2011,** *692*, 1-25.

219. Soukup, J.; Jandera, P., *Biologija* **2011,** *57*, 85-91.

220. Soukup, J.; Jandera, P., *J. Chromatogr. A.* **2012,** *1245*, 98-108.

221. Kumar, A.; Heaton, J. C.; McCalley, D. V., *J. Chromatogr. A.* **2013,** *1276*, 33-46.

222. Yi, Y. Capillary HPLC Separation of Selected Neuropeptides. University of Pittsburgh, Pittsburgh, 2012.

223. Mao, Y.; Carr, P. W., *Anal. Chem.* **2000,** *72*, 110-8.

224. Saifutdinov, B. R.; Emel'yanova, N. S.; Pimerzin, A. A., *Prot. Met. Phys. Chem. Surf.* **2014,** *50*, 317-325.

225. Kuznetsova, E. S.; Buryak, A. K., *Colloids Surf, A.* **2011,** *383*, 73-9.

226. Melmer, M.; Stangler, T.; Premstaller, A.; W., L., *J. Chromatogr. A* **2010,** *1217*, 6092-6096.

227. Gaudin, K.; Hanai, T.; Chaminade, P.; Baillet, A., *J. Chromatogr. A* **2007,** *1157*, 56-64.

228. Kwaterczak, A.; Bielejewska, A., *Anal Chim Acta.* **2005,** *537*, 41-46.

229. Moeckel, H. J.; Braedikow, A.; Melzer, H.; Aced, G., *J. Liq. Chromatogr.* **1991,** *14*, 2477-2498.

230. Snyder, L. R.; Dolan, J. W. *High-Performance Gradient Elution: The Practical Application of the Linear-Solvent-Strength Model*. John Wiley and Sons, Inc.: 2007.

231. Eghbali, H. S., K.; Tienpont, B.; Eeltink, S.; Sandra, P.; Desmet, G., *Anal. Chem.* **2012,** *84*, 2031-2037.

232. Madison, D. V.; Nicoll, R. A., *Journal of physiology* **1988,** *398*, 123-130.

233. Piguet, P.; North, R. A., *The Journal of Pharmacology and Experimental Therapeutics* **1993,** *266*, 1139-1146.

234. Yoshitake, S.; Ijiri, S.; Kehr, J.; Yoshitake, T., *Neurochem. Int.* **2013,** *62*, 314-323.

235. Lee, S. Y.; Park, S. H.; Chung, C.; Kim, J. J.; Choi, S. Y.; Han, J. S., *Sci Rep* **2015,** *5*, 18540.

236. Murphy, N. P., *ACS Chem Neurosci* **2015,** *6*, 94-107.

237. Andren, P. E.; Caprioli, R. M., *Brain Research* **1999,** *845*, 123-129.

238. Baseski, H. M.; Watson, C. J.; Cellar, N. A.; Shackman, J. G.; Kennedy, R. T., *J Mass Spectrom* **2005,** *40*, 146-53.

239. Emmett, M. R.; Andren, P. E.; Caprioli, R. M., *J. Neurosci. Methods* **1995,** *62*, 141-147.

240. Maidment, N. T.; Brumbaugh, D. R.; Rudolph, V. D.; Erdelyi, E.; Evans, C. J., *Neuroscience* **1989,** *33*, 549-557.

241. Zhou, Y.; Mabrouk, O. S.; Kennedy, R. T., *J Am Soc Mass Spectrom* **2013,** *24*, 1700-9.

242. Li, Q. Z., J.; Kennedy, R. T., *Anal Chem* **2009,** *81*, 2242-2250.

243. Maes, K.; Van Liefferinge, J.; Viaene, J.; Van Schoors, J.; Van Wanseele, Y.; Bechade, G.; Chambers, E. E.; Morren, H.; Michotte, Y.; Vander Heyden, Y.; Claereboudt, J.; Smolders, I.; Van Eeckhaut, A., *J Chromatogr A* **2014,** *1360*, 217-28.

244. Zestos, A. G.; Kennedy, R. T., *AAPS J* **2017**.

245. Song, P.; Mabrouk, O. S.; Hershey, N. D.; Kennedy, R. T., *Anal Chem* **2012,** *84*, 412-419.

246. Wong, J.-M. T.; Malec, P. A.; Mabrouk, O. S.; Ro, J.; Dus, M.; Kennedy, R. T., *J. Chromatogr. A* **2016,** *1446*, 78-90.

247. Raijmakers, R.; Berkers, C. R.; de Jong, A.; Ovaa, H.; Heck, A. J.; Mohammed, S., *Mol Cell Proteomics* **2008,** *7*, 1755-62.

248. Boersema, P. J.; Raijmakers, R.; Lemeer, S.; Mohammed, S.; Heck, A. J., *Nat Protoc* **2009,** *4*, 484-94.

249. Maiolica, A.; Borsotti, D.; Rappsilber, J., *Proteomics* **2005,** *5*, 3847-50.

250. Mitala, C. M.; Wang, Y.; Borland, L. M.; Jung, M.; Shand, S.; Watkins, S.; Weber, S. G.; Michael, A. C., *J Neurosci Methods* **2008,** *174*, 177-85.

251. Paxinos, G.; Watson, C., *The Rat Brain in Stereotaxic Coordinates*. Academic Press: 1998.

252. Hsu, J.; Huang, S.; Chow, N.; Chen, S., *Anal Chem* **2003,** *75*, 6843-6852.

253. Guo, K.; Ji, C.; Li, L., *Anal Chem* **2007,** *79*, 8631-8.

254. Lanckmans, K.; Clinckers, R.; Van Eeckhaut, A.; Sarre, S.; Smolders, I.; Michotte, Y., *J Chromatogr B Analyt Technol Biomed Life Sci* **2006,** *831*, 205-12.

255. Greco, S.; Danysz, W.; Zivkovic, A.; Gross, R.; Stark, H., *Anal Chim Acta* **2013,** *771*, 65-72.

256. Douglas, W. W.; Poisner, A. M., *J. Physiol.* **1964,** *172*, 1-18.

257. Chavkin, C. B., C.; Weber, E.; Bloom, F. E., *Proc. Natl. Acad. Sci.* **1983,** *80*, 7669-7673.

258. Podvin, S.; Bundey, R.; Toneff, T.; Ziegler, M.; Hook, V., *Mol Cell Neurosci* **2015,** *68*, 177-185.

259. Rocha, L.; Evans, C. J.; Maidment, N. T., *J Neurochem* **1997,** *68*, 616-624.

260. Rocha, L.; Maidment, N. T., *Hippocampus* **2003,** *13*, 472-80.

261. Rossier, J.; Vargo, T. M.; Minick, S.; Ling, N.; Bloom, F. E.; Guillemin, R., *Proc Natl Acad Sci U S A* **1977,** *74*, 5162-5165.

262. Simantov, R.; Kuhar, M. J.; Uhl, G. R.; Snyder, S. H., *Proc Natl Acad Sci U S A* **1977,** *74*, 2167-2171.

263. Hughes, J. K., H. W.; Smith, T. W., *Br. J. Pharmacol.* **1977,** *1977*.

264. Bloom, F.; Battenberg, E.; Rossier, J.; Ling, N.; Guillemin, R., *Proc Natl Acad Sci U S A* **1978,** *75*, 1591-1595.

265. Ploj, K.; Roman, E.; Gustavsson, L.; Nylander, I., *Brain Research Bull* **2000,** *53*, 219-226.

266. Nylander, I. V., M.; Terenius, L., *Brain Res* **1995,** *683*, 25-35.

267. Rupert, A. E.; Ou, Y.; Sandberg, M.; Weber, S. G., *ACS Chem Neurosci* **2013,** *4*, 838-848.

268. Ban, L.; Pettit, N.; Li, L.; Stuparu, A. D.; Cai, L.; Chen, W.; Guan, W.; Han, W.; Wang, P. G.; Mrksich, M., *Nat. Chem. Biol.* **2012,** *8*, 769-773.

269. Yates, N. A.; Deyanova, E. G.; Geissler, W.; Wiener, M. C.; Sachs, J. R.; Wong, K. K.; Thornberry, N. A.; Sinha Roy, R.; Settlage, R. E.; Hendrickson, R. C., *International Journal of Mass Spectrometry* **2007,** *259*, 174-183.

270. Bothner, B.; Chavez, R.; Wei, J.; Strupp, C.; Phung, Q.; Schneemann, A.; Siuzdak, G., *J. Biol. Chem.* **2000,** *275*, 13455-13459.

271. Van Noorden, C. J. F., *J. Histochem. Cytochem.* **2010,** *58*, 481-497.

272. Vandooren, J.; Geurts, N.; Martens, E.; Van den Steen, P. E.; Opdenakker, G., *Nat Methods* **2013,** *10*, 211-20.

273. Bivehed, E.; Stroemvall, R.; Bergquist, J.; Bakalkin, G.; Andersson, M., *Peptides (N. Y., NY, U. S.)* **2017,** *87*, 20-27.

274. OuYang, C.; Chen, B.; Li, L., *J. Am. Soc. Mass Spectrom.* **2015,** *26*, 1992-2001.

275. Wienkers, L. C.; Heath, T. G., *Nat Rev Drug Discov* **2005,** *4*, 825-33.

276. Kostel, K. L.; Lunte, S. M., *Journal of Chromatography B: Biomedical Sciences and Applications* **1997,** *695*, 27-38.

277. Freed, A. L.; Cooper, J. D.; Davies, M. I.; Lunte, S. M., *J. Neurosci. Methods* **2001,** *109*, 23-29.

278. Maidment, N. T.; Siddall, B. J.; Rudolph, V. R.; Erdelyi, E.; Evans, C. J., *Neuroscience (Oxford)* **1991,** *45*, 81-93.

279. Wen, X.-D.; Yang, J.; Ma, R.-H.; Gao, W.; Qi, L.-W.; Li, P.; Bauer, B. A.; Du, G.-J.; Zhang, Z.; Somogyi, J.; Wang, C.-Z.; Yuan, C.-S., *J. Chromatogr. B: Anal. Technol. Biomed. Life Sci.* **2012,** *895-896*, 162-168.

280. Sandeep, T. C.; Andrew, R.; Homer, N. Z. M.; Andrews, R. C.; Smith, K.; Walker, B. R., *Diabetes* **2005,** *54*, 872-879.

281. Sato, T.; Obata, T.; Yamanaka, Y.; Arita, M., *Br J Pharmacol* **1998,** *125*, 493-8.

282. Obata, T., *Life Sciences* **2002,** *71*, 2083-2103.

283. Wang, L.; Pi, Z.; Liu, S.; Liu, Z.; Song, F., *Sci. Rep.* **2017,** *7*, 1-11.

284. Rupert, A. E.; Ou, Y.; Sandberg, M.; Weber, S. G., *ACS Chem Neurosci* **2013,** *4*, 849-57.
285. Guy, Y.; Sandberg, M.; Weber, S. G., *Biophys J* **2008,** *94*, 4561-9.

286. Guy, Y.; Muha, R. J.; Sandberg, M.; Weber, S. G., *Anal Chem* **2009,** *81*, 3001-7.

287. Guy, Y.; Faraji, A. H.; Gavigan, C. A.; Strein, T. G.; Weber, S. G., *Anal Chem* **2012,** *84*, 2179-87.

288. McKinley, M. J.; Albiston, A. L.; Allen, A. M.; Mathai, M. L.; May, C. N.; McAllen, R. M.; Oldfield, B. J.; Mendelsohn, F. A. O.; Chai, S. Y., *The International Journal of Biochemistry & Cell Biology* **2003,** *35*, 901-918.

289. Aksit, A.; Arriaga, M.; Wang, X.; Watanabe, H.; Kasza, K. E.; Lalwani, A. K.; Kysar, J. W.; Arteaga, D. N.; Lalwani, A. K.; Kysar, J. W., *Biomed Microdevices* **2018,** *20*, 47.

290. Di Giacomo, R.; Krodel, S.; Maresca, B.; Benzoni, P.; Rusconi, R.; Stocker, R.; Daraio, C., *Sci. Rep.* **2017,** *7*, 45897.

291. Faraji Rad, Z.; Nordon, R. E.; Anthony, C. J.; Bilston, L.; Prewett, P. D.; Arns, J.-Y.; Arns, C. H.; Zhang, L.; Davies, G. J., *Microsystems &Amp; Nanoengineering* **2017,** *3*, 17034.

292. Hong, N.; Yang, G. H.; Lee, J.; Kim, G., *J Biomed Mater Res B Appl Biomater* **2018,** *106*, 444-459.

293. Lissandrello, C. A.; Gillis, W. F.; Shen, J.; Pearre, B. W.; Vitale, F.; Pasquali, M.; Holinski, B. J.; Chew, D. J.; White, A. E.; Gardner, T. J., *J Neural Eng* **2017,** *14*, 036006.

294. Malinauskas, M.; Baltriukiene, D.; Kraniauskas, A.; Danilevicius, P.; Jarasiene, R.; Sirmenis, R.; Zukauskas, A.; Balciunas, E.; Purlys, V.; Gadonas, R.; Bukelskiene, V.; Sirvydis, V.; Piskarskas, A., *Appl. Phys. A: Mater. Sci. Process.* **2012,** *108*, 751-759.

295. Marino, A.; Tricinci, O.; Battaglini, M.; Filippeschi, C.; Mattoli, V.; Sinibaldi, E.; Ciofani, G., *Small* **2018,** *14*.

296. Miller, P. R.; Boehm, R. D.; Skoog, S. A.; Edwards, T. L.; Rodriguez, M.; Brozik, S.; Brener, I.; Byrd, T.; Baca, J. T.; Ashley, C.; Narayan, R. J.; Polsky, R., *Electroanalysis* **2015,** *27*, 2239-2249.

297. Son, A. I.; Opfermann, J. D.; McCue, C.; Ziobro, J.; Abrahams, J. H., III; Jones, K.; Morton, P. D.; Ishii, S.; Oluigbo, C.; Krieger, A.; Liu, J. S.; Hashimoto-Torii, K.; Torii, M., *Sci. Rep.* **2017,** *7*, 1-16.

298. Suzuki, M.; Sawa, T.; Takahashi, T.; Aoyagi, S. In *Ultrafine three-dimensional (3D) laser lithographic fabrication of microneedle and its application to painless insertion and blood sampling inspired by mosquito*, 2015 IEEE/RSJ International Conference on Intelligent Robots and Systems (IROS), 28 Sept.-2 Oct. 2015; 2015; pp 2748-2753.

299. Xu, H.; Medina-Sanchez, M.; Magdanz, V.; Schwarz, L.; Hebenstreit, F.; Schmidt, O. G., *ACS Nano* **2018,** *12*, 327-337.

300. Fernando, R. N.; Luff, S. E.; Albiston, A. L.; Chai, S. Y., *J. Neurochem.* **2007,** *102*, 967-976.

301. Hernandez, J.; Prieto, I.; Segarra, A. B.; de Gasparo, M.; Wangensteen, R.; Villarejo, A. B.; Banegas, I.; Vives, F.; Cobo, J.; Ramirez-Sanchez, M., *Behav. Brain Res.* **2015,** *287*, 42-48.

302. Gray, A. C.; Coupar, I. M.; White, P. J., *Life Sci.* **2006,** *79*, 674-685.

303. Faraji, A. H.; Cui, J. J.; Guy, Y.; Li, L.; Gavigan, C. A.; Strein, T. G.; Weber, S. G., *Langmuir* **2011,** *27*, 13635-42.

304. Faraji, A. H.; Jaquins-Gerstl, A. S.; Valenta, A. C.; Weber, S. G., *J Neurosci Methods* **2019,** *311*, 76-82.

305. Hamsher, A. E.; Xu, H.; Guy, Y.; Sandberg, M.; Weber, S. G., *Anal Chem* **2010,** *82*, 6370-6.

306. Chen, K. C.; Höistad, M.; Kehr, J.; Fuxe, K.; Nicholson, C., *Journal of Neurochemistry* **2002,** *81*, 94-107.

307. Feng, J. F.; Liu, J.; Zhang, L.; Jiang, J. Y.; Russell, M.; Lyeth, B. G.; Nolta, J. A.; Zhao, M., *Stem Cell Reports* **2017,** *9*, 177-189.

308. Fekete, Z.; Pálfi, E.; Márton, G.; Handbauer, M.; Bérces, Z.; Ulbert, I.; Pongrácz, A.; Négyessy, L., *Sensors and Actuators B: Chemical* **2016,** *236*, 815-824.

309. Cepeda, D. E.; Hains, L.; Li, D.; Bull, J.; Lentz, S. I.; Kennedy, R. T., *J Neurosci Methods* **2015,** *242*, 97-105.

310. Koehler, C. J.; Arntzen, M. O.; de Souza, G. A.; Thiede, B., *Anal Chem* **2013,** *85*, 2478-85.